



**UiT**

THE ARCTIC  
UNIVERSITY  
OF NORWAY

Faculty of Geosciences

# Fluid flow and seafloor gas seepage studies of Tampen Spurr.

---

**Isaiah Oluwamayowa Olayiwola**

*Master's thesis in [Marine Geology and Geophysics]*





# **Abstract**

The southern areas of the North Sea are shallow waters with a depth of roughly 50m, which includes the German section, Dutch section, Danish and the UK sector of the North Sea. The north of the North Sea is much deeper but generally less than 200m, except within the Norwegian Trough/Trench towards the northeast, the only region of deep waters. Significant oil and gas discoveries have been made within the Norwegian sector of the North Sea, both within the Norwegian Trench and away to the west of the National boundaries towards the east Shetland platform.

Despite the discoveries of oil and gas. A lot remains unsaid about the complex history of tectonics systems underlying the North Sea and arguments supporting this area's complex structure. Notwithstanding, this short stint of research attempted to explain some reasons for gas leaks seen on the seafloor to the west of the Norwegian Trench related to Norway's sectioning, especially with areas on the part of the structural high westwards of the Norwegian North Sea.

In understanding some of these gas leaks to the seafloor on the embankment, seismic was being utilised with flare data and bathymetry of the area. The findings attempt to highlight Complex structures noted from the seismic underlying this area, with proven evidence of fluid release resulting from this complex structure beneath the base Cretaceous, marking a pivotal root source of fluid release charging the seafloor and possible pathway mechanisms.

The summary of these findings presents activities that might have fueled the shallow gas seen towards the seafloor within the Quaternary and Neogene sub divisions unit and into the seafloor through faults and possible fractures while invoking a known Petroleum system that has been studied as a likely explanation of the source of the fluid contributing to the shallow gas to the seafloor from base Cretaceous, linking it to the complexity tectonics shaping the North Sea and its complex stratigraphy.



# **Acknowledgement**

I want to thank God for taking me through this rigorous journey and seeing me through this program right from Nigeria to Norway. My special appreciation also goes to the department for providing an enabling environment with talented educators passionate about teaching and providing critical feedback to improve me through my academic journey.

I want to thank my parents for their financial support that brought me here and everyone from Nigeria who prayed and supported me towards my master's program.

I also want to thank my principal supervisor in the person of Professor Stefan Bünz, for assigning me this excellent topic, which I enjoyed and for providing the data, setup used and critical feedback that has helped fine-tuned my project to this stage. Also, I thank my co-supervisor in person at Andreia Plaza Faverola for her weekly meeting and for pushing me to try something new with PETREL; her feedback and weekly support proved pivotal to thinking things differently, for which I'm grateful.

An appreciation also goes to Kai Mortensen for his support as a student advisor, and I'm indeed grateful for that.

This also goes to those who have supported me at one point or the other with advice and for keeping me going through this journey. I collectively acknowledge you, and this project is all thanks to you.



## Table of Contents

1. Introduction .....	10
1.1 Study Area.....	11
1.2 Motivation / Objectives .....	13
2. Geological Setting & Margin Development.....	14
2.1 Basin Evolution .....	20
2.1.1 Triassic Basin Evolution .....	20
2.1.2 Jurassic Basin Evolution.....	20
2.1.3 Tertiary/ Cenozoic Basin Evolution .....	21
3. Quaternary Basin Evolution / Glacial History.....	22
4. General Stratigraphy & Sedimentary Process of North Sea.....	27
4.1 Mesozoic.....	29
4.1.1 Hegre Group .....	29
4.1.2 Statfjord Formation.....	30
4.1.3 Dunlin Group .....	31
4.1.4 Brent Group.....	31
4.1.5 Viking Group .....	33
4.1.6 Cromer Knoll Group & Shetland Group.....	33
4.2 Cenozoic .....	34
4.2.1 Rogaland Group.....	34
4.2.2 Hordaland Group.....	34
4.2.3 Nord-land Group .....	34
4.3 Sedimentary Processes and environment of north Northern Sea.....	36
5. Structures in the north Northern Sea .....	37
5.1 Major Fault Classification and Types.....	37
5.1.1 Polygonal Faults Systems.....	38
6. Petroleum Systems Framework.....	40
6.1 Porosity.....	40
6.2 Permeability.....	41
6.3 Capillary Pressure.....	41
6.4 Source Rocks .....	43
6.5 Reservoir Rocks .....	43
6.6 Seals and Traps.....	44

6.7 Migration.....	44
6.8 Pressure .....	44
6.9 Temperature.....	47
7. Compression and Shear Stress in Marine Sediments .....	47
8. Seismic Expressions & Fluid-Related systems .....	49
8.1 Compaction-controlled systems. ....	49
8.2 Volcanism Controlled Systems. ....	50
8.3 Petroleum Controlled Systems. ....	51
8.4 Gas Hydrates & systems.....	51
8.4.1 BSR (Bottom Simulating Reflector) - Bottom of Gas Hydrate .....	53
8.4.2 GHSZ - Gas Hydrate Stability Zone .....	53
9. Methodology & Data.....	55
9.1 Seismic Reflection Principles.....	55
9.1.1 Tuning Effect (Vertical Resolution).....	56
9.1.2 Fresnel Zone (Horizontal Resolution).....	57
9.2 Direct Hydrocarbon Indicators (DHI)/ Fluid Indicators.....	58
9.3 Data .....	61
9.1 Frequencies.....	66
9.1.1 Noise-to-signal ratio .....	66
9.1.2 Polarity of the Data (Examples).....	68
.....	68
9.2 Seismic Attributes Used and parameters .....	69
9.3 Time Slices Vs Horizons .....	70
9.4 Workflow .....	71
10. Results .....	72
10.1 Seismic Stratigraphy, Horizon Interpretation & subdivisions.....	72
10.2.1 Seismic Unit & Facies Descriptions.....	78
10.4 Seafloor Morphology and Description of Seabeds Surface.....	81
10.5 Fluid Indicators on Seismic Sections (High Anomaly) .....	89
10.5.1 Shallow amplitude anomalies towards the seafloor.....	89
10.5.2 Occurrence of V, W, and winglike amplitude anomalies with associated structures. ....	92
10.5.3 Deeper amplitude anomalies .....	98
10.6 Fault Description and Orientation.....	100
10.5.1 Small and Large Fault Components .....	101
10.5.2 Large Fault Component .....	105
10.5.3 Large Structures Underlying Base Cretaceous. ....	106



10.6 Possible Pathways / Fluid Flow related Structures.....	109
11. Discussions.....	121
11.1 Seismic Unit & Facies Descriptions.....	121
11.2 Glacier-induced Marks / Morphology and Glacier Expressions on Seabed. ....	121
11.3 Shallow Amplitude Anomaly towards the Seafloor .....	125
11.4 V, w, and winglike shaped Anomaly.....	126
11.5 Fault, fractures, and Structures Encountered Probably Associated with Fluid Flow .....	127
11.6 Fluid Flow Structures and Leakages on Tampen Spurr. ....	129
11.7 Potential Geological Model, rootpoint and Triggers for the North Northern Sea gas seepage. .....	130
12. Conclusion.....	133
13. Further Works.....	134



## 1. Introduction

A growing body of literature recognises the importance of understanding fluid flow in the subsurface. Judd (2004) emphasizes that gas seeps have only recently been acknowledged as a possible origin of atmospheric methane. Methane is a type of hydrocarbon, which is represented by the chemical formula  $\text{CH}_4$  and tends to be classified chemically as dry gas, a component of petroleum Selley & Sonnenberg (2015), it is an important greenhouse gas (GHG) that plays a significant role in influencing and altering the Earth's climate system. It is the second most important GHG (e.g Berndt, 2005; Böttner et al., 2020; A. G. Judd, 2004).

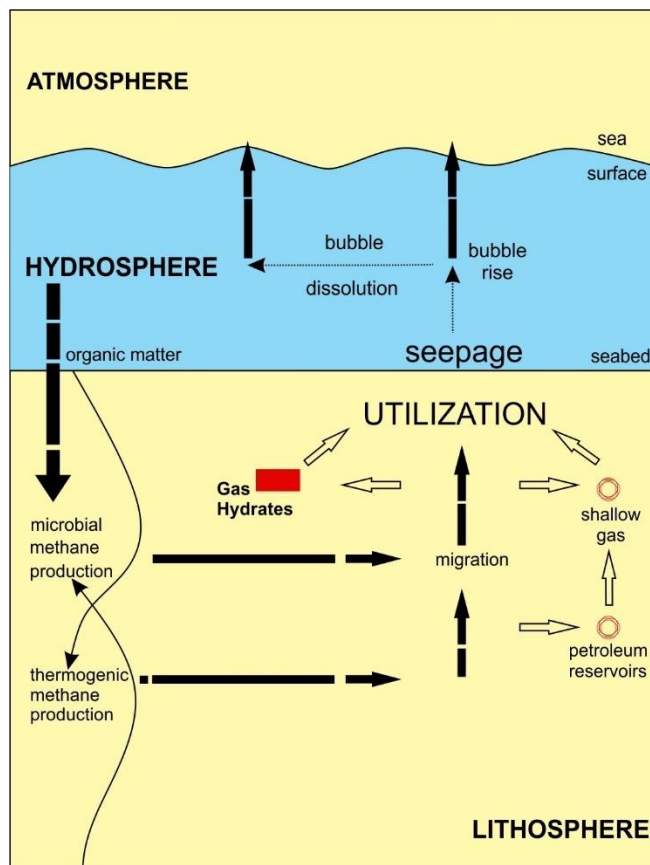
According to Böttner et al. (2020) while carbon dioxide, which is the number 1 GHG gas, is known in terms of production, generation, and consumption. Methane, with more warming effect on the atmosphere than carbon dioxide, has remained elusive in estimation and accounting for gases concerning climate input (Böttner et al., 2020). Its estimation comes with a lot of uncertainties that accompany its production, occurrence by degradation and methanotrophs and consumption by prokaryotes metabolizing methane's as a source of chemical energy and carbon known as methanogens (Judd, 2004; Judd & Hovland, 2009).

Berndt (2005) highlighted fluid flow as a field in marine geology that will be increasingly important in the coming decades due to its relevance and contribution to climate change, a hot topic (Berndt, 2005). Additionally, its application in understanding benthic ecosystems and how fluid affects and changes the ecosystem further highlights its significance. Lastly, fluid flow plays a crucial role in natural resources and its application to  $\text{CO}_2$  sequestration, making it a highly relevant area of study (Berndt, 2005; A. G. Judd, 2004; A. Judd & Hovland, 2009). Also, within the European Union, one of the largest funding in geosciences goes into ecological hotspots, which requires fluid flow understanding of the processes connecting the geosphere to the biosphere (Berndt, 2005).

Judd (2004) and Böttner et al. (2020) acknowledges the uncertainties and challenges concerning constraining the amount of methane from the seabed. Methane can be formed by various processes, some of which remain poorly understood. Researchers and authors have addressed the generation of methane from the sea beds by addressing different processes which might have led to the generation of methane into the atmosphere (Judd, 2004). Some of the authors who have studied the natural methane seeps from the seabed in marine areas are (Dimitrov,

2002; Hornafius et al., 1999; A. Judd et al., 1997) and globally, estimations have been done by (Böttner et al., 2020; Hovland, 2002; Kvenvolden & McMenamin, 1980).

Judd et al. (1997) provides the framework for estimating methane gases from natural gas seep into the atmosphere if they make their way through the water column, as shown in Fig.1. Despite the uncertainty of methane from natural gas seeps, this study focuses on seepages occurring in



a study area located north Norwegian Sea and possible methane emissions. It aids the understanding of atmospheric methane in a specific area north of the Norwegian Sea. It does not seek to generalise seepage occurrence across the North Northern Sea, but just a specific region limited to the North Northern Sea.

Figure 1: Possible origins of CH<sub>4</sub> from the lithosphere to the hydrosphere and the fate of fluids and natural gas seepage need to be explained. Inspired by (Judd, 2004).

The investigated area is a small study area on the North Northern Sea, with a history of complex tectonics shaping the basin with significant main events associated with a described Mesozoic rifting (Fossen, 1989; Ziegler, 1992). They are suspected

to contain leaks on the seafloor and are associated with significant discoveries of oil and gas fields on the north Norwegian Continental Shelf. Much similar work has been done using seismic and an integrated approach in understanding of fluids such as (Arntsen et al., 2007; Böttner et al., 2020; Løseth et al., 2009a, 2011). This study seeks to improve the understanding of fluid flow and related causal mechanisms using seismic, flare data, bathymetry data, and penetrating literature on the study area.

## 1.1 Study Area

Fig. 2 shows the subject of study, marked in red with corresponding seismic sections. This region is situated in the Tampen Spur area, lies to the north of the Gullfaks Field and to the

north-east of the Statfjord field, which is one of the largest oil fields in the North Sea, with a STOIIP (Stock tank oil initially in place) of more than  $1200 \times 10^6 \text{ Sm}^3$  (Caillet, 1993; Horstad et al., 1995). Structural investigations have revealed a connection to the Viken Graben, and the area is located within the coordinates around 58°E and 62°E (Caillet, 1993).

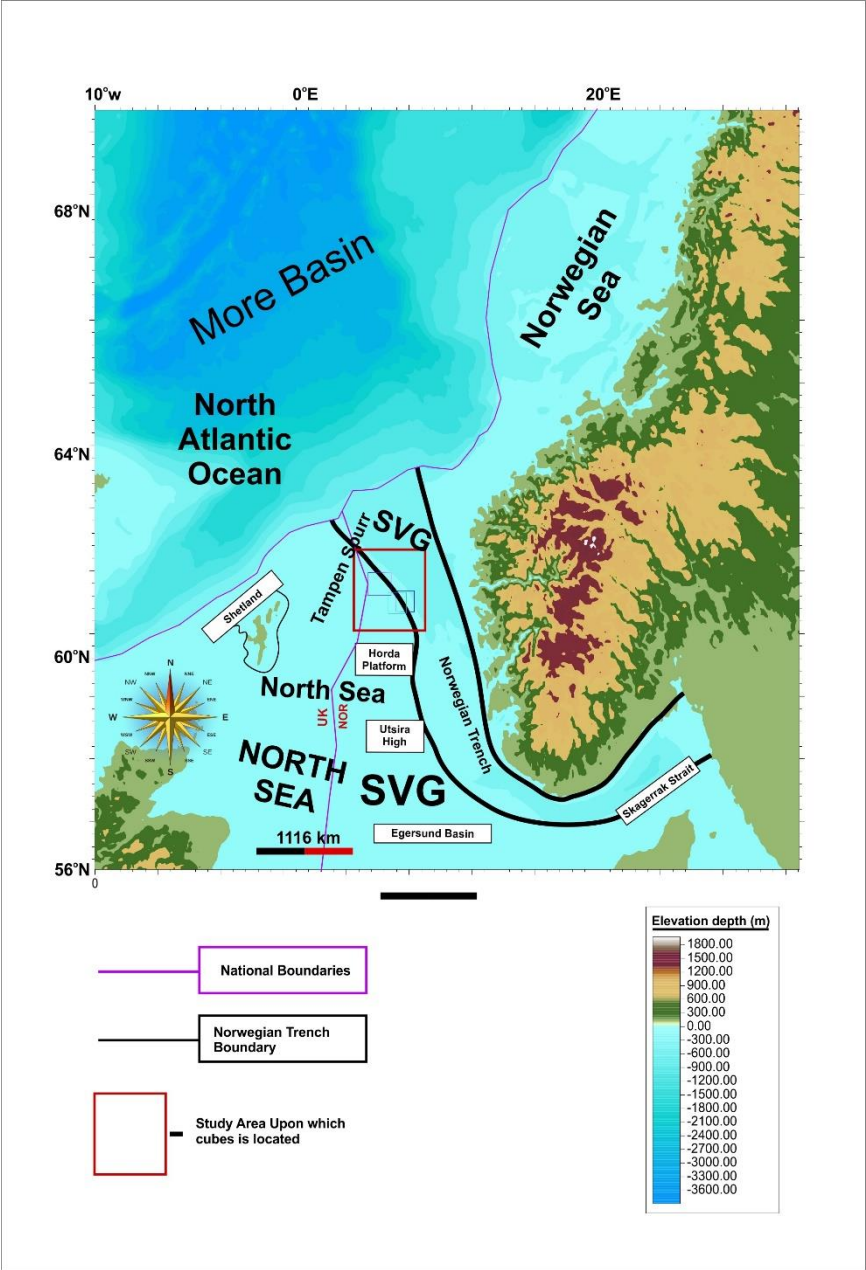


Figure 2: A bathymetry map showing the study area marked in red and corresponding seismic cubes (ST11MZ07, ST98M7 and NX0802) analysed with major subbasins. Where NVG is North Viken Graben, SVG is South Viken Graben.

Fig.2 shows that the area is connected to various structural elements and deformations associated with the Mesozoic rift system and the resulting Viking graben system that has been inactive since the late Jurassic and early Cretaceous with surrounding depocenters (Ziegler,

1990). Various explorations and activities on the Northern Sea have led to the mapping of numerous fault structures associated with the study area, with main faults orientating from NE to SW, while smaller faults orientates perpendicular and opposite to that of the main faults (see 3 for orientation of fault systems) (Fossen, 2016). This makes the Tampen area much more complicated due to various complex processes controlling the area, which hosts many giant oilfields (Fossen & Hesthammer, 1998; Horstad et al., 1995; Huuse & Mickelson, 2004; Ziegler, 1992) .

The Northern Sea, in which the study area is also located, also has a well-known glacial history that is linked to the Fennoscandian Ice Sheet (FIS), which covers entire Northern Europe during the last glacial period of the Weichselian glaciation, and the British-Irish Ice Sheet (BIIS), which covered Britain and Ireland during the Quaternary period (Becker et al., 2018). The impact of glaciers is often accounted for due to the role played in erosion, uplift, and deposition of sediments. Glaciers are also essential in understanding the Northern Sea's sediment influx and Cenozoic contribution. Hence, the glacier also plays a pivotal role in understanding the area.

## 1.2 Motivation / Objectives

The study area is being investigated through an integrated approach incorporating subsurface data, bathymetry data, and other available data to understand the region better.

The main goal of this project includes:

1. Is to aid in the better understanding of controlling mechanisms for the occurrence and development of gas seepage.
2. To identify fluid-focused features such as faults and/ or chimneys.
3. Also, to identify shallow gas accumulations on the western bank of the Norwegian Trench
4. Lastly, the influence of structural features and glacial evolutions on the distributions and intensity of this seepage in the study area must be constrained.
5. To, in an attempt, also contribute to the causes of existing knowledge of shallow gases, of which little ongoing research has been made due to the predrilling risk it poses.

## 2. Geological Setting & Margin Development

The North Sea basin shown in Fig.3 is underlain by the Caledonian basement rocks in most part observed in the German and Danish sector of the North Sea, while the eastern section of the North Sea basin is characterized by Precambrian basement. This characterizes the Pre-rift history and onset of the North Sea area with accompanying orogeny and complex crustal deformations (Ziegler, 1992).

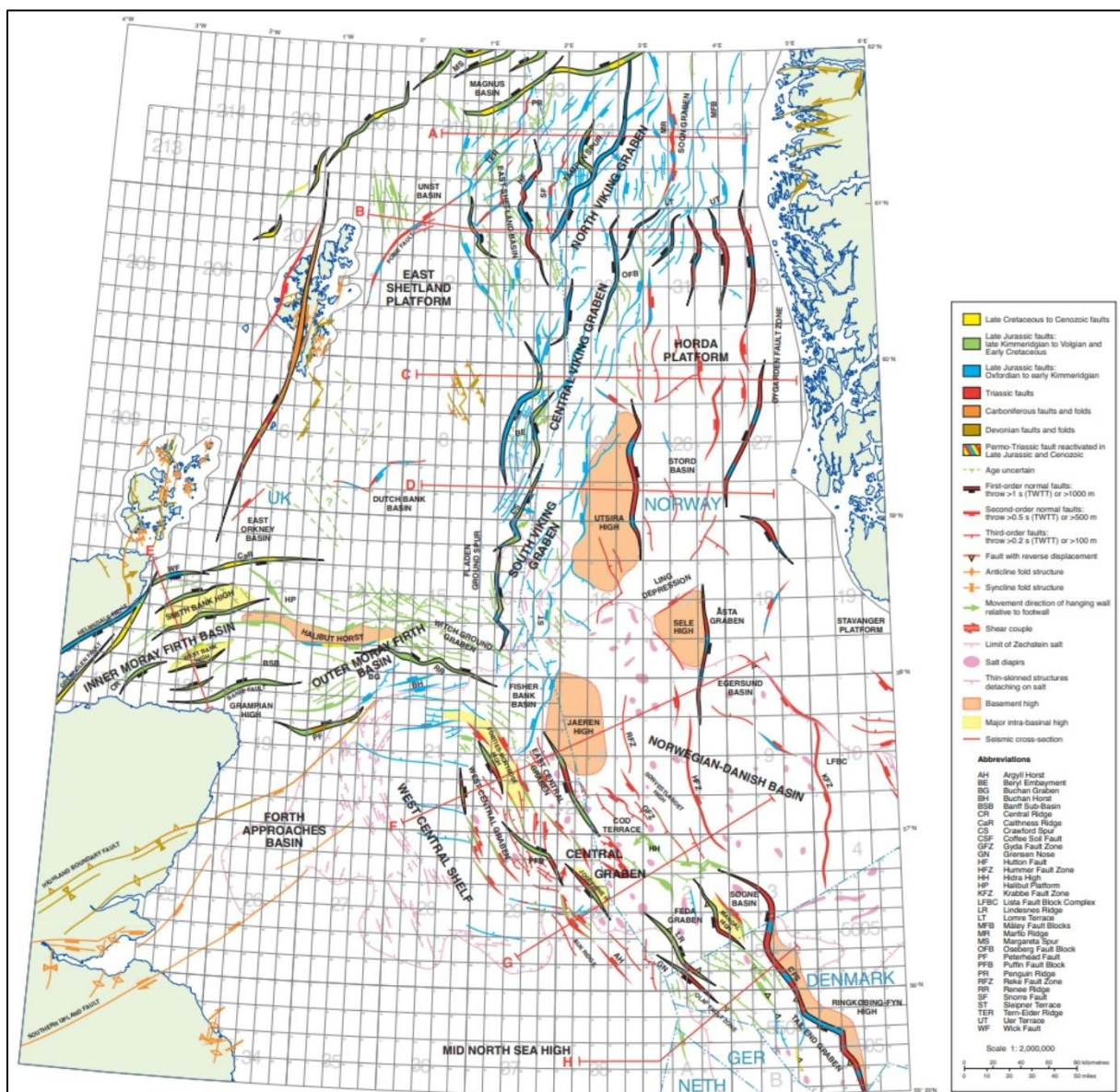


Figure 3: showing the structural map of the Northern Sea and its basins. Where alphabets A to H represents cleavage zones previously identified and mapped out. Modified from fig 4.2 Evans (2003)

**Triassic to early Jurassic** rifting stages characterizes the onset and acceleration of rifting associated with the Northern Sea marking the transition from Permian influence of the Paleozoic to Triassic of the Mesozoic time (Ziegler, 1990, 1992). This moment is characterized by an intense stress regimes which dominated the rifting systems. Mueller et al. (1997) described the stress regime in the North Sea as an average maximum horizontal stress with an orientation of north-west to south-east which is typical of the stress field in north-western Europe (Evans, 2003). Rifting cuts cross the Northern areas which is made up of the Viking and Central Graben (VG), Horda and Egersund Graben and Moray Firth - Witch Ground Graben causing subsidence noticed around the Northern Sea, with variability in maximum thickness of sediment following subsidence (Ziegler, 1992). This rifting also crosscuts the Caledonian basement and Permian Basins, which subside in response and are being cooled with accompanied contraction. No evidence of doming and crustal deformation was noticed in this rifting stage. Triassic rifting is often associated with low levels of volcanic intrusion (Ziegler, 1992).

**Mid Jurassic** signifies the period of thermal doming, crustal deformation, and intense volcanic intrusions. This event ranges from the late Aalenian and Bajocian seen as a broad arch uplifted in the central North Sea. In the Bajocian and Bathonian, a large volcanic intrusion developed at a triple junction of the Viking, Central and Moray Firth. Witch Ground Grabens with minor volcanics are documented in the southern Viking, Central Grabens, and the Iggesund Basin. The development of dome resulted in consistent crustal extension seen on the subsidence pattern of the northern Viking Graben (Ziegler, 1992).

Late Jurassic to early Cretaceous rifting stage is shown in Fig. 4 as an extension-vector triangle, and Fig. 5 shows its tectonic history. The extension triangle has been identified by most authors as the main extension accompanying the rifting stage consisting of the Viking graben, characterized by an acceleration of crustal extension during the Kimmeridgian to Berriasian / Valanginian, which concentrated tectonic activities on the Viking, Central and Moray Firth – Witch ground graben system. The late Jurassic to early Cretaceous system is controlled exclusively by the stress regime systems associated with the development of the Arctic-North Atlantic rift system. Regional seismic reflection data obtained from the northern Viking Graben estimates the faulting of Jurassic- early Cretaceous some of 19 km; however, the Triassic equivalent which accompanies crustal extensions are being unable to be quantified for lack of regional occurrence of base of Triassic reflector (Ziegler, 1992). However, Fossen (1989) has argued that the extension during the upper Jurassic to lower Cretaceous event is also



accompanied by transpressional tectonics identified from available seismic reflection acquired from Gullfak field north Northern Sea. Fossen (1989) argued that there is a transpressional tectonics event accompanying extensional structures, leading to the formation of thrust, reverse faults, compressional folds, dextral strike-slip faults and deformation occurring perpendicular to the primary fault orientation occurring northeast-southwest noticed at Gullfaks field. Several authors agree that the late Jurassic and early Cretaceous were the main rifting that shaped the North Sea basin, which is mainly extensional but not on the transpressional tectonics happening contemporaneously with the extension (Ziegler, 1992).

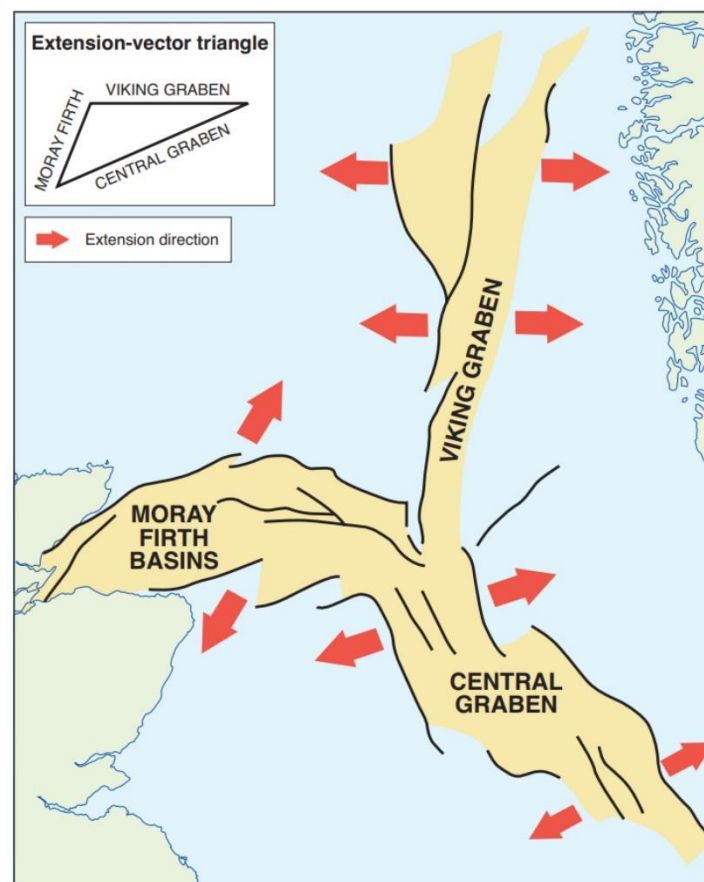


Figure 4: Extension of the North Sea basin during the late Jurassic to early Cretaceous rifting stage. Modified from Evans (2003)

**Late Cretaceous to Paleocene** signifies the late rifting stage, which abated but remained active with accompanied crustal extension into a transition from the Paleocene into the Eocene times (Ziegler, 1990, 1992). Faults accompanying the base of the early Cretaceous rifting system die out upwards within the late Cretaceous, with only a few master faults showing continuity in displacement within the late Cretaceous and Paleocene time. The regional scale shows the termination of faults at the end of the Paleocene. At the same time, the late Cretaceous extension along northern Viking Graben amounts to about 2.5km, and the Central Graben accounts for

1.5km crustal extension (Ziegler & Van, 1989). Analysis of facies and isopach maps indicates that events during the late Cretaceous and Paleocene periods coincided with extensions in the North Sea. Basin suggests thermal subsidence to play a significant role along eustatically rising sea levels, resulting in stepping and overstepping of progressive basin margins. The corresponding event led to the deposition of chalks seen on the southern and central North Sea, which thickens towards erosional edges. Northern sections of the chalks are described to grade into pelagic marls and clays, ranging in thickness within the Viking Graben from 1000m to 2000m. The seafloor topography of the Viking and Central Grabens was gradually filled with chalk sediments. Still, it was never observed in the axial parts of the North Sea that there were shallow water conditions. (Ziegler, 1992).

In the Senonian period, which marks the end of the Cretaceous era, there was a significant increase in activity of large igneous intrusions. This sudden increase continued into the Paleocene era and ended abruptly after a separation of Greenland from Europe resulted in significant changes in the Earth's crust. An uplift in the northern British Isles was observed following the Thulean thermal event, which is indicative of Paleocene Uplift..(Ziegler, 1992). The resulting Paleocene uplift led to the denudation and lowering of the Shetland Platform and Scottish Highlands by erosion to form complex progradation of major deltaic deposits into margins of a Viking graben and central Graben partly controlled by faults of water depth of the order of 500m. The occurrence also resulted in debris on the slope due to the density currents' transportation caused by the failure of the slope. This led to the already present fan deltaic fan complex, which is associated with the Thulean thermal events, as suggested by the decreasing water depths (Ziegler, 1990).

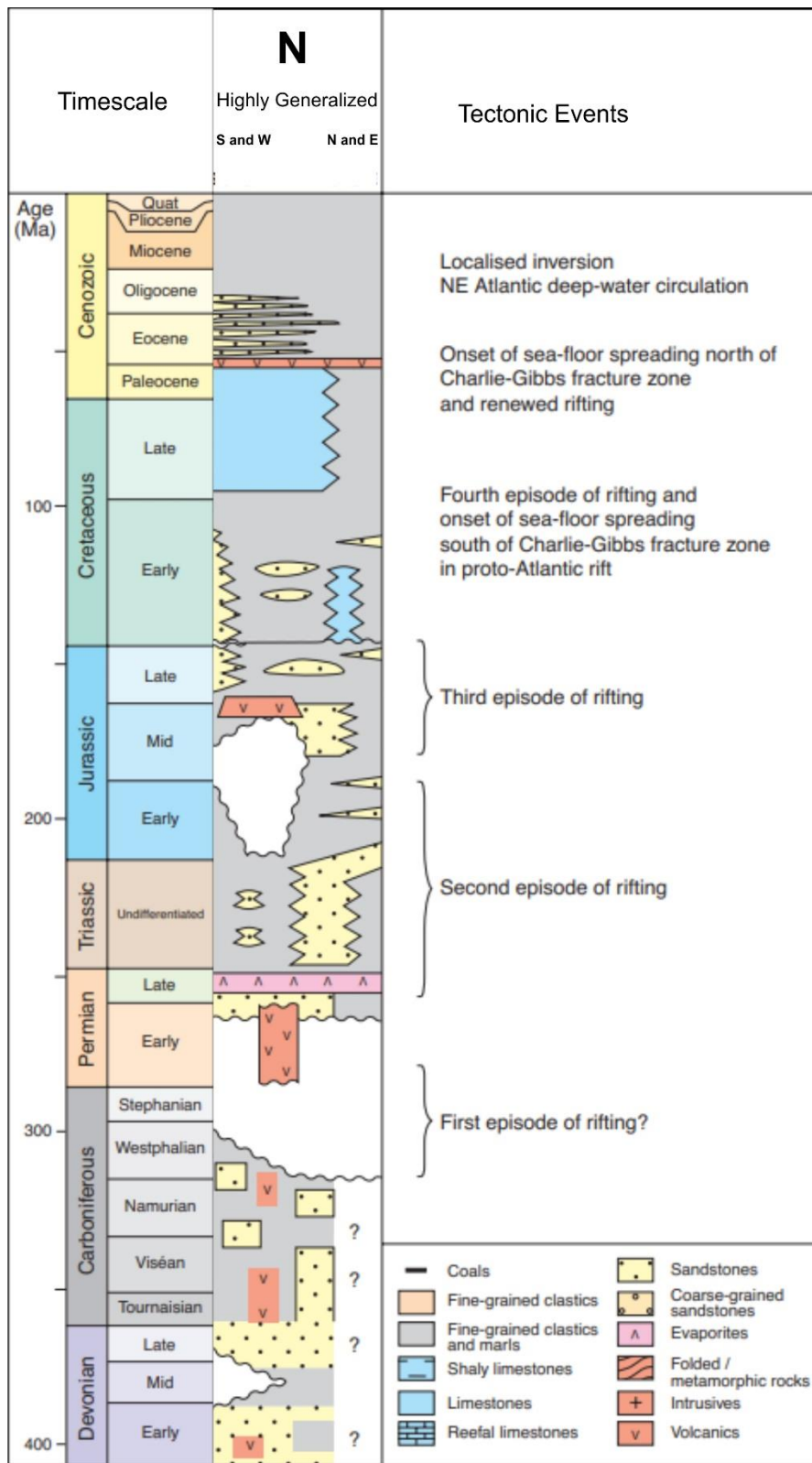


Figure 5: Tectonic History of the North Sea Basin and corresponding lithologies, showing the 3 main rifting episodes (Highly generalized for the North sea). Modified from Evans (2003).

Senonian and Paleocene stress regime which is attributed to compressions exerted and caused inversion of the northern foreland as result of the Alpine orogeny associated with an uplift. The inversion

representing an uplift is accounted for in the southern Central Graben but dying out northwards of the central North Sea. These stresses have been pivotal to the subsidence of the North Sea Basin (Cloetingh & Kooi, 1992). Wherein the northern part of the North Sea was only affected to a small extent by the Paleocene thermal doming, which is evident on the eastern Shetland platform, resulting in a progradation of the delta complex into the Viking Graben (Ziegler, 1990).

Eocene to recent represents the post rifting stage of the North Sea and the last event of tectonics documented of the complex Northern Sea basin. During this period, it has been characterised by quiet tectonic events accompanying a thermal cooling of the lithosphere and low sediment influx. Infilling of sediments into the Northwards sections of seafloor topography is primarily from erosion of the British Isles and the progradation of deltaic systems from Germany and Denmark, from northwest and westwards, respectively (Ziegler, 1992). These events have been prevalent throughout the basin since Pliocene times. The deeper troughs of the Skagerrak straight and the Norwegian trench/ channel are not associated with tectonic activities but are rather glacially induced structures (Ottesen et al., 2018; Sejrup et al., 2003; Ziegler, 1992). The Norwegian trench and Skagerrak straight are features described by Fossen (2016), as glacial tectonics resulting from deformation caused by glaciers and often forms at the toes of advancing ice sheets. Late Pliocene and Quaternary uplift of both the British Isles and Fennoscandian Shield are paralleled to an increasing subsidence of the North Sea Basin which can be related to the buildup of present NNW- SSE of compressional stress regime in Northern Sea basin (Cloetingh & Kooi, 1992; Ziegler, 1992).

## 2.1 Basin Evolution

### 2.1.1 Triassic Basin Evolution

During most of the Triassic period, the offshore region of Norway located south of 62°N degrees north latitude served as an area where continental deposition occurred. Within this region, a rapidly subsiding intracratonic rift system existed, which was bounded to the east and northeast by the Fennoscandian shield, to the west by the East Shetland Platform, and to the south by the Mid-North Sea and Ringkøbing-Fyn Highs. Throughout this time, thick successions of sedimentary sequences accumulated within this area.(Vollset & Dore, 1984).

Movements were observed on the bounding faults throughout the Triassic period, which were accompanied by some tensional faulting within the basin. The early Triassic was marked by documented fast phases of rifting. (early Kimmerian movements) (e.g (Ziegler, 1990) ).

Near the edges of the rift, deposits of coarse-grained sediment were found whereas towards the center of the basin, there was a prevalence of alluvial, flood plain, or lacustrine deposits which were finer-grained.(Clemmensen et al., 1980).

Intervals of high eustatic sea levels allowed for marine influences from the Boreal and Tethyan oceans to penetrate the northern and southern extremities of the rift system associated with the North Sea. The middle Triassic Muschelkalk transgression was particularly crucial in the south, coming into prominence from Tethys and proceeding northwards via the Norwegian-Danish Basin (Vollset & Dore, 1984).

Marine influence of this age has been documented as far north as the Egersund Sub-basin, where limestones and evaporites were reported. A more widespread transgression from both north and south beginning in latest Norian-Rhaetian times (Clemmensen et al., 1980) brought an eventual end to continental sediment deposition and an indication of the marine-dominated environment of the Jurassic (Vollset & Dore, 1984).

### 2.1.2 Jurassic Basin Evolution

The Jurassic basin evolution in the southern Norwegian province is reported to be affected by events of earth motions broadly categorized together as the Kimmerian tectonic episode. Rifting and related faulting of blocks and erosion of the sediments in the basin, occurred throughout the Jurassic times within the general rift framework inherited from the Triassic (e.g. (Ziegler, 1990, 1992; Ziegler & Van, 1989)). Events of more intense activity occurred at the beginning and end of the Middle Jurassic, and during the Late Jurassic (Vollset & Dore, 1984).

A rise in the sea level known as eustatic rise started during the Triassic period. This rise was observed in all marine conditions across the study area during the early Jurassic era. During the Middle Jurassic period, a significant amount of volcanic activity occurred mainly in the Forties and Piper Fields in the United Kingdom sector. Additionally, there was a smaller volcanic event in the Egersund Sub-Basin. Associated erosion removed much of the presumed pre-existing Lower Jurassic marine cover, resulting in these sediments having only a patchy distribution south of the Egersund Sub-Basin and Ling Graben. During the Middle Jurassic period, deltaic systems spread outwards radially from the volcanically up domed area. The sands which form the Brent Group were deposited in the northern area, including the East Shetlands Basin, North Viking Graben, and Horda Platform. Meanwhile, the southern area, including the South Viking Graben, Central Graben, and Norwegian-Danish Basin, saw the deposition of the basal vestland Group. (Vollset & Dore, 1984).

Marine conditions returned to most of the study area due to the collapse of the domed areas in the Callovian of the Jurassic times and rising sea levels. The basin centres saw an accumulation of shales, while local marine sands were formed on the basin flanks and around intra-basinal highs. Block faulting and tilting during the Late Jurassic era caused erosion and non-deposition, particularly in marginal regions. These movements persisted into the early Cretaceous period. The resulting unconformities and non-sequences exhibit varying intensity and timing across different areas. (Vollset & Dore, 1984)

### 2.1.3 Tertiary/ Cenozoic Basin Evolution

Tertiary to Cenozoic basin evolution of the Tampen Spur Basin to the west of the Viken Graben is formed through gravity-driven deformation by glaciers, known as Glaciotectonics. This process results in the formation of the Norwegian Trench and the Skaggerak trenches, which occur perpendicular to the ice sheets. (Ottesen et al., 2018).

Debris flow lateral progradation forms a resulting outcome of this basin, which shapes the Tampen Spurr and creates a sediment contribution in the north Northern Sea (Ottesen et al., 2018; Ziegler, 1992).

### 3. Quaternary Basin Evolution / Glacial History

Basin infill of the North Sea varies across different sectors of the North Sea basin, from Dutch, Denmark, Norway, and the British sector. Quaternary sediments are the thickest along the NNW- SSE central axis which are composed of Quaternary sediment of up to 1030m where the accommodation space is maximum at 56°N. Quaternary sediment thickness of about 1600m being confirmed to be present in the northern North Sea at roughly 61°N (Ottesen et al., 2018). Variability in thickness of sediments differs from the southern, central, and Northern basin of the North Sea. Ottesen et al.(2018) has roughly estimated the Quaternary sediment volume across the North basin at about 140 000 km<sup>3</sup>.

Southern and Central basins of the North Sea are primarily dominated by fluvial and glaciofluvial processes and sediment influx from hinterlands, while the northern North Sea basin corresponding to the Norwegian sector is dominated and consists of glaciogenic processes (Ottesen et al., 2016, 2018, 2020; Sejrup et al., 2003, 2016). In comparison to the central and southern northern sea of shallower waters. The North Northern Sea is filled with contributions from glacier-dominated processes on the North Sea (Ottesen et al., 2016, 2018, 2020) .

The Northern sea basin is described as a representation of glaciation representing the Last Glacial Maximum (LGM) known as the Weichselian in North Western Europe and as Devensian in the British regional stage divisions, which was an initial coalescing of the Fennoscandian Ice Sheet to the east and the British- Irish Ice Sheet (BIIS) to the west (Clark et al., 2012; Hughes et al., 2016; Sejrup et al., 2015). The influx of deltaic and deltaic sediments, ranging from sub glaciers to glacial-induced sediments, which are products of glaciomarine and glaciofluvial sedimentary inputs, characterizes the North Sea basin. Understanding the paleoclimate and sediment rate of accumulation in formerly glaciated regions such as the Northern Sea is aided through studying the stratigraphic evolution of Quaternary, the thickness of successions in quaternary sediments input into the Northern Sea basin is sufficient in preservation of both climate and environmental changes within the last approximately 2.6 million years (Løseth et al., 2022; Phillips et al., 2017) .

Quaternary evolution is the history of glacial and interglacial periods shown in Fig. 6 through the marine isotope stages (MIS), where the even numbers are low in oxygen-18, which implies cold glacial periods, and odd numbers of stages are indications of low oxygen-18, which are interglacial periods. These stages which have shaped the advancement and retreat of ice sheets,

which has shaped the coastlines margin areas and brought about varying sediment input along margins of the North Sea basin (Becker et al., 2018; Phillips et al., 2017). Glaciers have played a significant role in shaping shorelines and accompanying marine transgression caused by the last glaciation maximum known as Weichselian. The last glacial maximum extent is shown in Fig. 7 by Sejrup et al., (2003). These glaciers have been responsible for sediment redistribution and realignments of coastlines after deglaciation, hence its importance during the Cenozoic (Phillips et al., 2017).

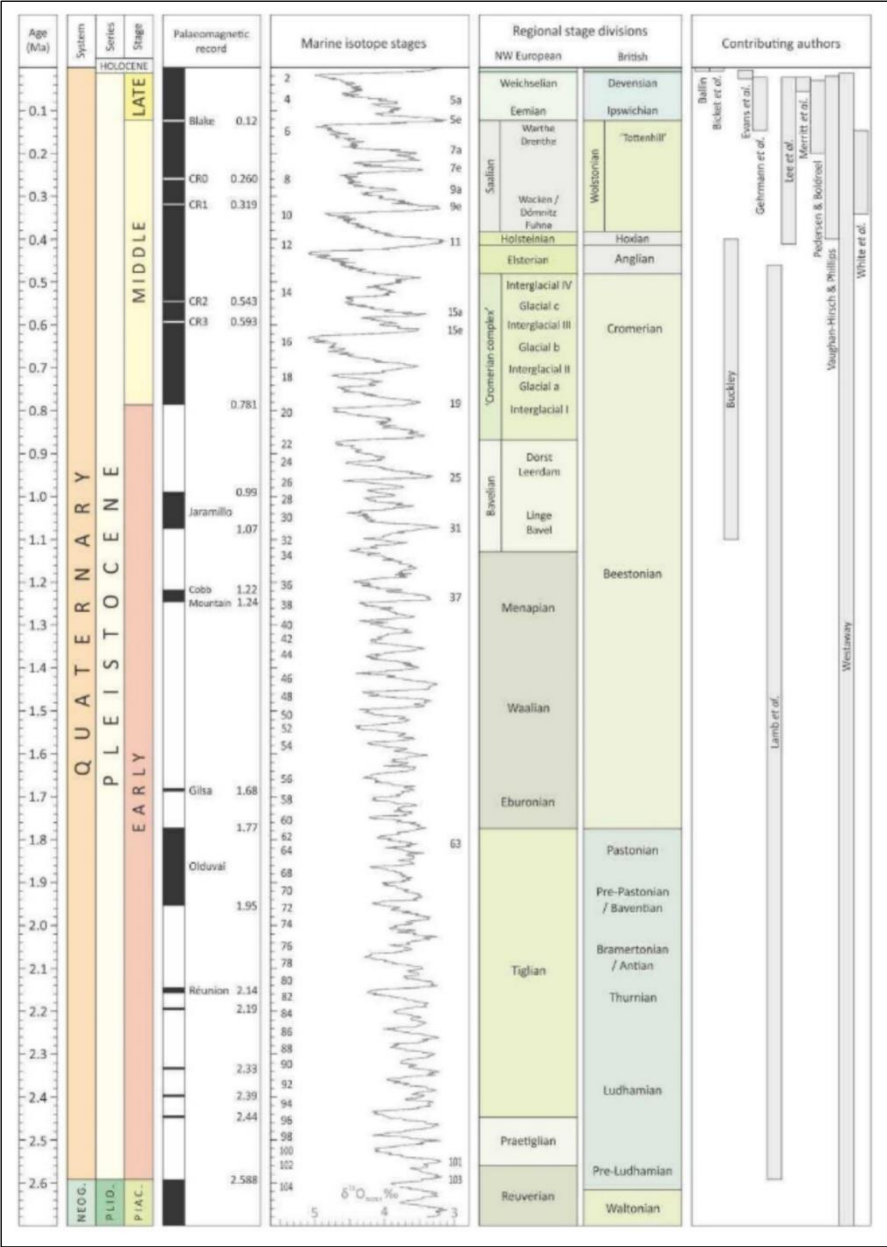


Figure 6: Stratigraphic column of the Quaternary with timescale, palaeomagnetic column, marine isotope stages, and regional stage divisions from diverse authors for the North Sea basin. Image modified from figure 2 of Phillips et al. (2017).



The north Northern Sea which forms a part of the Northern Sea basin adjacent to the East Shetland Platform was a formerly glaciated region covered by the Fennoscandia shield (FS) and previous British Irish- ice sheet (BIIS). Large land masses being covered by continental ice sheets severally throughout the Quaternary (Becker et al., 2018). Fast ice streams greatly influenced and brought in the influx of sediments into the North Sea basin which represents the pathway for large scale transport of glacially derived sediment into the Atlantic ocean which consists of (e.g. (Bradwell et al., 2021; Hjelstuen et al., 2012; King et al., 1996, 1998).

Ice streams drains fans carrying sediment into the northern sea basin like the modern analogue of ice draining the Greenland and Antarctica ice caps. These fast-moving streams of ice are very crucial in understanding the features created by ice-sheets occupying Quaternary in understanding the paleo ice history of the northern European ice masses, in particular the BIIS and FIS (Becker et al., 2018; Løseth et al., 2022; Phillips et al., 2017). Figure 7 shows a map by (Sejrup et al., 2003) showing every possible scenarios of the maximum glaciation occurring around the Nordic region, showing the extent and impact of glaciers covering the Northern basin. The BIIS and FIS are the main continental ice sheets coalescing to form the Eurasian ice sheet (Becker et al., 2018), melting of these ice sheets led to a rapid influx of sediments as deltaic and pro-delta fans into the Northern sea, and forming well-defined lithostratigraphic units that have been identified by several studies occurring during the regional mapping from the 1970s, 1980s, and well into the 1980s (Phillips et al., 2017).

The north Northern section of the Quaternary sediments successions are primarily subdivided majorly into (Stoker et al., 2011) :

- The Zulu Group composed of pro-deltaic shallow marine sediment of marly to middle Pleistocene age.
- The Reaper Glacigenic Group is composed of glaciogenic formation of middle to late Pleistocene age on the central and northern North Sea.

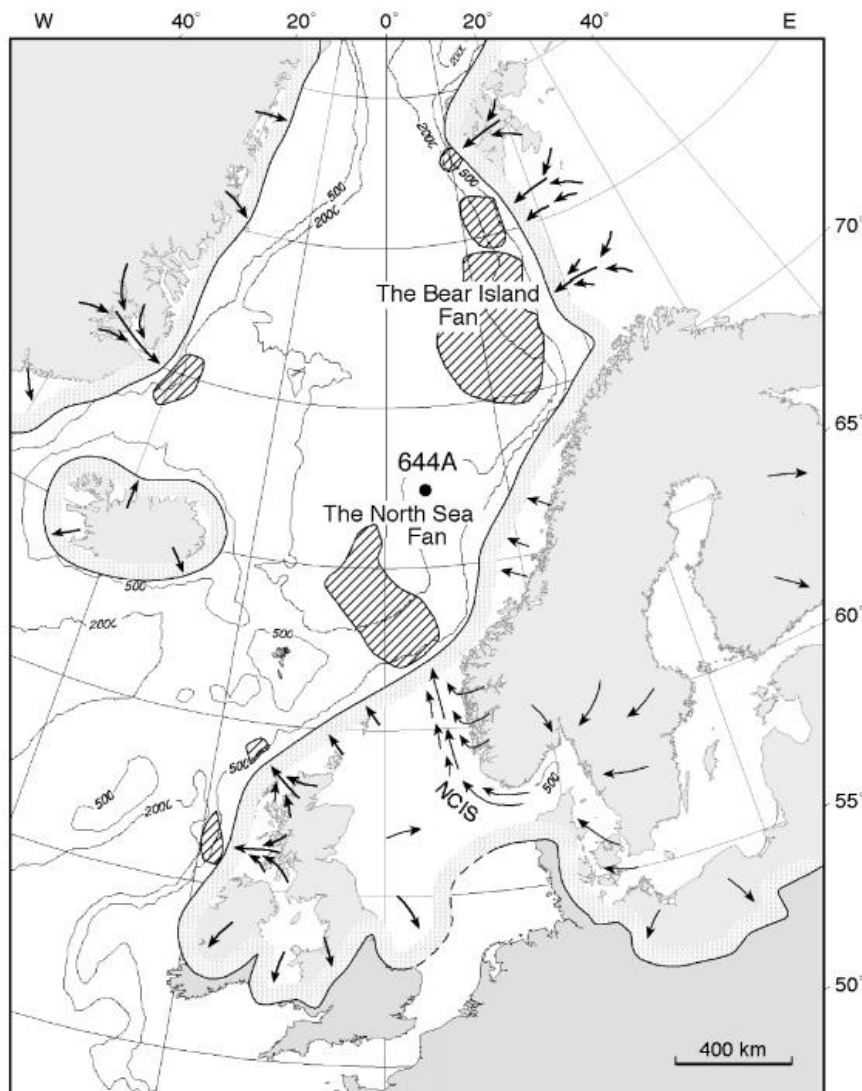


Figure 7: showing a map of possible maximum glaciation scenarios of the Nordic Sea cutting across Northern Sea. Figure from Sejrup et al. (2003)

There are pressing issues in understanding the glaciations of the onshore and offshore equivalent of sedimentary, while the onshore equivalent is understandable. The offshore correlation of the impact of glaciation has proven not to be straightforward (Phillips et al., 2017). Identifying tunnel valleys, which are paleo-ice indicators, has proven to be a pivotal instrument and evidence in understanding the impact of ice and its contribution to the North Sea basin. The Norwegian trench, also known as Norwegian Channel is a large paleo ice tunnel valley has aided the understanding of glaciers' contribution into the North sea basin through the identification of diamictons attesting to the impact of glaciers and also the separation path of the Eurasian sheet into the formerly coalesced Fennoscandian ice sheet and British Irish Ice sheet (Bradwell et al., 2008; Sejrup et al., 1995, 2003, 2016). Norwegian trench shouldn't be

confused with a subduction region but rather an erosional area carved out by fast flowing ice streams (Ottesen et al., 2018; Sejrup et al., 2016) .

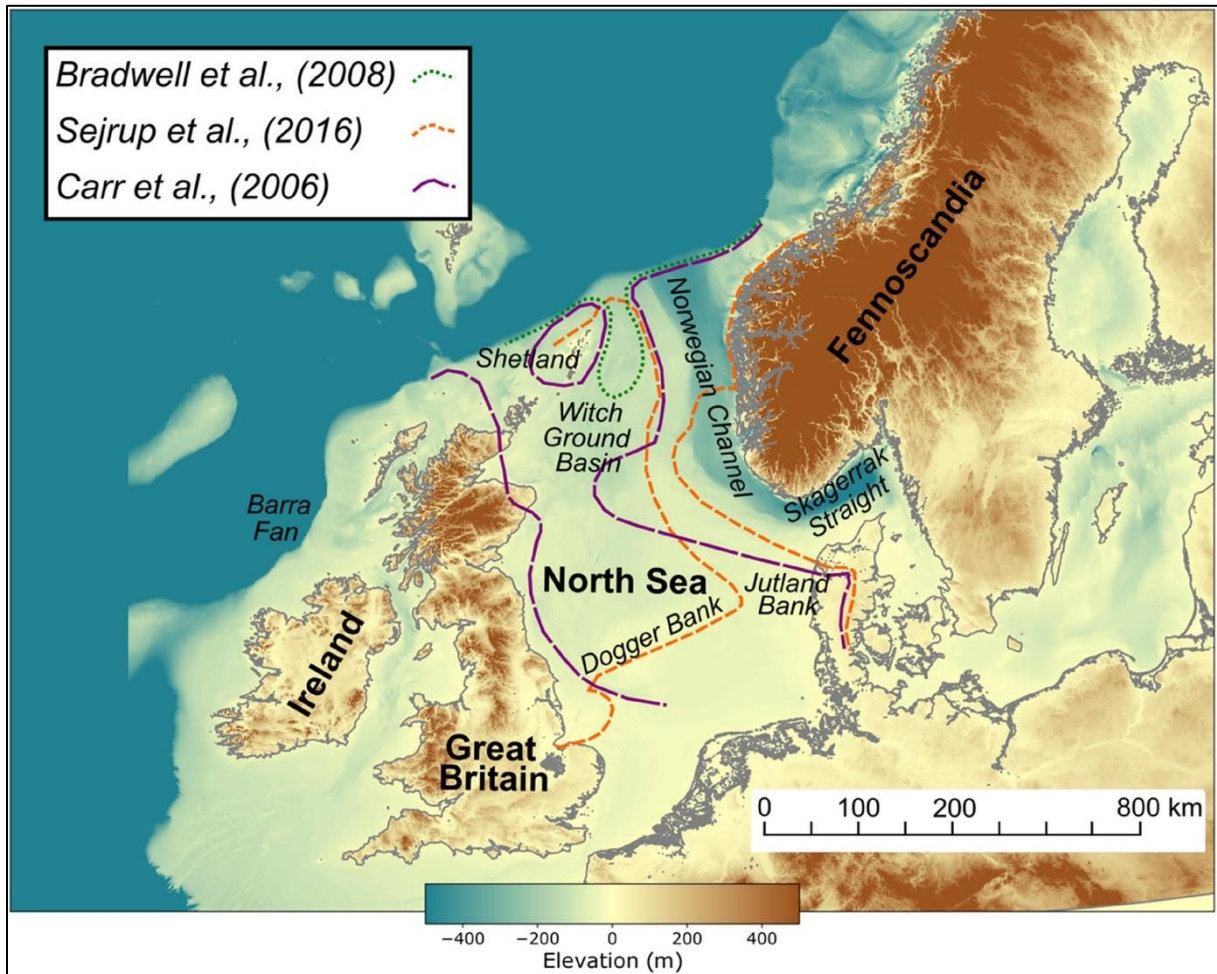


Figure 8: showing the extent, collapse of the Eurasian sheets attested to by several authors. Modified from Gandy et al. (2021)

The subject of ice advances, retreat, timing, processes, and dynamic nature of ice sheets are still subjects of contentions, and advancements are still ongoing in understanding the dynamic nature of ice and its contribution to the North sea basin, as shown by different authors in figure 8 (e.g (Becker et al., 2018; Evans, 2003; Phillips et al., 2017).

## 4. General Stratigraphy & Sedimentary Process of North Sea

In defining the complex stratigraphy of the Northern Sea wherein our study area lies in. (Deegan & Scull, 1977) made and adopted the lithostratigraphy nomenclature of the Northern sea which was revised and modified by a committee led by (Vollset & Dore, 1984), while some modifications were made to Deegan & Scull (1977) lithostratigraphic nomenclature, some formations and stratigraphic classifications remains untouched. According to international standards, lithostratigraphy adheres to the guidelines set by the Subcommittee on Stratigraphic Classification (Hedberg, 1976).

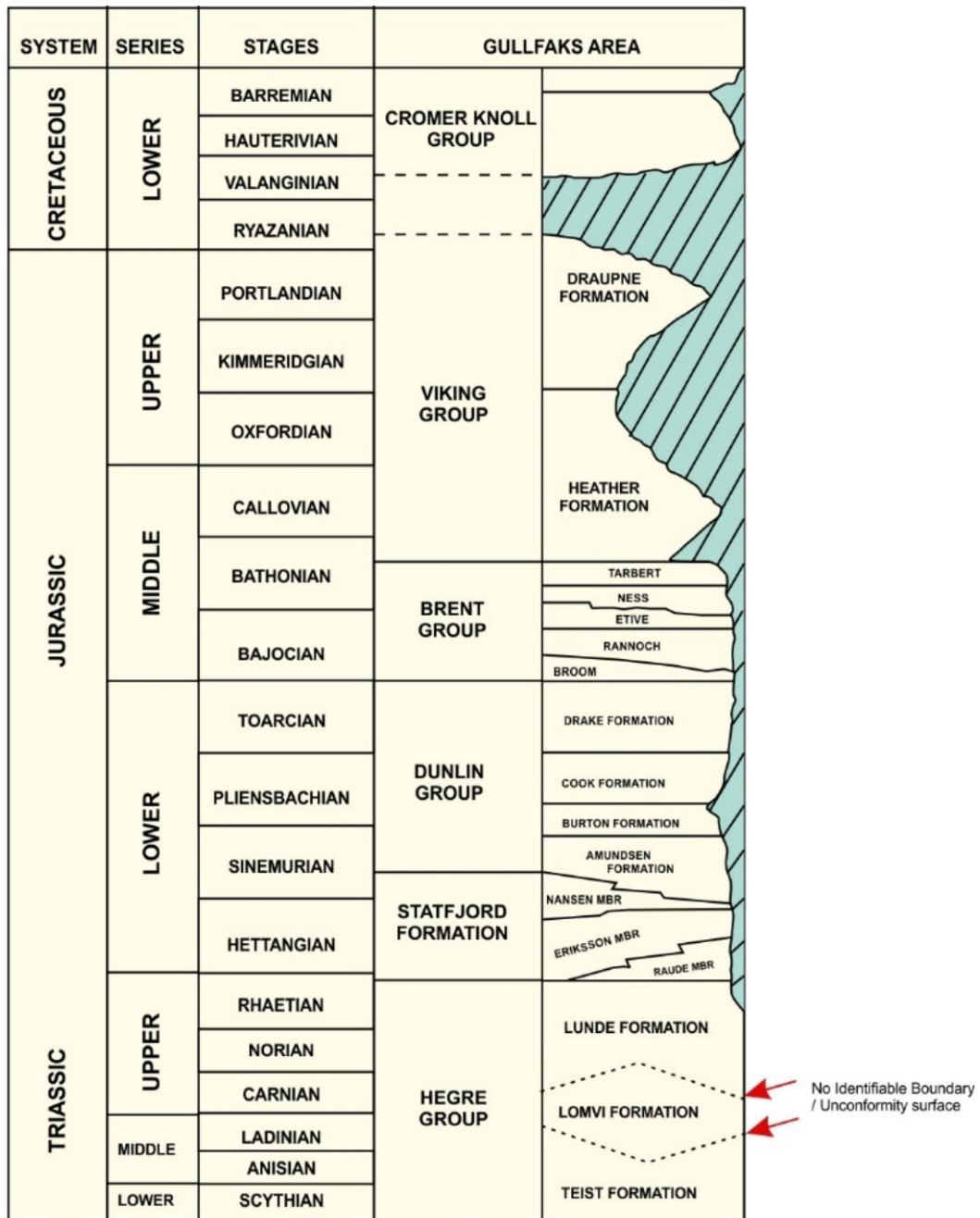


Figure 9: Lithological Nomenclature using the Gullfaks field. The Green area in Inspired by Figure 15 Pettersen et al.(1990).

## 4.1 Mesozoic

### 4.1.1 Hegre Group

Hegre group makes up part of the Triassic successions. No well has penetrated the complete succession. The maximum drilled sequence is 1839m in well 33/12-5 (Vollset & Dore, 1984).

According to recent analysis of deep wells within the Tampen Spur region of the Statfjord Field, the Hegre group and its subdivisions - Teist, Lomvi, and Lunde Formations are based on areas west of the Viking Graben ( Vollset & Dore, 1984).

The Hegre group consists of intervals of interbedded sandstones, claystone, and shales associated with sequences of dominant sand or shale/claystone. The shales are reddish, while the sandstones are described to show ranges from white, light grey, and orange to brick red. Grain sizes vary from very fine to very coarse, and the sediments are in parts of a pebbly nature. It also has a supporting presence of white limestones, anhydrite and brownish-red mud (Vollset & Dore, 1984).

Regarding boundary, the Hegre group base has been reached in places of structural highs on the Northern Sea. Hence, the Hegre Group remains a name for interim use till a base of formation is established in deeper basins across the Northern Sea (Vollset & Dore, 1984).

The Hegre Group is classified as apparent in the northern North Sea. However, (Deegan & Scull, 1977) relation of the lithostratigraphic units down south of the Northern sea remains unclear (Vollset & Dore, 1984).

#### *4.1.1.1 Teist Formation*

Teist formation is a subdivision of the Hegre Group as shown in Figure 8. It is made up of interbedded sandstone, claystone, and marble. The sandstones are described as being dominantly fine to fine-grained, dark red brown and calcareous in composition. Along with its description, it is white and pink, medium to coarse sandstone present in upper levels of the succession. Red marl makes up the main argillaceous (shale) lithology with green to dark grey claystone's as subordinate constituents ( Vollset & Dore, 1984).

The geological formation is composed of fine-grained sandstone in the north of the Northern Sea, specifically near a reference well marked as 33/5-1. Lithology is the most dominant feature that characterizes most of the formation, except the lowermost 24 meters, made up of red marl. This lowermost layer is distinguishable from the rest of the formation due to its unique colour

and composition, which sets it apart from the surrounding fine-grained sandstone ( Vollset & Dore, 1984).

#### *4.1.1.2 Lomvi Formation*

It consists of fine to coarse-grained kaolinitic sandstone with supporting presence of thin red marl and claystone ( Vollset & Dore, 1984).

#### *4.1.1.3 Lunde Formation*

This formation consists of an interbedded sequence of very fine to very coarse-grained sandstones (2 to 10m thick), claystone's, marls and shales ( Vollset & Dore, 1984).

Lithologically, the sandstones are white, pink or grey in colour and cemented to a variable degree with kaolinite, anhydrite and carbonates. Fine grained sandstones identified on upper portion of the formation (core data from UK well 211/134-1) shows sedimentary structures such as small-scale ripple cross stratifications, bioturbation and incorporated mud clasts and mud balls. It may also have small fining upward sequence ( Vollset & Dore, 1984).

#### *4.1.2 Statfjord Formation*

With respect to the Gullfak fields on the north Northern Sea. The Statfjord is further divided into; the Raude, Eiriksson, and Nansen Members. It is described to have formed in an alluvial environment. It forms as a result of periodic draining of semi-arid settings to a more humid, alluvial plain composed of poorly drained, swampy overbank areas and channel generated flow based on a confidential report by Collinson, 1985 for statoil (Pettersen et al., 1990).

##### *4.1.2.1 Raude Member*

This is broken into three reservoirs (Raude 1, 2, and 3) for characterization on the Gullfak field. The bottom end unit is a coarsening upward sequence of shale/silt unit with reservoir qualities that are considered pore and a net to gross ratio of 0.1. Where Raude 2 and 3 are formed from periodic flooding events in a dry climate. They are generally of moderate reservoir qualities owing to kaolinitic content which tends to seal pores and lower its permeability(Pettersen et al., 1990).

##### *4.1.2.2 Eiriksson Member*

Eiriksson is subdivided into Erikson 1, 2, and 3 for characterization for the Gullfaks field located north North Sea. It is deposited in a fluvial environment characterized by meandering channels and swampy overbanks. It is described lithological to be as a reservoir to exhibits excellent reservoir properties with a porosity value as high up as 28% and a net/gross ratio of

0.60. And makes a up a good reservoir as a result of its stacked fluvial channels (Pettersen et al., 1990).

#### *4.1.2.3 Nansen Member*

This formation is heterogenous in its upper part. But, characterized as coarse-grained channel sandstones which exhibits a great to moderate reservoir qualities with a porosity up to 28% and a net/gross ratio of 0.60. Nansen is described to be laterally extensive but can be broken by presence of shale periodically.

#### *4.1.3 Dunlin Group*

This is separated based on the lithological nomenclature of the north Northern Sea into the Amundsen, Burton, Cook, and Drake formation. It is deposited by marine transgression which terminates the Statfjord formation, southeastwards. It is composed of 170 to 180m thick claystones of the Amundsen and Burtin formation which were deposited (Pettersen et al., 1990; Vollset & Dore, 1984).

##### *4.1.3.1 Cook Formation*

Cook formation is an intra-dunlin formation. It is described to have form due to regression because of regression, accompanying tectonics, and leading to deposition of silt and sand to be deposited on the East Shetland basin, depositing the cook basin. In Gullfaks field it is further subdivided into cook 1, cook 2, and cook 3 having different characteristics ranging from open marine silty claystone having no reservoir characteristics in cook 1 to cook 2 forming on inner marine shelf with cook 3 consisting of an intercalation of sand and shale with clear to cleaner sands upwards forming an excellent reservoir. A transgressional event which occurs generally continued after cook formation was deposited to form the Drake formation which varies in thickness and composed of marine shale with varying silt composition (Deegan & Scull, 1977; Pettersen et al., 1990; Vollset & Dore, 1984).

#### *4.1.4 Brent Group*

Brent group are further subdivided into the Broom, Rannoch, Etive, Ness, and Tarbet formation, all having different compositions of lithology. All formations that makes up the brent group has been classified collectively as a river delta systems (Deegan & Scull, 1977; Pettersen et al., 1990; Vollset & Dore, 1984).

##### *4.1.4.1 Broom Formation*

Broom formation resulted from the river deltaic formation of a wave to fluvial/dominated delta type that forms part of the Bajocian Delta lobe deposit along with the Rannoch, Etive, Broom,



and Ness Formation. It is made up of thin layers of coarse sandstone, gravelly beds which forms as a prodelta delta deposits in an open marine environment (Deegan & Scull, 1977; Pettersen et al., 1990; Vollset & Dore, 1984).

#### *4.1.4.2 Rannoch Formation*

This formation forms part of the delta sequence of formation and exhibits a general coarsening upward sequence. It is composed of mainly shoreface micaceous sandstones. And are further subdivided into Rannoch-1, Rannoch-2 and Rannoch-3 exhibiting difference characteristics. Due to its near shoreface development, the common sedimentary structure that forms is the hummocky cross-stratification which forms due to an high wave disturbance (Deegan & Scull, 1977; Pettersen et al., 1990; Vollset & Dore, 1984).

#### *4.1.4.3 Etive Formation*

Etive formation are classified as barrier bar complexes and forms the main depositional environment that characterizes this formation. Due to the presence and heavy observations of laminations, large scale cross – stratification and grain sizes from cores obtained an high energy environment typical of beaches are inferred (Deegan & Scull, 1977; Pettersen et al., 1990; Vollset & Dore, 1984).

They have been described to have excellent reservoir qualities, because of lateral prevalence of sandstones with minor mica and clayey mineral content. It has an estimated porosity as high as (30 to 36%) and permeability as a high as 1.0 to 4.0 darcys reflecting great reservoir qualities (Pettersen et al., 1990).

#### *4.1.4.4 Ness Formation*

An occurrence of coal at the top of Etive formation, serves as the base of the Ness formation. 11 subdivisions have been made on the Gullfak field to characterize the Ness formation and it has been described to have formed in a delta plain environment (Pettersen et al., 1990). However, a characterization of the Ness formation into several sub units has led to identification of a formation composed of siltstones/ claystones, channelized sands typical of fluvial environment, and interdistributary fill deposits of a bay setting (Pettersen et al., 1990).

#### *4.1.4.5 Tarbert Formation*

This formation is separated from the Ness formation by an unconformity caused by the Kimmerian erosion. In the studies of its reservoir, it has been subdivided into sub units for the purpose of characterization using a core and well log (Pettersen et al., 1990).

Sedimentary structures, characterizing tidal flats and shoreface deposits are found in cores obtained from Tarbert Formation. Tarbert formation lithology ranges from shales, siltstones, and coalbeds to medium to coarse-grained sands with mineral cementation of calcite sealing off pores. It is underlain by the shales of Heather formation of the Viking group after a Kimmerian unconformity (Pettersen et al., 1990).

#### 4.1.5 Viking Group

Upper boundary of Viking group is well known on the northern Northern Sea, it ranges from Bathonian to Ryazanian in age of the Jurassic age. This is composed of the Draupne formation which makes up a main source rock of the north Northern Field and the Heather Formation at Gullfaks and known to an extent on the Norwegian sector of the north sea (Pettersen et al., 1990; Vollset & Dore, 1984).

Lithology wise, it composed of dark, grey to black marine mudstones, shales and claystones with occasional replacement of sandstones. (Vollset & Dore, 1984)

##### 4.1.5.1 Draupne Formation

This is of Oxfordian to Ryanian age. According to Pettersen et al. (1990) Draupne is a key source rock on the Gullfaks field. It is composed of dark grey to brown, non-calcareous, and carbonaceous claystones which forms in a marine environment with restricted bottom circulation and anaerobic conditions favourable for organic matter generation of hydrocarbon (Deegan & Scull, 1977; Pettersen et al., 1990; Vollset & Dore, 1984).

##### 4.1.5.2 Heather Formation

It ranges in age from Bathonian to Kimmeridgian in age. It consist often of silty claystones deposited into an open marine environment as a result of marine transgression which also brought about the formation of the youngest Brent group (Deegan & Scull, 1977; Vollset & Dore, 1984).

#### 4.1.6 Cromer Knoll Group & Shetland Group

This makes up the Cretaceous formation of the Tampen spur characterized by erosion (Horstad et al., 1995). This Cretaceous sediments is mainly described lithologically to be dominated by mudstones and siltstones, making them a good seal. They often are composed with sandstones with good reservoir properties but that are often not evaluated according to the Norwegian offshore directorate.

## 4.2 Cenozoic

### 4.2.1 Rogaland Group

This makes up the Paleocene formation of the north Northern Sea. They are composed of fine-grained sediments and described to have been sourced from sands located to the north and west of the Norwegian continental shelf. The main sand reservoir of this formation is the Danian Egga sandstone, as reported by the Norwegian offshore directorate.

### 4.2.2 Hordaland Group

According to Deegan & Scull, (1977), this is described as an Eocene to Early Miocene marine claystones with minor sand stone equivalent known to have formed contemporaneously with the Brygge formation in Norwegian sea. However, no further subdivision has been done in detail to describe this group of the north Northern Sea. In the Viking graben of the North Sea. This group reaches only just a few hundred of meters on the north Northern Sea with its maximum thickness developing in the central and southern parts of the North Sea. Environment of deposition has been described to be in an open marine environment and setting by the University of Oslo research team (NORLEX). The Frigg's formation is composed of sandstone with lenses and traces of claystone as described by the Norwegian Interactive Offshore Stratigraphic Lexicon (NORLEX). This is missing from Fig.10, as this classification is updated years later.

### 4.2.3 Nord-land Group

Nordland group is dominated by marine claystone. Lithologically are described in colour to be of greenish-grey and brownish gray , soft, and locally composed of silts and mica minerals (Deegan & Scull, 1977). The Viking graben section, the Nordland group formation comprises of sandstones being assigned to the Utsira Members. Where the upper part is grouped and composed of unconsolidated clays and sand, and an occasional amount of glacier induced sediments known as ice-rafted detritus input. The content of glacial deposits increased in the uppermost part of the group from Miocene through Pliocene, as shown by the general stratigraphy in Fig.10.

The base of the group coincides with the Oligocene and Miocene uniformity. Drilled core of this section also suggests gravity flow of sandstone, siltstone with basaltic ash and lapilli (Mørk & Duncan, 1993). The Nordland group is described as thick as 1000m in the Viking Graben area(Isaksen & Tonstad, 1989). The Nordland Group has been described to be deposited in an open marine environment, with an influx of glacio-marine deposits in the upper part as depicted

in Fig. 9 (Deegan & Scull, 1977; Eidvin, et al., 2000; Hald & Vorren, 1984; Isaksen & Tonstad, 1989; Mørk & Duncan, 1993).

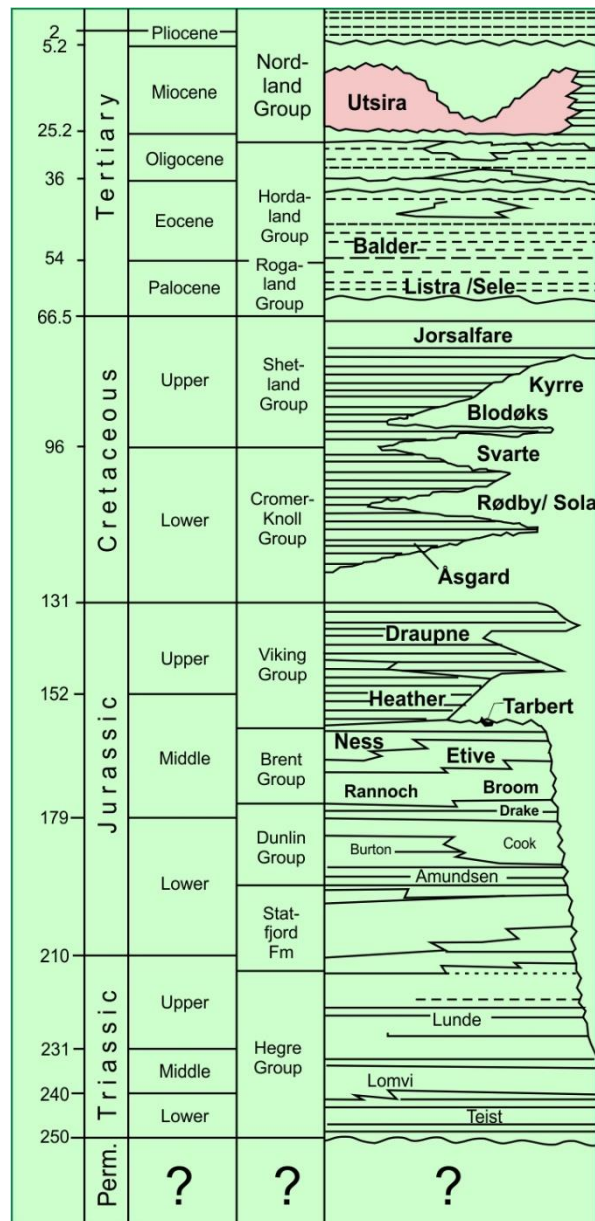


Figure 10. General stratigraphy cutting across Tampen Spurr. Inspired by Fig. 3. Horstad et al. (1995)

### 4.3 Sedimentary Processes and environment of north Northern Sea.

Most notable Cenozoic sediment processes and environment of deposition into the Northern basin continued during the Miocene and Pliocene, resulting in a series of progradation wedges (Eidvin & Rundberg, 2007; Fyfe et al., 2003; Rasmussen et al., 2010; Thöle et al., 2014). An uplift of East Shetland Platform during the late Cenozoic resulted into the creation of lateral and ubiquitous sand accumulations found in the northern North Sea, which forms part of the Utsira Formation of the Miocene and Pliocene age, which have been interpreted to have formed from high energy marine current typical to nearshore environments (De Schepper & Mangerud, 2018; Eidvin & Rundberg, 2007; Galloway, 2002; Gregersen & Johannessen, 2007). This event is followed by the deposition of sediments derived from debris flows also occurring within the Utsira Formation, which marks an unconformity and a hiatus transitioning into the Quaternary sediments of the north Northern Sea (Ottesen et al., 2016).

## 5. Structures in the north Northern Sea

An understanding of the North Sea, a reference to a major rift system during the Mesozoic of a late Jurassic and early Cretaceous, has been identified as the primary and most recognizable events in seismic reflection that has shaped the North sea basin and its evolution (Fossen, 2016; Ziegler, 1992). These rifting systems have been described as primarily generating faults that trend north-south. Fossen (1989), argued that beyond the north sea rifting system, transpressional tectonics led to features and faults occurring perpendicular to the main fault orientation in the east-west direction of Gullfaks field, leading to dextral strike-slip faults, compressional folds, reverse and thrust faults accompanying such compressional and seen on a seismic reflection data (Fossen, 1989, 2016; Fossen & Hesthammer, 1998; Pettersen et al., 1990).

Fossen (2016) indicated that tectonics study involves a regional study of deformation involving dynamics, kinematic and geometric analysis at a wide range of basin extent of the North Sea. And oftentimes, deformation accompanies a reorganisation of grains, which occurred in the North Sea during the rifting stages carving out the basin (Ziegler, 1992).

North Sea rifting is an associated passive rifting model that differs from an active one. A passive rifting implies that the rift systems identified on the North Sea are associated with far-fetched inherited stresses at weak zones and often associated with shear zones (Fossen, 2016).

### 5.1 Major Fault Classification and Types

According to the Seismological Facility of Geosciences. Faults are grouped basically into the three fault types with corresponding causal stress accompanying their formation. As shown and described in Fig.11. Other types of faults, such as listric and growth faults, are often caused by internal deformation and further displacement hinged on these three main fault systems shown in Fig. 11. Often, there is a combination of faults and orientation in most cases. Such is the case of the North Sea basin during the late Jurassic to early Cretaceous main rifting stage (Fossen, 2016; Ziegler, 1992; Ziegler & Van, 1989).

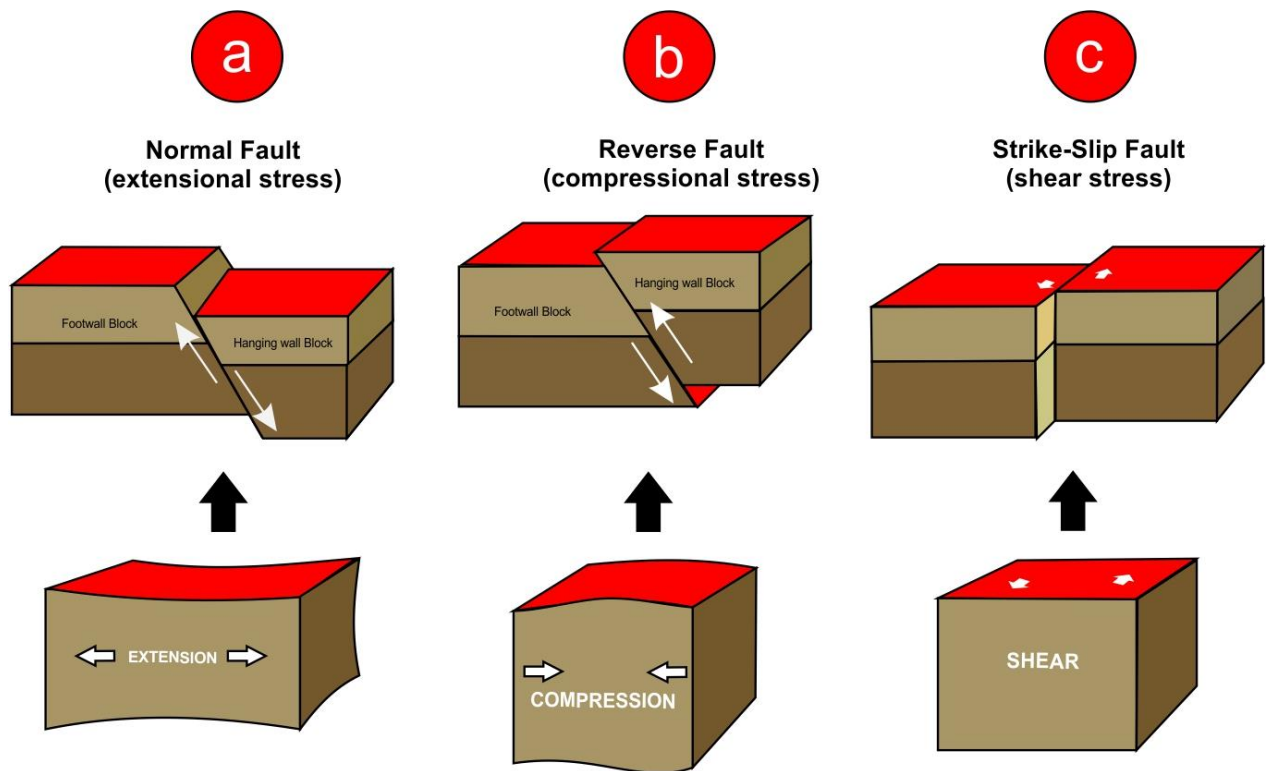


Figure 11: The basic type of faults with corresponding stress regimes. A). Normal fault caused by extensional stress B). Reverse Faults caused by compressional stress C). Strike- Slip fault accompanied by shear stress.

Faulting and fracture formations are interrelated and formed by process that considers the growth and connection of smaller structures such as minor fractures. Once a fracture develops, it represents zones or planes of weakness (Fossen, 2016).

### 5.1.1 Polygonal Faults Systems

Fluid flow systems are often associated with a fault reported commonly. The actual causes of this fault are still poorly understood, and little information is available about this fault system. Three processes are said to be responsible for the generation of this system: the columnar Syneresis of clay minerals, Basin inversion, and Gravitational collapse (Berndt, 2005; Cartwright & Lonergan, 1996). There is still much about how they interact is unknown, which is still subject to further work and research (Cartwright & Lonergan, 1996; Huuse & Mickelson, 2004).

General characterisation of the structures of the Northern Sea based on available field from Gullfaks Field has been attempted by Fossen & Hesthammer (1998). Fossen & Hesthammer (1998), has described the faults on the North Northern Sea to be a major domino system, which are synrifted faults limited by a horst structure on the Northern Sea following the extension phase of the north basin. Fig.12 shows the phases, inclination and how this fault type forms as reported by Fossen (2016) on Gullfak field located north Northern Sea.

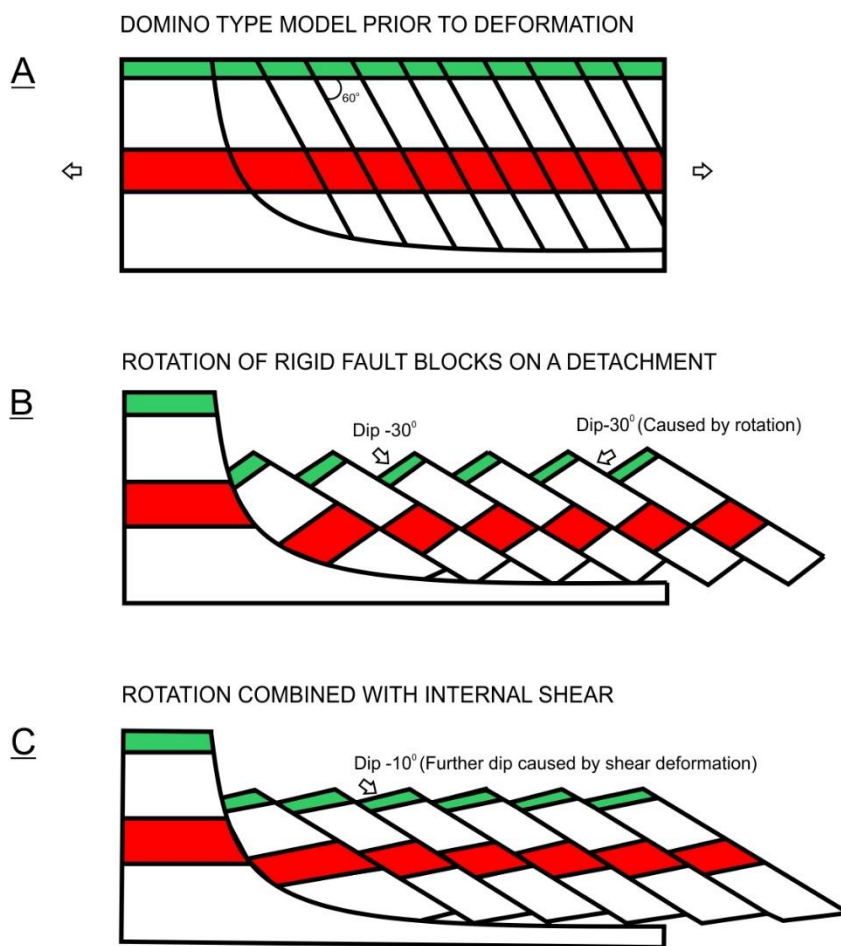


Figure 12: Domino/ Structural Type Model accompanying extension of north Northern Sea. A). shows the lithology prior to deformation B). Dipping of fault following rotation at an angle  $30^\circ$  C). Further dips of  $10^\circ$  due to shearing and realignment of grains. Inspired by Fossen (2016), Pettersen et al. (1990) & Ziegler (1992)

Cartwright & Lonergan (1996) has worked extensively to understand the genesis of polygonal faulting. The role of this fault system has been pivotal in understanding fluid flow, as it transmits fluid from a shallow depth and often is strata bound. However, their origin still poses a debate (Cartwright & Lonergan, 1996).



## 6. Petroleum Systems Framework

Petroleum systems are investigative tools used on a separate level to understand the origin and location of hydrocarbons. A framework which encompasses an active pod of source rock formed from organic matter named kerogen to all essential elements that leads itself to the accumulation of oil and gas (Magoon & Dow, 1994).

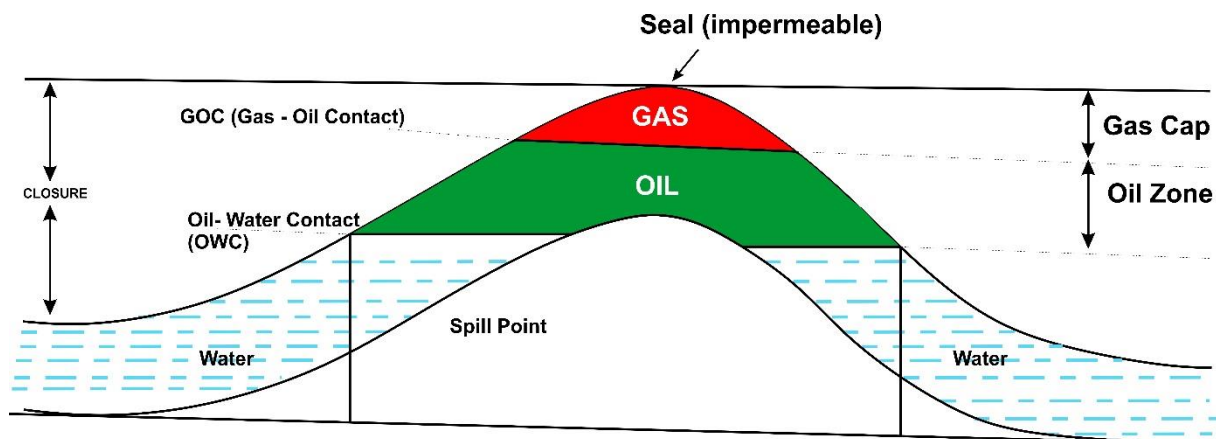


Figure 13: A simple cross section of a Petroleum system. Inspired by figure 7.1 (Selley & Sonnenberg, 2015).

The system includes a source rock, reservoir rock, seals and traps in form of faults, folds etc. and also processes such as migration, which leads to the entrapment of hydrocarbon as shown in Fig. 13 of a simple petroleum system (Magoon & Dow, 1994).

### 6.1 Porosity

Porosity is one of the essential attributes of a reservoir rock. They are void spaces or pores in a reservoir rock that can be filled with a fluid either in form of gas or oil. They are initially filled with connate water or brine and expressed below as in percentage as (Selley & Sonnenberg, 2015). As a percentage, it is expressed as equation 1;

#### EQUATION 1

$$\text{porosity (\%)} = \frac{\text{Volume of voids}}{\text{total volume of rocks}} \times 100$$

Or

$$\text{Porosity} = \Phi = \frac{V_p}{V_b}$$

Where  $V_p$  is volume of pores and  $V_b$  is bulk volume of a rock. It is often signified with the Greek alphabet phi ( $\Phi$ ). The porosity can either be effective or ineffective. Effective porosity

refers to pores that are connected to each other, while ineffective porosity occurs when there is no connection or a closed pore. This can be measured either from well logs or cores obtained during drilling (Selley & Sonnenberg, 2015). They are often measured from cores or logs obtained from drilling activities.

### 6.2 Permeability

Permeability is an important parameter used to estimate a reservoir rock. Outside its porosity. Porosity alone doesn't make a suitable reservoir rock, but its connectivity and the ability of fluids to pass or transmit through them which is the permeability (Selley & Sonnenberg, 2015).

This was demonstrated and illustrated in 1856 by French engineer H. Darcy. Where he tried to measure the flow rates of a spring in Dillion in France. A simple sketch to illustrate the experiment is shown in Fig.14.

Darcy's law is an equation shown in equation 2 describing how fluids flow through a permeable medium:

**EQUATION 2**

$$Q = \frac{K (P_1 - P_2)A}{\mu L}$$

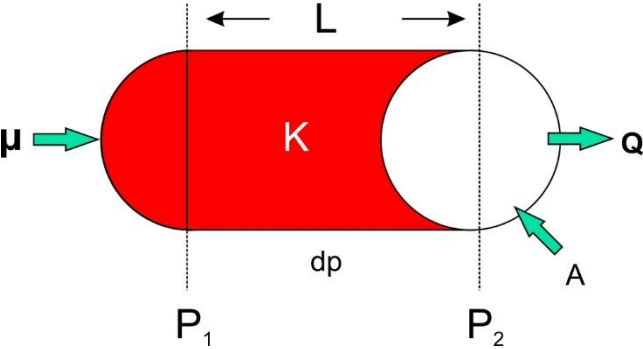


Figure 14: A simplistic illustration of Darcy's Experiment.

The unit itself is referred to as Darcy (Selley & Sonnenberg, 2015).

### 6.3 Capillary Pressure

The concept of capillarity pressure is used to understand the wettability of pores. This term describes the phenomenon where a liquid can enter a pore or void by exerting pressure. The variation in pressure between a fluid column and the surrounding pressure is the capillary pressure. (Selley & Sonnenberg, 2015). It can be defined as the difference in surface tension between two fluids, i.e. water and oil.

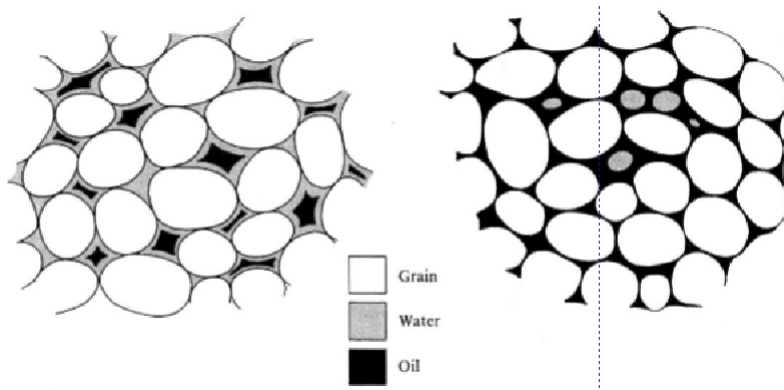


Figure 15: Showing fluid replacement due to capillary pressure and wettability of different fluids. Figure 6.14 of (Selley & Sonnenberg, 2015)

In geological terms and reservoir application, the capillarity entry pressure of a

fluid increases with decreasing pore throat and fluid diameter. Fig.15 shows how fluid shows how oil replaces fluids gradually and Fig.15 shows how the hydrocarbon squeezes into the pore space, and it is expressed with equation 3 as;

**EQUATION 3**

$$P_{\text{Capillary Entry Pressure}} = \frac{2\gamma \cos(\beta)}{r} = P_{\text{wetting}} - P_{\text{nonwetting}}$$

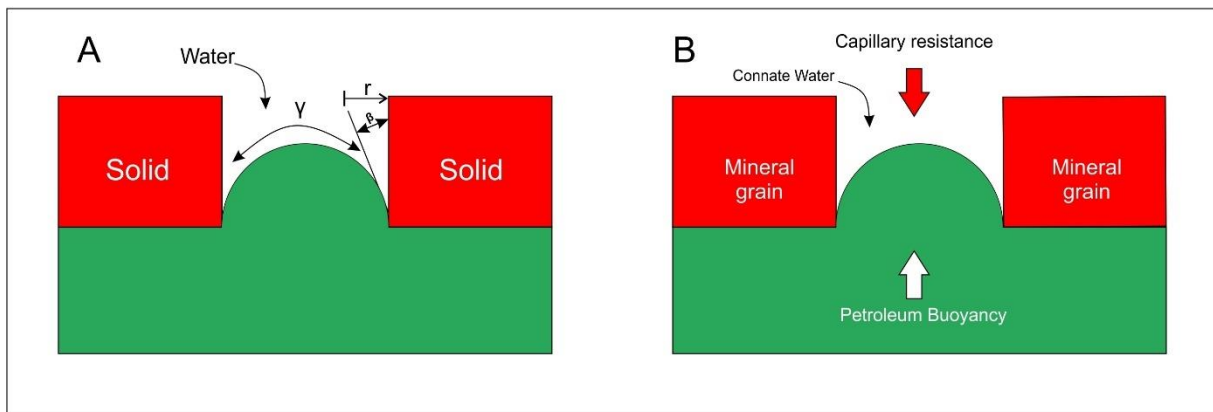


Figure 16: showing the entry of petroleum into a water filled reservoir.

For a petroleum breakthrough and entry into a water-filled reservoir as shown in Fig. 16, thus equation 3 is defined as:

$$P_{\text{cap}} < \rho_{\text{Water-oil}} \times g \times h_{\text{column}}$$

Where  $P_{\text{cap}}$  is often less than the density difference of oil ( $\rho_{\text{Water-oil}}$ ), acceleration due to gravity ( $g$ ) and height of column ( $h_{\text{column}}$ ) in which fluid occurs.

## 6.4 Source Rocks

This is the primary source and generation of hydrocarbon. It is often rich in organic matter called a kerogen. The type of kerogen suggests if a source rock generates either gas or oil according to the Van Krevelen diagram shown in Fig. 17 (Selley & Sonnenberg, 2015).

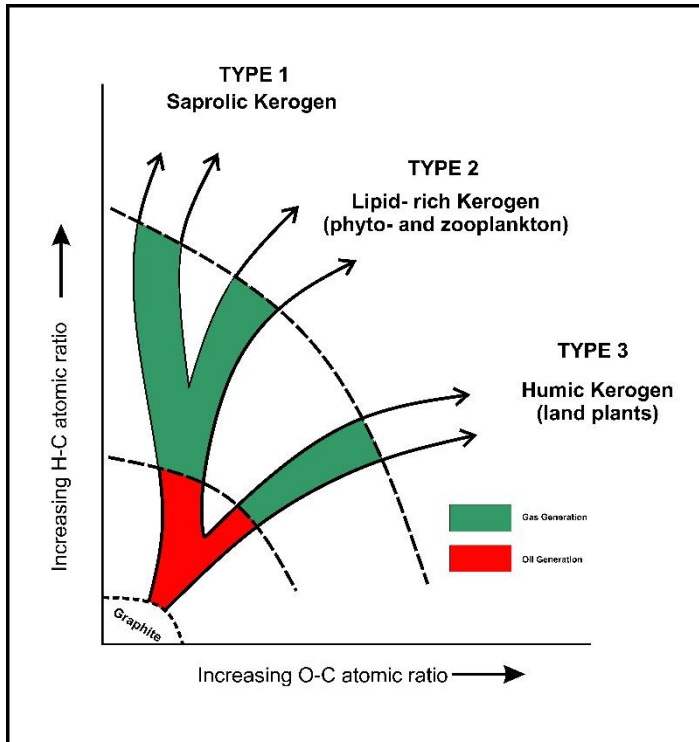


Figure 17: Van Krevelen diagram. Inspired by Selley & Sonnenberg (2015)

The origin of kerogen, and its preservation are the necessities needed in generation of an hydrocarbon in either its gas or oil form (Magoon & Dow, 1994; Selley & Sonnenberg, 2015).

## 6.5 Reservoir Rocks

Reservoir rock is one of the essential components and for the commercial accumulation of oil and gas. An example of reservoir are sandstones and carbonates which have been known to make up general reserves over the world, including the North Sea basin (Selley & Sonnenberg, 2015).

For a reservoir to contain fluid in form of either oil or gas. It must contain pores and must have the pores must be connected to aid in the transmissivity of fluids. Hence, a reservoir is characterized based on its permeability and porosity. A change in a reservoir often changes as a result of diagenesis, compactions and as a result of its provenance (Selley & Sonnenberg, 2015).

## 6.6 Seals and Traps

Traps are major component of a petroleum system. It has been defined as a barrier that bars fluids from moving further. It is characterized by lower permeability. Geologically, examples of seals are often clay, shales and mudstones.(Selley & Sonnenberg, 2015)

Seals and Traps can be broadly classified into structural traps, stratigraphic traps and combination traps (Selley & Sonnenberg, 2015).

## 6.7 Migration

This is an important process and concept that seeks to explain the drainage of hydrocarbons in either its gas or oil form into a reservoir. This movement can be either laterally through permeable and carrier beds which are often sandstones or siltstone, or vertically from a source rock in which it is generated at a sufficient temperature and pressure known as the oil window or gas window (Magoon & Dow, 1994; Selley & Sonnenberg, 2015).

The divisions of migration can be primary, secondary migration or tertiary migration. Wherein primary migration occurs from the source rock, secondary migration is movements within carrier beds, and Tertiary migration occurs through faults or leakage when a seal is broken or deformed(Magoon & Dow, 1994; Selley & Sonnenberg, 2015).

## 6.8 Pressure

Pressure is the force exerted over a unit area on a surface measured in either kilogram per square centimeter or in psi. The types of pressure that can be experienced at the subsurface is generally termed an overburden pressure, which can be subdivided into lithostatic pressure and hydro pressure (Selley & Sonnenberg, 2015).

Lithostatic pressure is due to the weight and pressure of rock due to its grain-to-grain compaction and composition. The lithostatic gradient varies with depth according to the overburden density and the grain-to-grain relationship with water pressure. It is usually estimated to be at an average of **1psi/ft** (Selley & Sonnenberg, 2015).

Fluid pressure or Pore pressure between pore spaces. It is often expressed by the Terzaghi's law (Hubbert & Rubey, 1959; Li et al., 2022; Terzaghi, 1936) which is stated in equation 5 that:

### EQUATION 4

$$S = P + O$$

where:

$S$  = overburden pressure

$P$  = lithostatic pressure

$O$  = fluid pressure / pore pressure

The effective stress is alternatively referred to as the pressure exerted on the solid framework of a sediment. The difference between the overburden pressure ( $S$ ) and its pore pressure (Fluid pressure). Fig.18 shows the relationship and effects of marine sediments. The effective stress can also be referred to as the differential pressure if its coefficient is equal to 1 (Li et al., 2022) :

Can be rewritten as equation 6:

#### EQUATION 5

$$\sigma = S - P$$

$\sigma$  is the vertical effective stress;

Overpressure is a pressure concept used in describing when the pore pressure is greater than the hydrostatic pressure in a marine sediment. It is defined as the difference between the pore pressure (Fluid pressure) and hydrostatic pressure. Figure 19 shows the relationship and within marine sediment and when an overpressure is established (Li et al., 2022) .

Generally, the oil industry according to Selley & Sonnenberg (2015) generally calculates the fluid pressure as follows in equation 7:

#### EQUATION 6

$$P = 0.052 \times wt \times D$$

where:

$P$  = hydrostatic pressure (psi)

$wt$  = mud weight (lb/gal)

$D$  =depth (ft)

Fluid pressure can either be **hydrostatic** or **hydrodynamic pressure**. The pressure exerted by a fluid column at rest is known as hydrostatic pressure. Column of fresh water with a density

of 1.0, has an hydrostatic gradient of 0.433psi in comparison with saline water with about 55,000ppm of dissolved salts with an hydrostatic gradient of 0.45psi/ft , when saline water contains 88,000ppm of dissolved salts, hydrostatic gradient is 0.465psi. Hydrostatic gradients are dependent on temperature, a relationship between lithostatic pressure and hydrostatic pressure is shown in Fig.18 (Selley & Sonnenberg, 2015).

Hydrostatic pressure, alternatively known as normal pressure is  $P_h$ , it arises as a result of the weight of fluid column and is defined in equation 8 as;

**EQUATION 7**

$$P_h = \rho_f gh$$

where  $\rho_f$  , g and h are fluid density, acceleration of gravity, and the height of the fluid column, accordingly (Li et al., 2022).

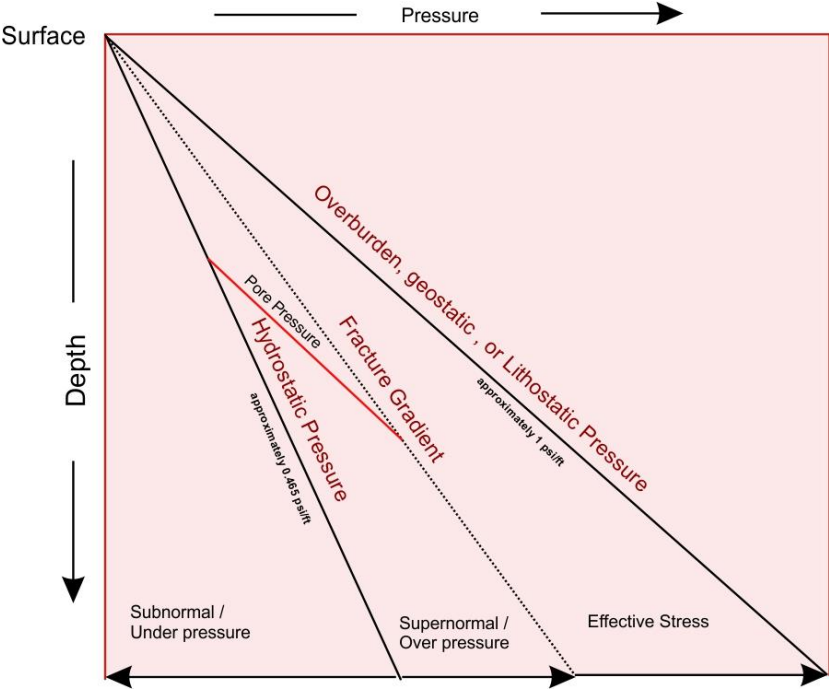


Figure 18: Depth and Pressure relationship illustrating hydrostatic and lithostatic (geostatic) pressures and concepts inspired by (Selley & Sonnenberg, 2015) & (Li et al., 2022)

**Hydrodynamic pressure** is the fluid potential gradient resulting from a fluid flow (Selley & Sonnenberg, 2015).

Overpressure often occurs when the pore pressure exceeds the hydrostatic pressure which causes the deviation from hydrostatic pressure shown in Fig. 18 & 19 (Li et al., 2022).

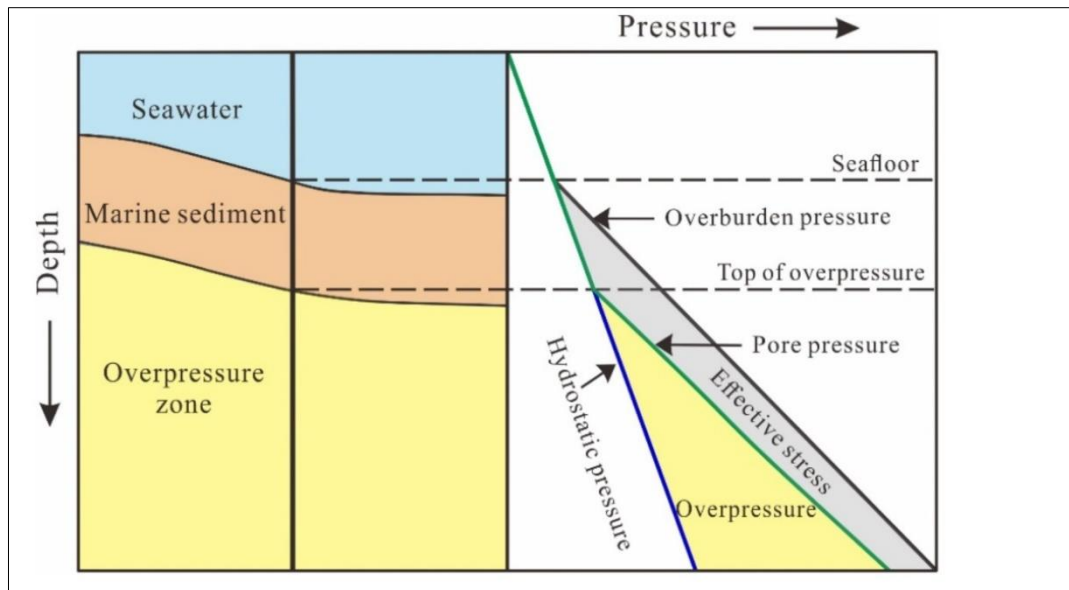


Figure 19: Pressure and Depth relationship of Marine sediments and corresponding stress. modified from fig 1 of (Li et al., 2022)

Understanding hydrocarbon accumulation and well drilling in marine sediment requires a good grasp of different types of pressure as depicted in Fig.19. Additionally, overpressure is a fundamental component in comprehending fluid migration, including shallow gases, which are a type of dry gas (Li et al., 2022; Selley & Sonnenberg, 2015).

## 6.9 Temperature

Temperature is known to increase from the surface of the earth to the core, known as the centre of the earth which is described as being very hot, very dense centre of the earth system (Selley & Sonnenberg, 2015).

Understanding the generation of hydrocarbon and its fluid form. Temperature is very important ingredient along with pressure. Hence, the BHT (Bottom Hole Temperature) that is being obtained from drilling for hydrocarbon is measured with care while drilling as a result of influence of the temperature of drilling mud and corrected using the Horner plot when obtaining well logs to characterize sediments and its fluid (Selley & Sonnenberg, 2015).

## 7. Compression and Shear Stress in Marine Sediments

In understanding fluid migrations, stress regimes are often studied in a basin to study tectonic activities that might have played an important role in the migration of fluids. Stress is built up when there is a movement of the plates relative to one another. It can be compressional stress or shear stress, often associated with convergent and divergent plate boundaries (Evans, 2003; Fossen & Hesthammer, 1998; Ziegler, 1992).



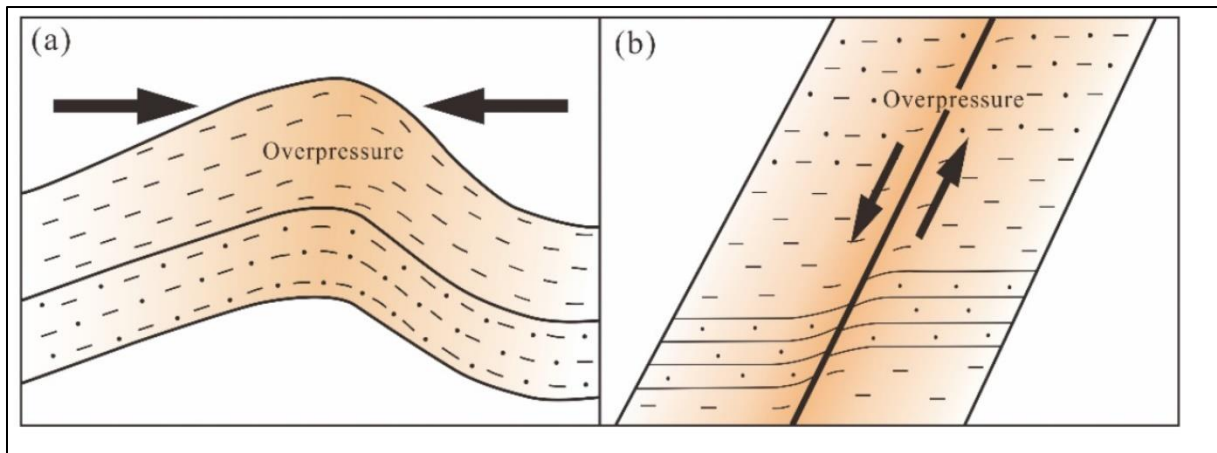


Figure 20: shows a.) compressional stress applied to a strata b.) A shear stress applied to a strata. Both result in the overpressure of fluids. Modified from figure 6 of (Li et al., 2022).

Stress plays a vital role in the migration of fluid. Fig. 20 seeks to show how this stress affect marine sediment (Li et al., 2022). . The North Sea, which is a significant basin, is characterised by shear stress due to the rifting system and history, which is typical of divergent plate boundaries (Ziegler, 1992). Two everyday stresses have been applied in the study of the North Sea, which are simple shear stress and pure shear stress (Evans, 2003).

## 8. Seismic Expressions & Fluid-Related systems

### 8.1 Compaction-controlled systems.

These are fluid systems that forms mainly in non-permeable formations that experiences faster rate of deposition faster than it lets out its pressure. Therefore, leading to overpressure by fluid and gas- This often common in lithologies such as shale

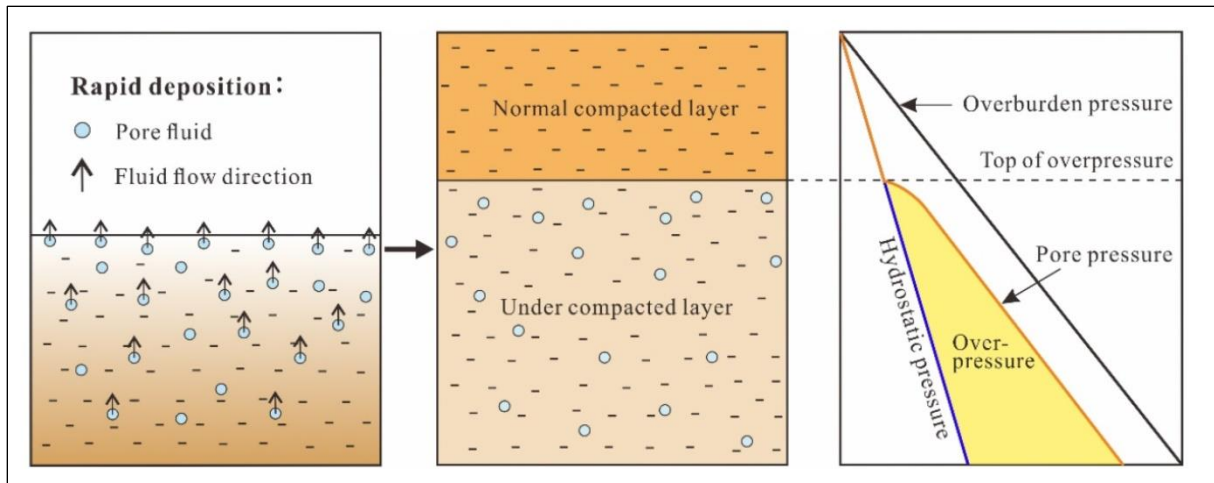


Figure 21: showing a compaction fluid-controlled system and pressure regime in a marine sediment. Modified from figure 2 of (Li et al., 2022).

Fig. 21 shows the formation of compacted sediments and its relationship with overpressure in fluids by (Li et al., 2022). Figure 24 shows related seismic expressions and structures associated to a compaction controlled system and corresponding pockmarks (Berndt, 2005).

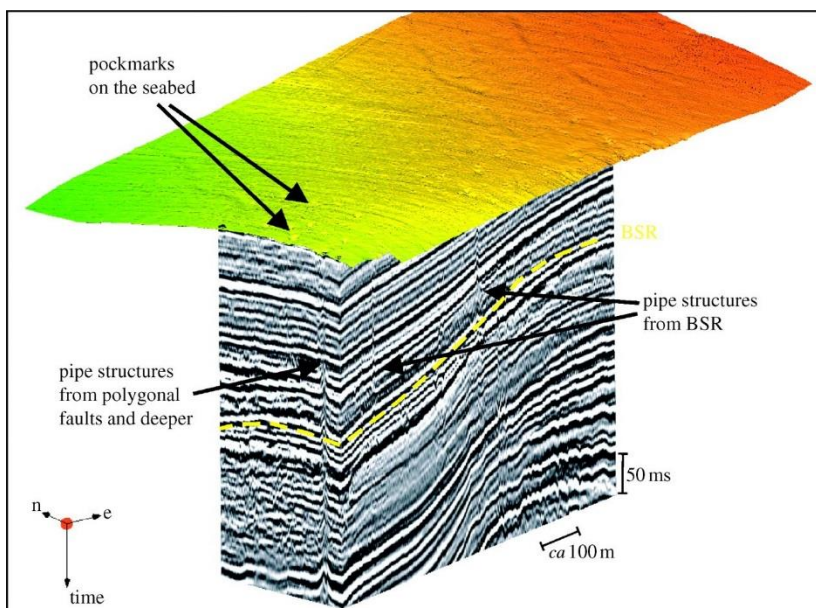


Figure 22: Compaction controlled fluids and related seismic structures and its expressions as a pockmark on seafloor. Image from Berndt (2005)

The term "craters" is sometimes used interchangeably with "pockmarks" in certain publications. These features are often accompanied by seabed deformation and serve as a point of leakage

for hydrocarbons into the water column (Løseth et al., 2009a, 2011, 2022). Most fluid leaks are often expressed as pockmarks or craters as shown in Fig.22. Some are buried, as shown on Vestnesa ridge by (Plaza-Faverola et al., 2015).

## 8.2 Volcanism Controlled Systems.

The largest input of carbon ever documented from the seabed is because of the Paleocene-Eocene Thermal Maxima (PETM). These systems are often estimated to contribute the most methane into the atmosphere from the seabed. They often form because of intrusions and the emplacement of magma, which heats up rocks with already high amounts of organic matter. Heat is transferred from magma emplacement to organic matter-filled rock, resulting in the release of large amounts of carbon-containing gases, mainly methane, through the water column and into the atmosphere.(Berndt, 2005; Li et al., 2022).

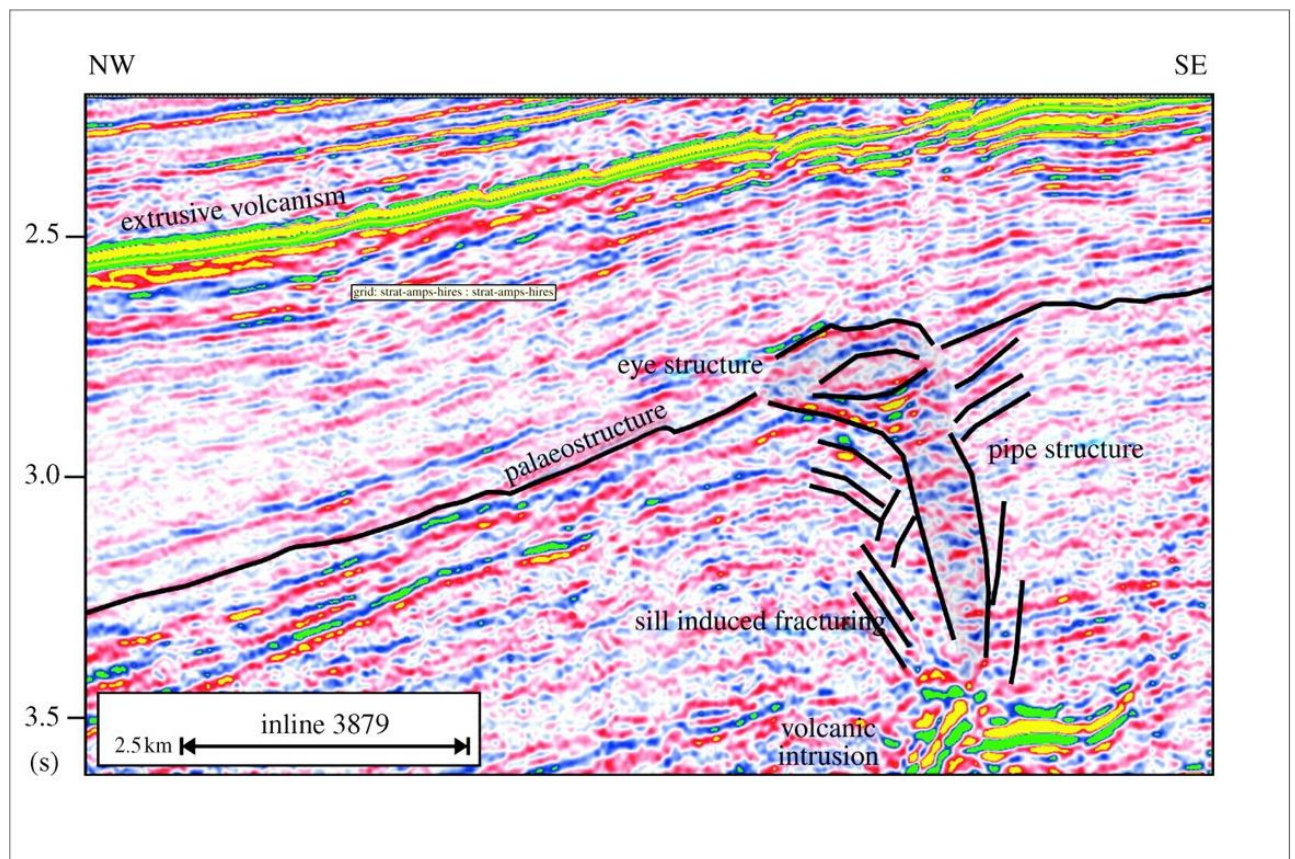


Figure 23: Seismic expressions in a volcanic controlled fluid system. Modified from Berndt (2005)

Fig. 23 by (Berndt, 2005) perfectly describes a volcanic-controlled system and its equivalent seismic expression. This results in heating the existing pore fluid with organic content to release an enormous amount of methane gas. (Berndt, 2005; Svensen et al., 2003).

### 8.3 Petroleum Controlled Systems.

A significant amount of research has been conducted on the fluid controlled by the petroleum system in the offshore region of Nigeria's Niger Delta. Regions where hydrocarbon traps are already charged and filled often give rise to petroleum systems. The offshore region of Nigeria is a prime example (Løseth et al., 2009a, 2011, 2022). Fig. 24 shows a typical example of seismic expression accompanying gas seeps from a potential hydrocarbon trap and accompanying acoustic blanking and hydrocarbon expression (Berndt, 2005; Løseth et al., 2009a).

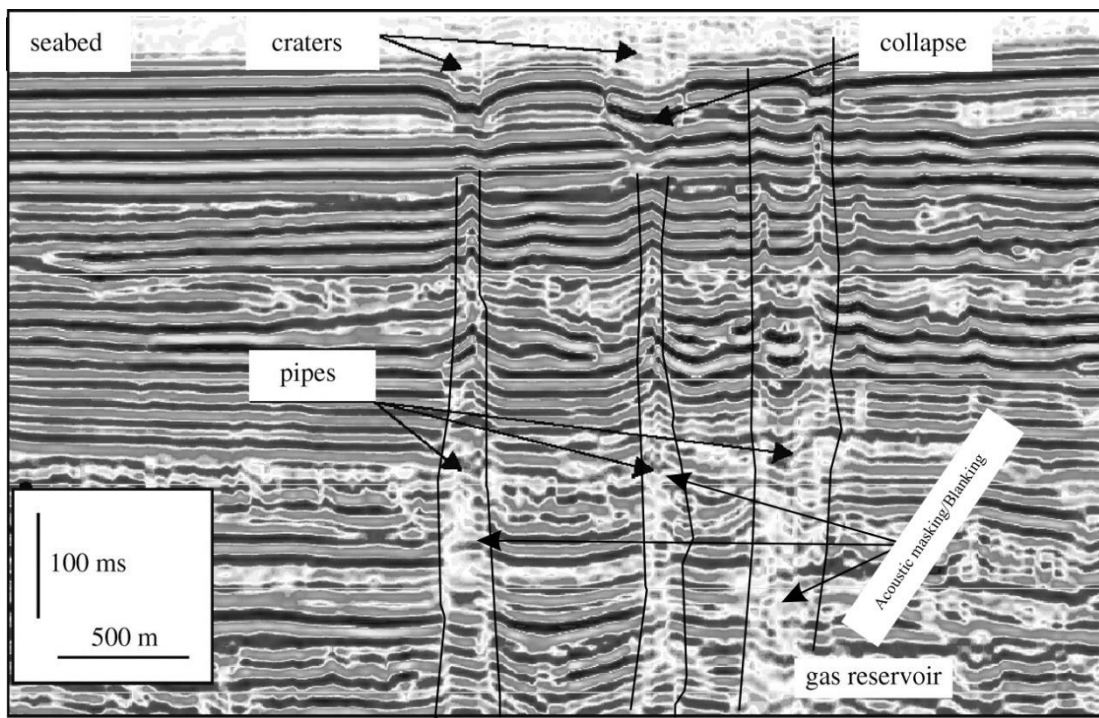


Figure 24: Løseth et al. (2001) natural gas-controlled fluid system from Niger delta. Modified from Berndt (2005)

The pipes have no evident roots associated with leaks as shown in Fig.24. Its seabed expression is referred to as craters and pockmarks. And this pockmarks on seabed are often associated with permanent deformation of the seabed and lithology (Løseth et al., 2009a, 2011, 2022).

### 8.4 Gas Hydrates & systems

Gas hydrates are described as composition of frozen water that is containing gas molecules (Kvenvolden & McMenamin, 1980). The frozen water molecules are being referred as a **clathrates** (Sloan, 1990). It physically looks like a white powdery snow and has a crystal structure of 12Å holding around eight methane molecules inside of 46 water molecules (Selley & Sonnenberg, 2015) .

The lattice structure does not only contain methane but also can contain ethane, hydrogen sulphide, and carbon dioxide. It can also consists of larger hydrocarbon molecules of the pentanes and n-butanes (Selley & Sonnenberg, 2015).

Gas hydrates occurs at certain pressure and temperature requirements and are generally seen as stable at an high pressure and low temperature, hence the concept of GHSZ (Gas hydrate stability zone) used in describing the nature of occurrence of clathrates. The stability of a Gas hydrate increases in pressure logarithmically of a linear thermal gradient as and its relationship is showing gas hydrate development in Fig.25 ( Selley & Sonnenberg, 2015).

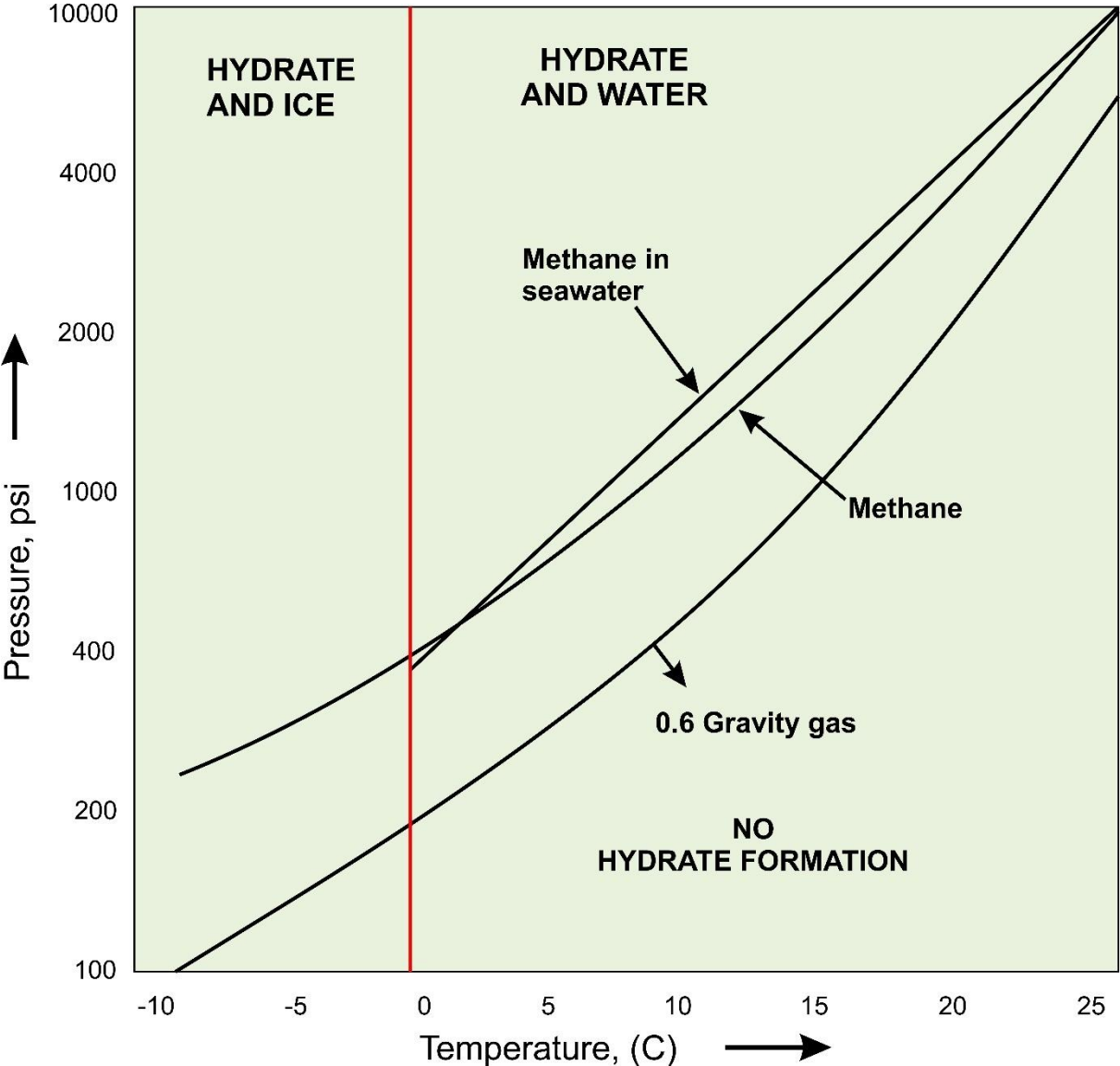


Figure 25: Pressure and Temperature Graph showing the stability field of gas hydrates. Inspired by Hunt (1996) & Selley & Sonnenberg, (2015).

Gas hydrates can occur both in deeper oceanic deposits and shallow arctic sediments deposits. Gas hydrates have been described to have existed both in Siberia and Alaska. In Alaska, the range for gas hydrates occurrence is from 750 m to 3500 m (Holder et al., 1976). While in Siberia, where the geothermal gradient is described as being lower, they extend in occurrence down to roughly about 3100m (Makogon, 1981; Makogon et al., 1971).

#### 8.4.1 BSR (Bottom Simulating Reflector) - Bottom of Gas Hydrate

Bottom simulating reflector mimics the seafloor, has an opposite polarity in comparison to the seafloor and is characterized by a strong wave impedance contrast on a seismic which indicates the presence of gas hydrates. It is often parallel as shown in figure 24 by Berndt (2005) and underlies a gas-bearing layers (Li et al., 2022; Plaza-Faverola et al., 2015).

However, bottom simulating reflectors on seismic do not in every case infer a presence of gas hydrate (Berndt, 2005; Li et al., 2022).

#### 8.4.2 GHSZ - Gas Hydrate Stability Zone

Gas hydrate stability zone are zones suitable for the formation of gas hydrates and it is represented by a seismic expression associated with gas hydrates (Plaza-Faverola et al., 2015). These zones are often characterized by thermobaric conditions, occurring at high pressure and low temperature (Li et al., 2022). Seasonal dissociation of gas hydrate has been identified as the cause of an intermittent release of methane from gas hydrate deposits, which appears to be triggered by fluctuations in temperature (Plaza-Faverola et al., 2015).

BSR are important seismic features that shows bright spots that can be interpreted as a surface located below gas hydrate which contains free gas accumulation and often looked out for when identifying gas hydrates (Selley & Sonnenberg, 2015).

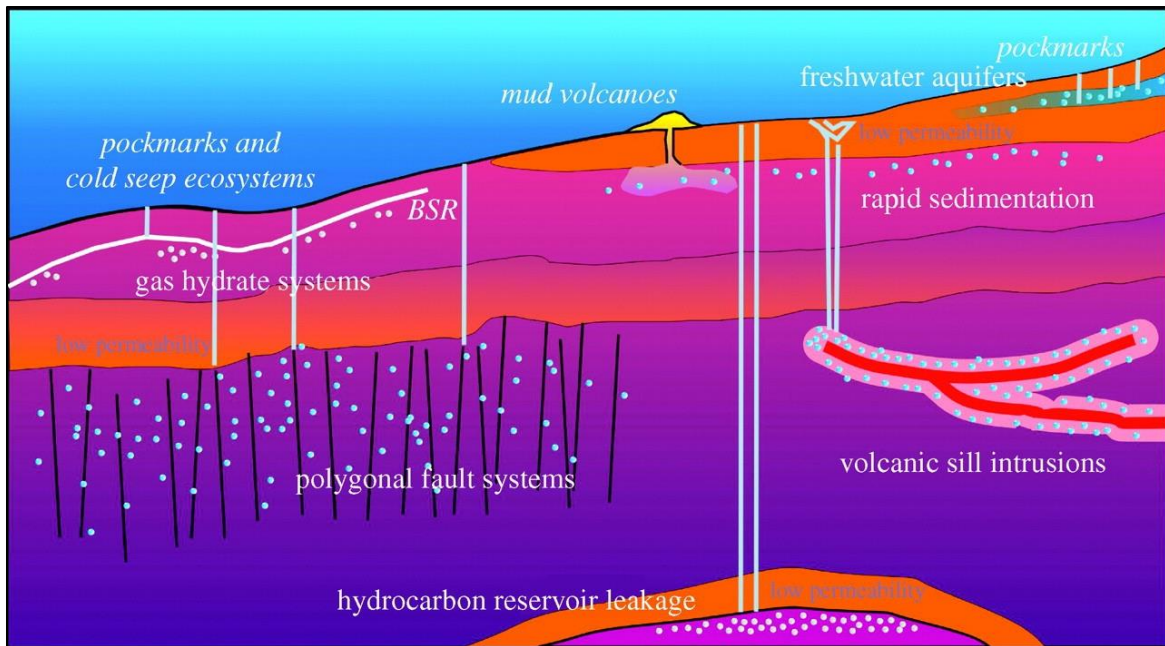


Figure 26: A Model showing different fluid-controlled systems and its equivalent surface expressions on seabed for a passive continental margin. Image from Berndt (2005)

Fig. 26 by Berndt (2005), shows a model associated with different causes of fluid migration and its equivalent expression on the seafloor to explain possible fluid migration and movement in a passive continental margin.

## 9. Methodology & Data

### 9.1 Seismic Reflection Principles

Seismic reflection principles start with a sound wave generated from an air gun or vibroseis in a marine or land environment. Fig.27 shows a simple picture showing how a vessel transmits signals using an air gun captured with a hydrophone. Waves are transmitted in a marine environment through the sea beds with the aid of a vessel and processed afterwards using different mathematical filtering and techniques to bring out the best from signals depicting the subsurface. (Badley, 1985).

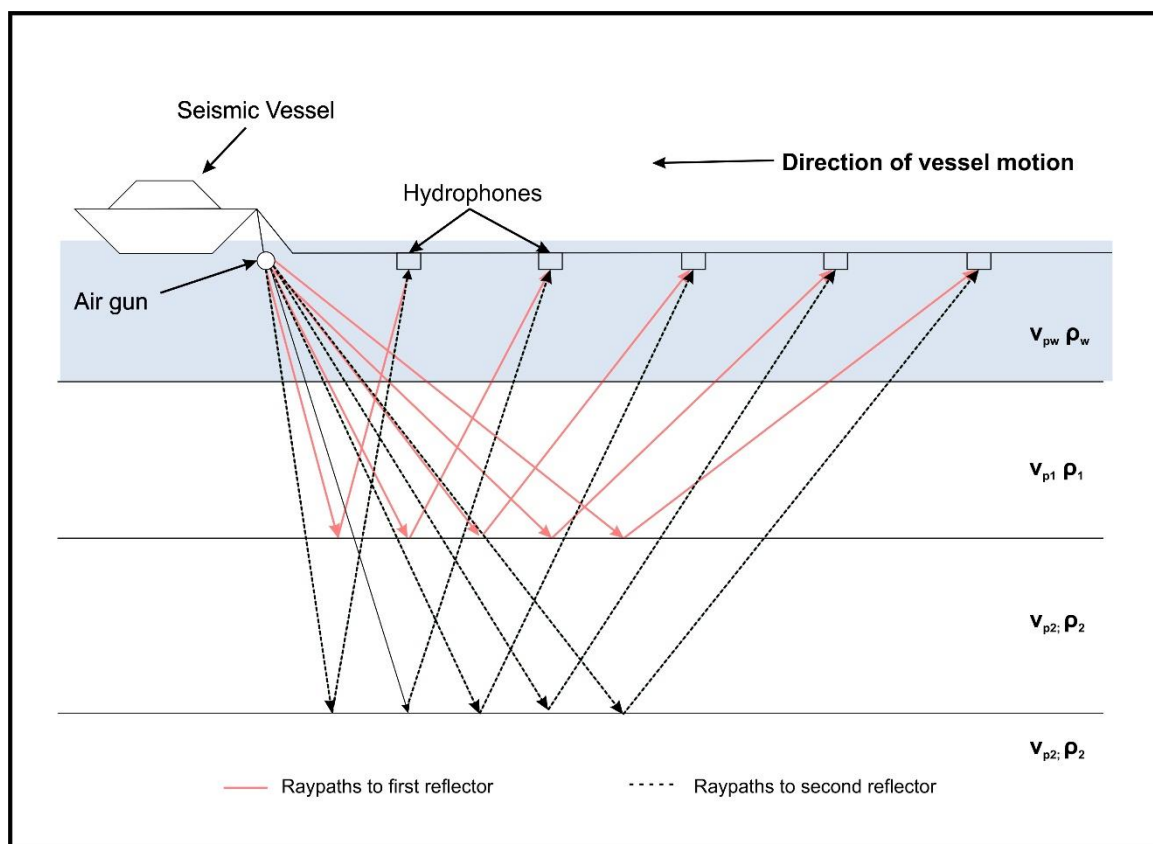


Figure 27 showing a marine towed streamer seismic survey with raypaths from a single shot of an airgun with streamers containing 5 hydrophones:

The properties of a ray to be changed into the ground surface are known as acoustic impedance ( $Z$ ), and  $Z$  is represented in equation 10 as:

#### EQUATION 8

$$Z = \rho V$$

The acoustic impedance, represented by  $Z$ , is the result of multiplying the density ( $\rho$ ) and the velocity ( $V$ ) (Badley, 1985).



Another relevant parameter is the reflection coefficient, which is defined as:

**EQUATION 9**

$$RC = \frac{Z_2 - Z_1}{Z_2 + Z_1}$$

Where:

$Z_2$  = the acoustic impedance of the upper layer

$Z_1$  = the acoustic impedance of the lower layer

The reflection coefficient measures the reflectivity of the higher boundary to the lower boundary in Fig. 27, from boundary 2 to 1 and boundary 3 to 2 and so on. This briefly summarises the acquisition and processing of seismic data interpreted for this project.

9.1.1 Tuning Effect (Vertical Resolution)

Vertical resolution and tuning are well known by most geophysicists because of spectral decomposition, which defines a stratigraphy to resonate at wavelengths which rely on a bedding thickness. The tuning effect is a critical concept caused by thin beds that amplify or weaken a reflection based on seismic reflectors' constructive or destructive interference.

The equation below corresponds to the vertical resolution, which can image certain subtle thickness variations, discontinuities, and thickness of the formation:

**EQUATION 10**

$$Resolution (R) = \frac{\lambda}{4}$$

The above corresponds to a vertical resolution that can image a reflection.

The use of this equation was used in the estimation of the vertical resolution shown in Table 1, the assumption that water column velocity is:

$$Velocity = 1500 \text{ m/s}$$

Vertical resolution is dependent upon the frequency output of the source and the processing of the seismic.

### 9.1.2 Fresnel Zone (Horizontal Resolution)

The Fresnel zone represents the extent to which it produces reflections. This determines the horizontal resolution of the given seismic data. It represents a quarter reflection wavelength that returns to the hydrophone after reflection. The contributions from this Fresnel zone result in the reflection that is produced and acquired (Badley, 1985).

For the unmigrated section, the zone produces rays from this zone defined by equation.13 (Badley, 1985);

#### EQUATION 11

$$R_f = \frac{V_2}{2} \sqrt{\frac{t}{f}}$$

Where  $R_f$  = Radius of Fresnel zone,  $V$  = average velocity,  $t$  = two-way time in seconds and  $f$  = dominant frequency in hertz.

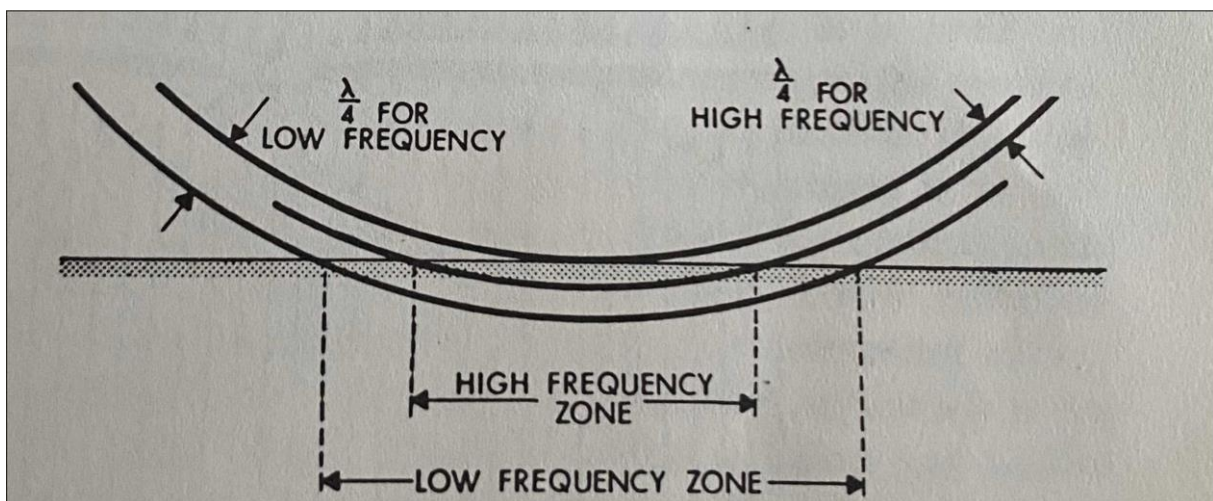


Figure 28: Showing the Fresnel zone for a low frequency and high frequency. Low frequency covers larger zones, while high frequencies cover smaller zones. From fig. 2.18 Badley( 1985)

The horizontal resolution is dependent upon the depth, frequency, and velocity. Fig 28 shows the relationship between higher frequency and low frequency along with its coverage. The deeper the event, the lower the horizontal resolution. The horizontal resolution still seems less understood by most Geophysicists and tends to be more driven by the acquisition and processing of the data. A horizontal resolution before migration is equal to the Fresnel zone, while after migration, the imaging aperture shrinks to a small circle equal to  $\frac{\lambda}{4}$  (Schulte, 2024).

## 9.2 Direct Hydrocarbon Indicators (DHI)/ Fluid Indicators

Methane is a dry gas that is classified as hydrocarbons (*Selley & Sonnenberg, 2015*). Direct hydrocarbon indicators utilize certain seismic expressions when identifying hydrocarbons and their occurrence on seismic. These indicators are crucial in identifying potential pathways of fluids and their occurrence on a seismic, although they do have their limitations, which are mentioned. This expression was utilized used to analyze high-amplitude reflections.

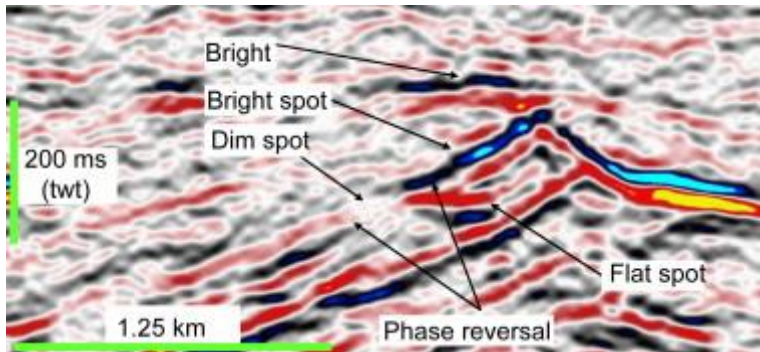


Figure 29: Direct Hydrocarbon/ Fluid Indicators Løseth et al. (2009).

### 9.2.1 Bright Spots

According to the Society of Exploration Geophysicists (SEG), bright spots are often linked with an increasing amplitude. Bright spots are one of the Direct hydrocarbon indicators (DHI), based on the observation that sand has a lower acoustic impedance than shale when filled with water. When sand, usually unconsolidated sediment, is filled with hydrocarbons, it increases in bulk density and velocity. This results in an increased amplitude at the top of the sand-bearing hydrocarbon, as shown in the seismic Fig. 29.

### 9.2.2 Dim Spots

Dim spots are hydrocarbon indicators that occur in highly consolidated sediments compared to bright spot occurrence on seismic, according to the Society of Exploration Geophysicists (SEG wiki). It is shown in the seismic. It is often associated with significant acoustic impedance in highly consolidated sand overlain by shale. Hydrocarbon occurrence in tight pores can decrease the velocity and density of such sediments, but such a decrease can't reverse the polarity of its reflection coefficient. As shown in Fig. 29.

### 9.2.3 Flat Spots

Flat spot is commonly used to detect hydrocarbons associated with gas and oil, oil and water, or gas and water. For a flat spot to appear on a seismic section, the thickness of the hydrocarbon reservoir must be greater than the vertical resolution. Locating this direct hydrocarbon indicator can be challenging due to low angles, steep beds, faults, and processing artefacts that may be

mistaken for flat spots. According to the Society of Exploration Geophysicists (SEG wiki), flat spots can also occur due to lower gas saturation in a reservoir. See Fig.31 for a corresponding sample of what a flat spot looks like.

#### *9.2.4 Phase Changes/ Reversals*

Phase changes are also fluid indicators or hydrocarbon indicators that are alternatively known as phase reversals by the Society of Exploration Geophysicists (SEG wiki). It is often associated with an overlying reservoir with lower reservoir rock. A typical example occurs when partly consolidated sands become wet, resulting in an acoustic impedance slightly higher than the overlying shale. The signal given results in the sand's top, resulting in a weak positive reflection coefficient. As hydrocarbon gradually fills pore spaces of sand, there is a decrease in acoustic impedance, which is lower than that of overlying shale. Hence, reflection at the top changes in phase from peak to a weak trough. However, phase changes can be challenging to identify by interpreters due to the assumption that the top of sandstone is often represented by a continuous reflection, according to the Society of Exploration Geophysicists (SEG wiki). See Fig.31 for an example of what a phase change looks like in a seismic.

#### *9.2.5 Gas Chimneys*

Gas chimneys occur primarily due to the buildup of hydrocarbon gas release, usually from fault planes or fractures. The overlaying shale of permeable zones is often characterized by lower velocity. Gas chimneys on seismic are generally seen as areas of poor data or data masking. They do not have economic value in occurrence but have grown vastly common in identifying possible traps and the occurrence of hydrocarbons in the form of gases. See section 8 for excellent examples.

#### *9.2.6 Shadow Effects*

Shadow effects are also hydrocarbon and fluid indicators that result in lowering velocities in hydrocarbon buildup. It often increases in travel times, resulting in reflection sinks. Shadow effects occur at the top of bright spots due to high amplitude processing. See Fig.29.

#### *9.1.3.7 General Limitations/Pitfalls of Using DHIs as (Fluid Indicators)*

The following are pitfalls and often unsuspecting events encountered while using fluid indicators on a seismic. This includes, but is not limited to, the following:

- Tuning effects in steeping beds can lead to overamplifying seismic responses, either resulting in a bright spot or dampening seismic amplitude, leading to a dim spot.
- Noises on seismic can result in a direct hydrocarbon indicator on seismic.
- Flat spots on seismic can be caused by lithological variation and not by fluid contact.

- Lithology with low impedance characteristics, such as mud volcanoes, low-density shales, ash, and coal, can be mistaken for a hydrocarbon or fluid indicator.

### 9.3 Data

Fig.30 shows the surrounding land mass and area corresponding to where the 3D seismic was obtained; area coverage of seismic and data information is covered in table information. Boundaries are established from given bathymetry and existing literature. (Ottesen et al., 2018) . Fig.31 shows an up-close view of this seismic box and areas that fall on the Norwegian Trench and its closeness to the east section of the Shetland platform.

Fig.31 shows that some of these seismic cubes overlap, hence a possibility of matching the interpreted seafloor. However, the challenge was a lack of a chronostratigraphic and 2-D seismic information marker to constrain interpretation properly. So, rough interpretations were made to determine the seafloor and reliance on previous works. (Ottesen et al., 2018). Also important to note is the lack of missing coverage from parts of seismic overlaps.

The availability of 3D seismic data made it possible to carry out an attribute and utilise time slices to reveal some features from previous literature and works carried out. See table for information and estimation made regarding seismic data.

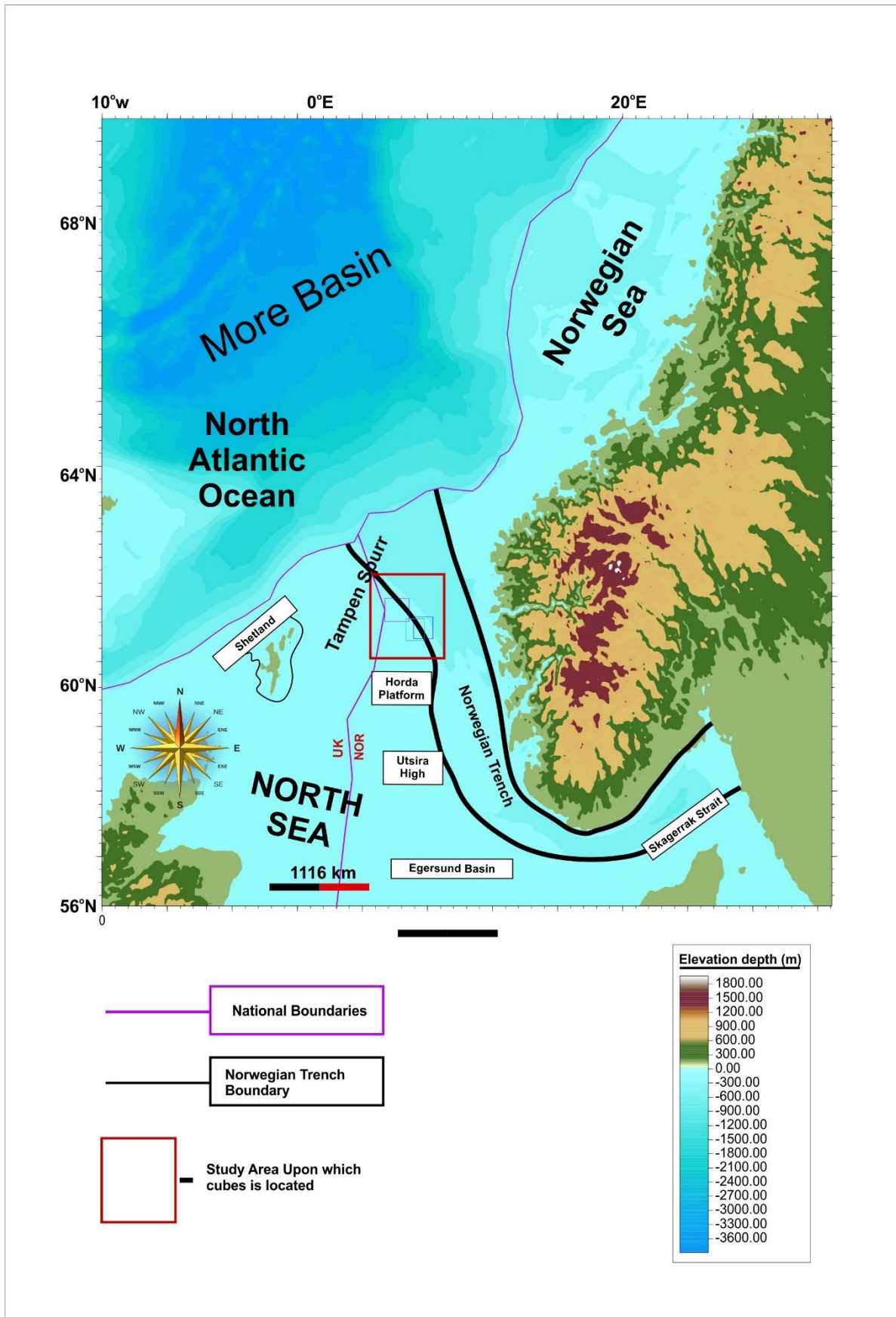


Figure 30: Map of Study Area with surrounding basin and associated landmasses.

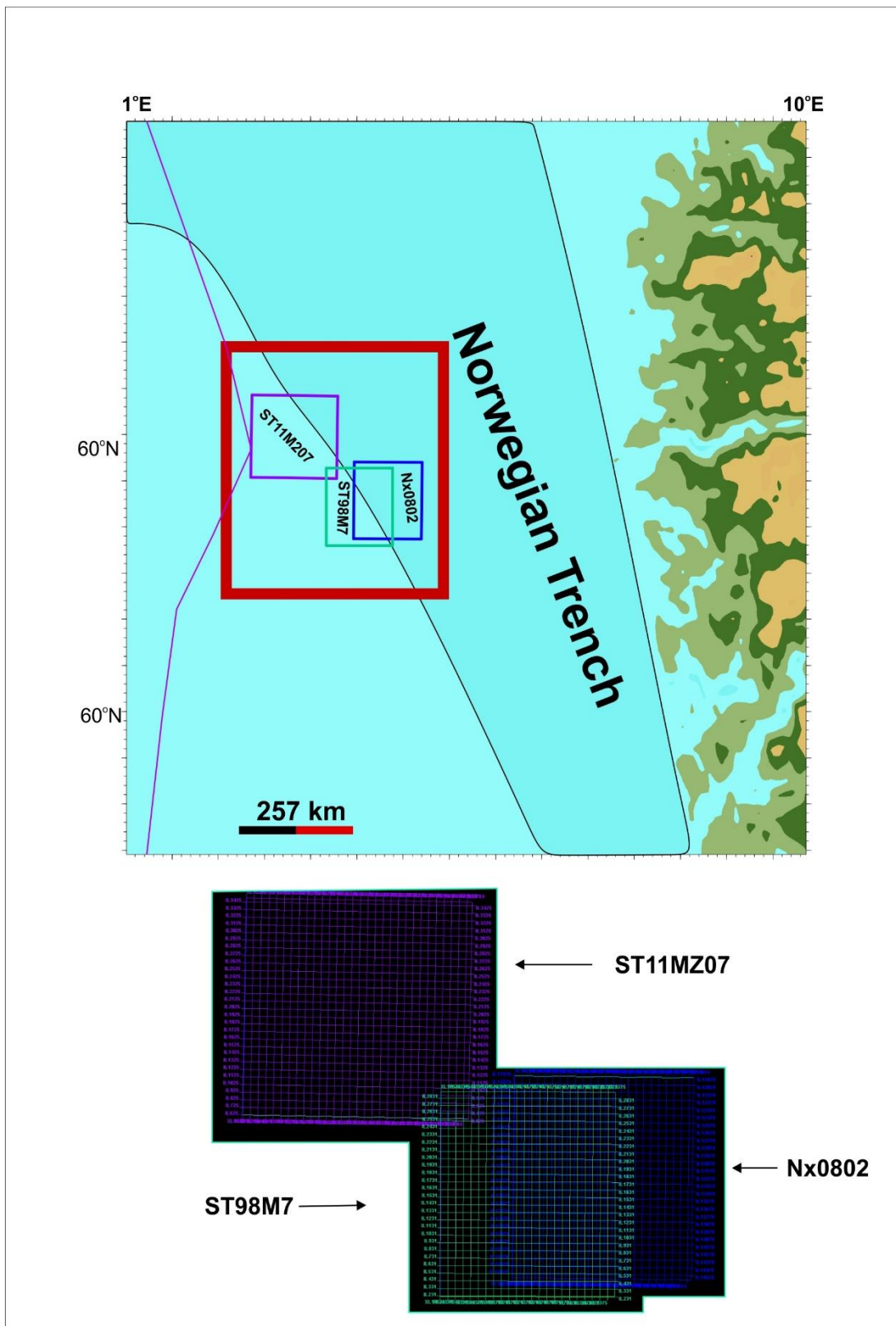


Figure 31: showing a zoomed section of the study area, placement on the Norwegian Trench and corresponding seismic coverage Inline and Crosslines..



Table 1: 3D seismic Data Acquisition and Processing Information

Data Information	Nx0802	ST11MZ07	ST98M7
Source	Tuned Boltgun	Flip Flop	Bolt Gun
Survey	3-D	3-D	3-D
Processing Company	WesternGeco	WesternGeco	Ensign Geophysics
Year Acquired	2009	2012	1998-1999
Client	Nexen	Statoil	Statoil

Table 2 shows the vertical and resolution of the 3D seismic data used. Frequencies used are selected from spectral analysis and inspecting of 3D data (See Fig.29 for dominating frequencies used ).

Seismic Parameters	Nx0802	ST11MZ07	ST98M7
Frequencies (Inset Lines)- Used in estimation (Referenced with seafloor)	21.5 Hz	13 Hz	17.5Hz
Polarity	Zero Phase Polarity	Zero Phase Polarity	Zero Phase Polarity
Vertical Resolution- ( $\lambda/4$ ) (Reference: Seafloor- using xline and inline )	17.44	28.846	21.4285
Horizontal Resolution (Retreived from Petrel)	12.50	12.50	12.52

**Assumption: Water Column (1500m/s)**

Table 3: shows Vertical Resolution based on chronostratigraphic age concerning dominant frequencies used in estimating seismic cubes ( See Fig.29 for dominating frequencies used ). Information obtained from previous studies in the area with well logs(Sebastian, 2022)

Seismic Parameters	Average. Int. Velocity (m/s)	Nx0802	ST11MZ07	ST98M7
Cretaceous	2835	33	55	41
Paleocene- Early Eocene	2317	27	45	33
Eocene	2108	25	41	30
Lower Oligocene	1742	20	33.5	25
Intra- Oligocene Wedge	2084	24	41	30
Lower Miocene	2135	25	41	31
Upper Miocene	2127	25	41	30
Pliocene	2113	24.6	41	30.2
Pleistocene- Holocene	2000	23	38.5	28.6

Vertical Resolution based on chronostratigraphic Marker

**EQUATION 14**

$$V_{int} = \frac{Z_{int}}{t_{int}}$$

Where  $V_{int}$  = interval velocity (m/s),  $Z_{int}$  = interval thickness (m) and  $t_{int}$  = one-way travel time (OWTT).

The vertical resolution is estimated in Table. 2 assumes that the water column is 1500m/s. The resolutions estimated for different chronostratigraphic markers in Table. 3 are based on well-log information obtained around the study area (Sebastian, 2022). This isn't strict and is just a rough assumption. These velocity estimates can determine the depth of interest in seismic but don't factor in velocity variations in steeping beds.

Assumptions are made in these estimations; the proper way is to integrate velocity intervals from calibrated sonic velocity intervals to known seismic units to estimate vertical resolution and in time-depth conversion.

## 9.1 Frequencies

### 9.1.1 Noise-to-signal ratio

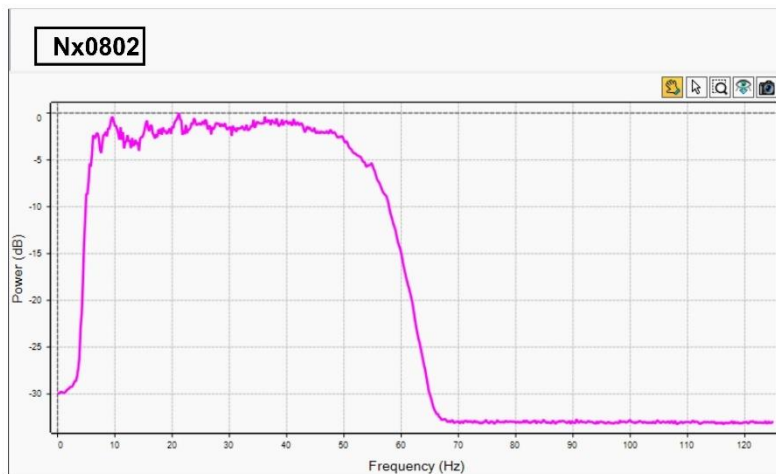
The noise-to-signal ratio of seismic is the first step in identifying the right signals, which detect features from the seismic section and the noises acquired while obtaining seismic.

The decomposition spectral analysis tools are pivotal in screening the right signals from noises on seismic sections. The focus is often on dominating frequencies.

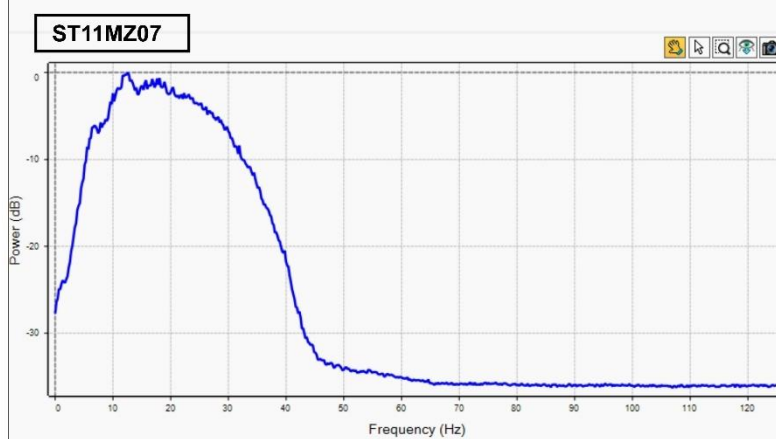
Dominant frequencies used in estimating this resolution of the given seismic are on NX0802, ST11MZ07, and ST98M7, which are 10-20 Hz primarily. Shown in Fig.29:

Noises in seismic can come from ground rolls, vessels at the surface and noises from other marine activities, which are inevitable. Hence, finding the right signals is essential in seismic analysis.

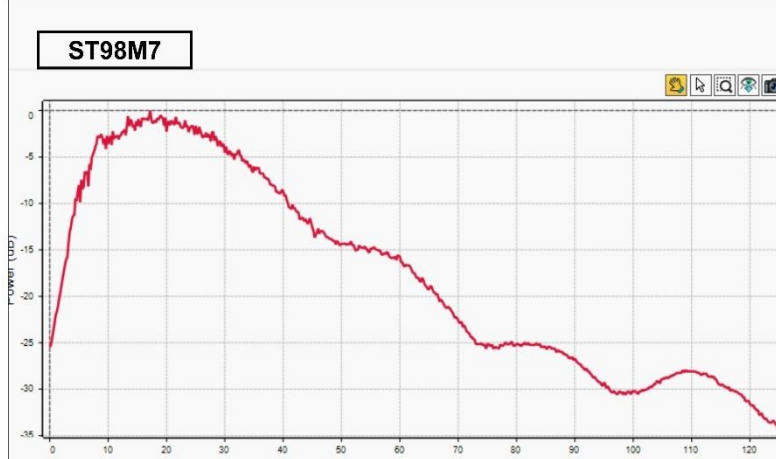
## Peak Frequency



**21.5 Hz**



**13 Hz**



**17.5 Hz**

Figure 32: Spectral Analysis of data set to inspect for the dominating frequencies used in Table 1 and estimation of the vertical resolution of the 3D seismic data.

### 9.1.2 Polarity of the Data (Examples)

Polarity helps determine reversal changes and understand potential fluid occurrence within the subsurface. Fig.30 shows examples of polarity and corresponding classification for the seafloor and inline.

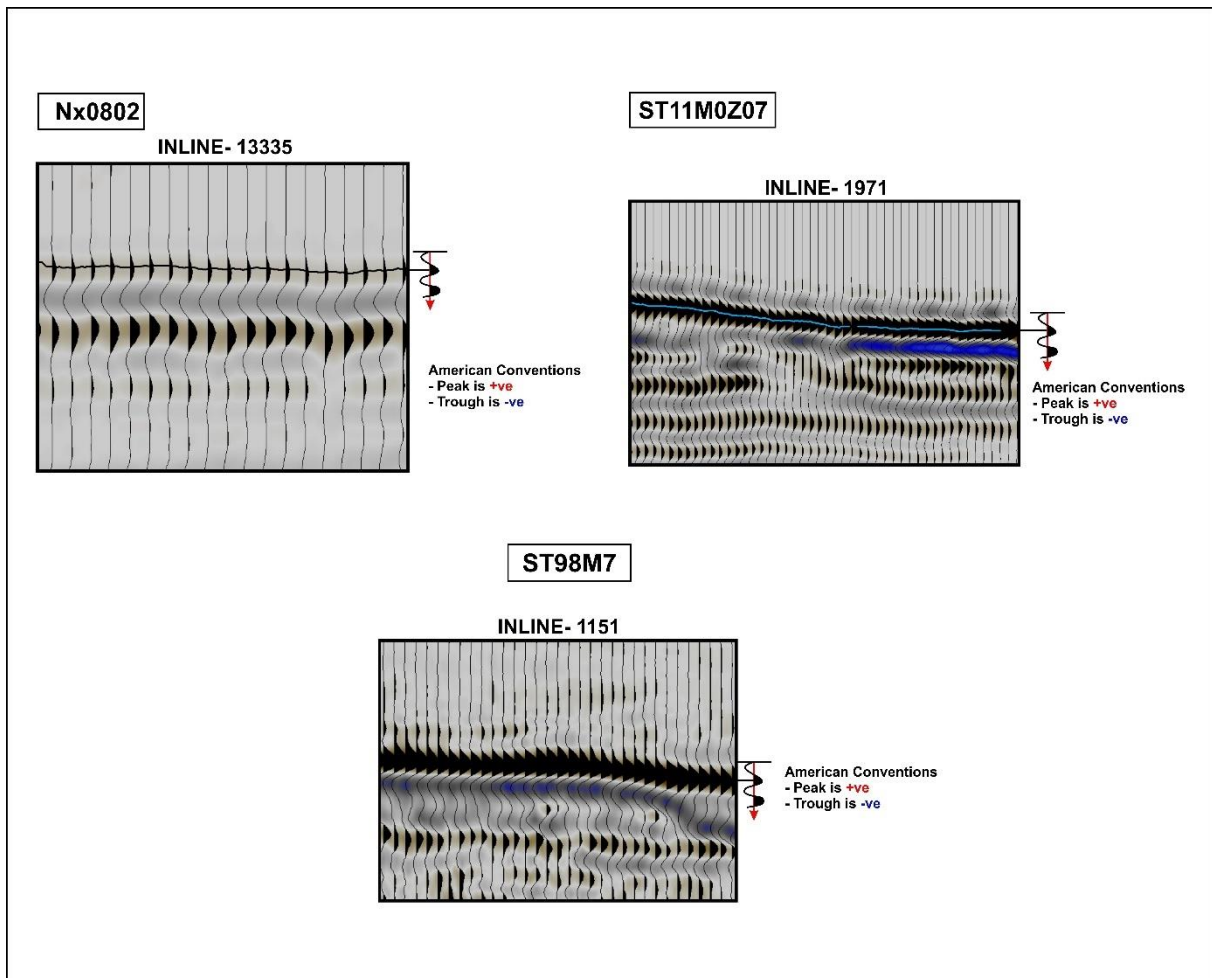


Figure 33: Showing examples of data's polarity with reference to the seafloor on 3D seismic cubes used in analysis.

## 9.2 Seismic Attributes Used and parameters

Seismic attributes are used to analyse different features within the subsurface. This feature includes unconformities, mapping faults, and identifying complex structures such as channels, diapirs, doming, etc. One of those attributes used for this project is attached in Table 3 and what it measures.

Table 4: Seismic attributes are used in interpretation, and what are they measured.

Seismic Volume Attributes	Parameter It Measures / Application
Variance	- Applicability in stratigraphy, depositional environments including; reefs , channels... - Responsible for fault detection and also discontinuities
RMS amplitude	- Detection of Lateral Variation and High Anomalies.
Antracking Variance	- Structural attributes that identifies fractures and faults aggressively, or passively using the stereonet that relies on selective dip magnitude and Azimuth

Table 5: Parameters Inputted for both Volume and surface attribute. (Most are default settings except that of the antracking)

RMS	Variance	Antracking
<b>ST11MZ07</b>		
<b>Parameters Used:</b> <b>Volume Attributes</b> Seismic attribute: RMS Amplitude Input: ST11MZ07 [Realized] 1 Window: 9	<b>Parameters Used:</b> <b>Volume Attributes</b> Input: ST11MZ07 [StructSmooth] [Realized] 1 Inline range: 3 Crossline range: 3 Vertical smoothing: 15 Dip correction: Off	<b>Parameters Used:</b> <b>Volume Attributes</b> Seismic attribute: Ant tracking Input: ST11MZ07 [Crop] 1 [StructSmooth] [Var] [Realized] 2 Ant mode: Aggressive Initial ant boundary: 5 Ant track deviation: 2 Ant step size: 3 Illegal steps allowed: 2 Legal steps required: 2 Stop criteria (%): 10
<b>Nx0802</b>		
<b>Parameters Used:</b> <b>Volume Attributes</b> Seismic attribute: RMS Amplitude Input: Nx0802 [Crop] 1 [Realized] 1 Window: 9	<b>Parameters Used:</b> <b>Volume Attributes</b> Seismic attribute: Variance (Edge method) Input: Nx0802 [Crop] 1 [Realized] 1 Inline range: 3 Crossline range: 3 Vertical smoothing: 15 Dip correction: Off	<b>Parameters Used:</b> <b>Volume Attributes</b> Seismic attribute: Ant tracking Input: Nx0802 [Crop] 1 [StructSmooth] [Var] [Realized] 1 Ant mode: Aggressive Initial ant boundary: 5 Ant track deviation: 2 Ant step size: 3 Illegal steps allowed: 2 Legal steps required: 2 Stop criteria (%): 10
<b>ST98M7</b>		
<b>Parameters Used:</b> <b>Volume Attributes</b> Seismic attribute: RMS Amplitude Input: ST98M7 Full Cube [Crop] 1 [Realized] 1 Window: 9	<b>Parameters Used:</b> <b>Volume Attributes</b> Seismic attribute: Variance (Edge method) Input: ST98M7 [Crop] 1 [Realized] 1 Inline range: 3 Crossline range: 3 Vertical smoothing: 15 Dip correction: Off	<b>Parameters Used:</b> <b>Volume Attributes</b> Seismic attribute: Ant tracking Input: ST98M7 [Crop] 1 [Crop] 1 [StructSmooth] [Var] [Realized] 1 Ant mode: Aggressive Initial ant boundary: 5 Ant track deviation: 2 Ant step size: 3 Illegal steps allowed: 2 Legal steps required: 2 Stop criteria (%): 10

A strict compliance to default settings were used for volume attributes. Except for antracking attributes that was somewhat played with to capture what might look like a fracture. Attributes generated are contained in Table.5. However, some orientation and parameters is not well understood with respect to the stereonet utilizing inlines and crosslines.

### 9.3 Time Slices Vs Horizons

Picks along a particular time or depth are called time slices. Seismic horizons are picks along noticeable seismic reflectors that involve picks along different times or depths on a seismic section. When it comes to geological features such as channels, a time slice reveals them partly, while horizons, which are often manually picked, reveal the full extent of channels and lateral discontinuities. Fig.34 shows the difference between a time slice and a horizon from a supposed 3D seismic cube.

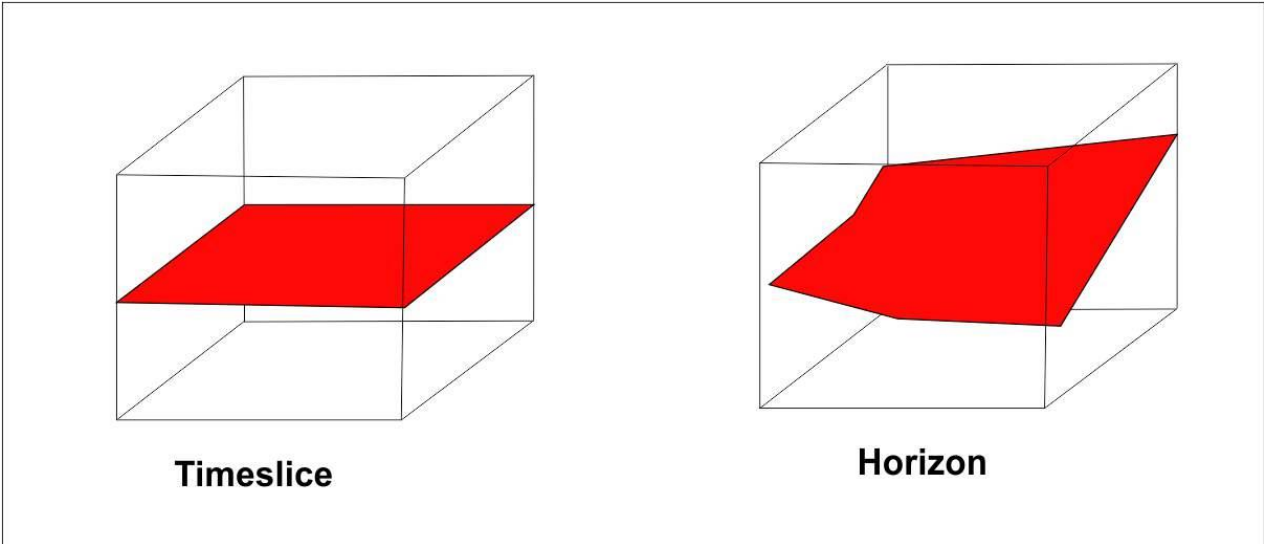


Figure 34: Showing a difference between a Timeslice and a Horizon

*Time slices* are a single time. *Horizons* are different times the interpreter picks based on noticeable continuity of reflection from a seismic, which is often subjective from one interpreter to another. This was used and implemented as interpretation.

## 9.4 Workflow

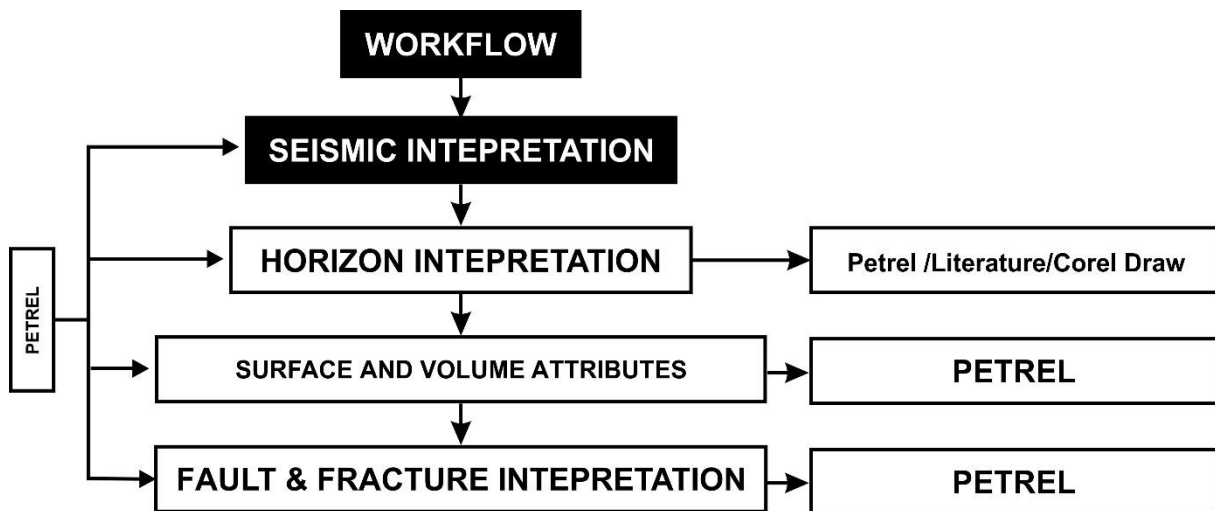


Figure 35: showing a described workflow that was implemented during this project.

Fig.35 shows a workflow of various methods used in executing the tasks given a general perspective. While Petrel remains the software used in interpretation, Corel Draw was used at some point for presenting results and adjusting somewhat questionable horizon picks. The 2D and 3D horizon tracking were the tools most utilised in Horizon Interpretation. The 3D horizon tracking was used to track horizons along the seismic cubes. 2D was utilised in areas where it was challenging to pick horizons, such as the horizon 3 picks. Choosing horizons is based on identifiable events and unconformities along with continuous seismic reflections from existing literature given as identifiable unconformities, especially with the Northern Sea.

Surface and volume attributes were generated with petrel and using parameters documented in part at the Data and Method section. A 3-D seismic, which combines inlines and crosslines, making it possible to generate volumetric attributes such as the RMS, variance, and ant-tracking variance volume attributes. Surfaces generated from horizons makes extracting values from already generated volume attributes possible with the surface attribute of Petrel.

Fractures and faults were often manually interpreted from the interpretation window and using time slices from volume attributes generated, along with extracting values of the surface attributes from volume attributes already generated.



## 10. Results

### 10.1 Seismic Stratigraphy, Horizon Interpretation & subdivisions

The basis of horizon picks was based on previous literature identifying clear event boundaries. The seismic units are defined based on distinct and explicit events documented in previous works (i.e. (Horstad et al., 1995)). Fig.37 shows an example of subdivisions associated with ST11MZ07, which was severally referenced in the description of seismic events and facies. The breakdown of these picks goes thus:

Horizon 1 (Fig.38): was the most chaotic of the pick regions, with cross-cutting continuous reflections overlying a chaotic zone. Hence, an horizon pick was placed at that boundary, corresponding to the Neogene-aged deposit of the Nordland group with an Unconformity above Utsira (see Fig. 37 for basis of picks). An attempt at a well-known unconformity region (However, it was a failure using both the 2D and 3D tracking tools). Hence, CorelDraw adjusted traces along continuous reflection overlying the Utsira formation unconformity with reference to Fig.36 for basis of pick. It includes the Nordland group of Miocene age as part of the Neogene period.

Horizon 2 (Fig.39) These identifiable picks show continuity across seismic areas. This corresponds to Paleogene deposits, which consist of Frigg's formation, named by NORLEX (Norwegian Interactive Offshore Stratigraphic lexicon) and Balder's formation underlying the Eocene mudstone. They are represented by sand lithology that might have intruded into the mudstone. Hence, a pick was placed at that distinct boundary using existing literature. Beneath this is the Sele formation and group (Hordaland group, Shetland group, and Cromer Knoll Group).

Horizons 3 (Fig.40): represents a clear-cut boundary indicating the base Cretaceous, which makes up the Viking Groups. This is a well-documented unconformity. Hence, a pick was introduced in that region. The Viking Group is a well-documented petroleum system and represents the main rifting event boundary associated with the late Cretaceous and early Jurassic events. See Fig.36 for corresponding lithology.

However, a strict approach will utilise well logs to establish the right boundaries and characterise lithology and fluids. Hence, approximate subdivisions were made based on

literatures and areas of an approximate Clear-Cut Boundary (Unconformity) or continuous boundary of horizon 2 of Paleogene period.

UHR: This represents a region of unconformity identified as being challenging to locate, as some reflections might appear to be conformable to lithology; hence, references were made and indicated as a significant event. and surface included belong to the onset of Pliestocene (which is very subjective and difficult to identify in most seismic sections).

A general example of a description of seismic facies was given and presented on this basis in tables 6, 7 and 8 based on this subdivision (Fig. 36). Note the corresponding stratigraphy that has been described in section 4).

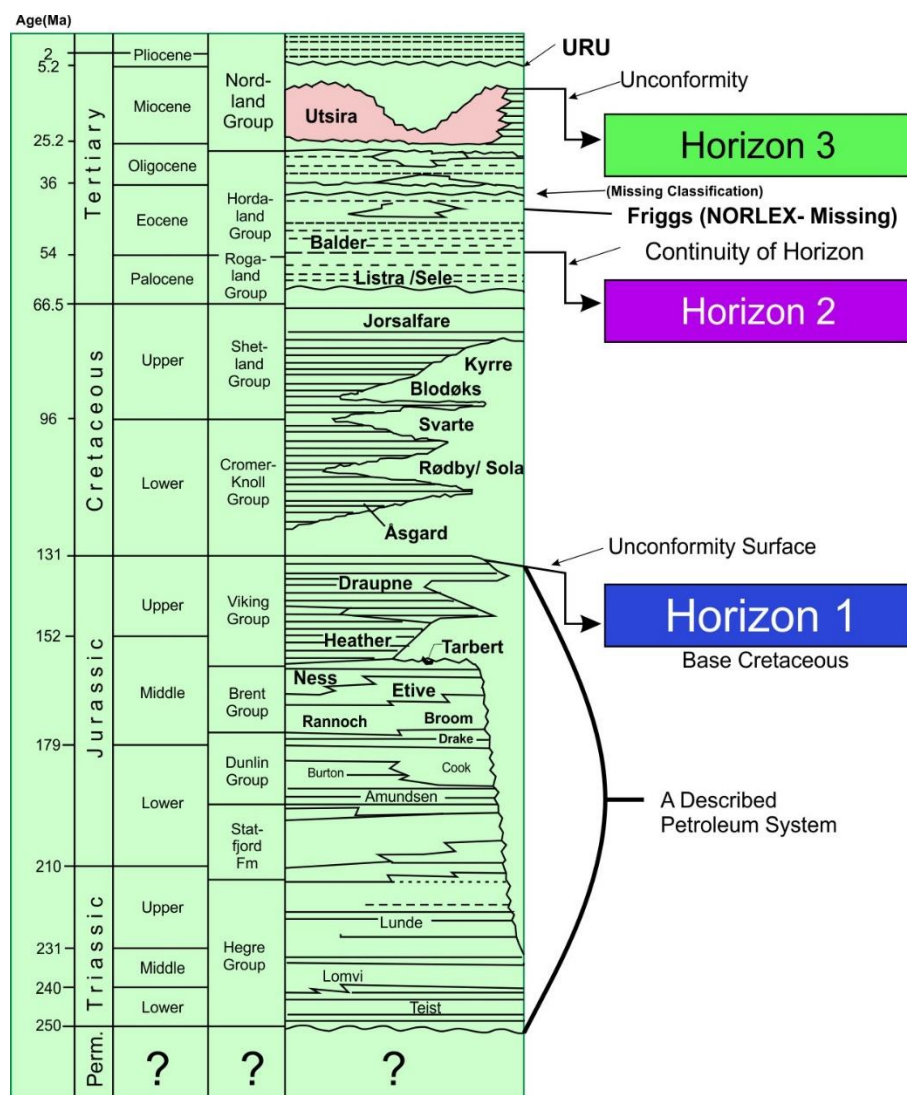


Figure 36: Basis of Stratigraphic Picks and Horizons (see section 4 of fig.10 for general seismic stratigraphy ). Inspired by Fig. 3. Horstad et al.( 1995). Note colour codes used and referenced with corresponding lithologies

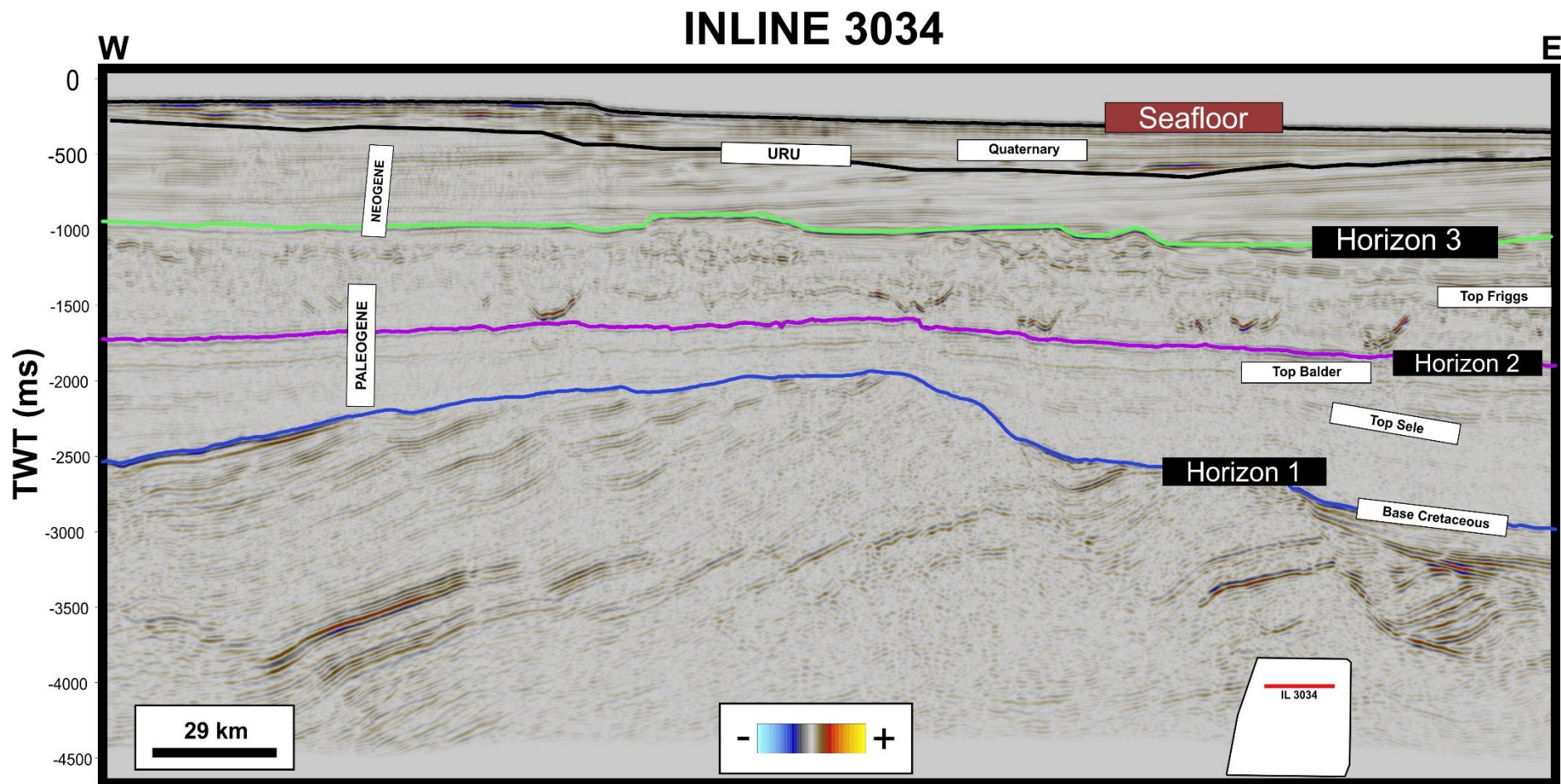


Figure 37: shows Inline 3034 of reference Horizon picks only of ST11MZ07

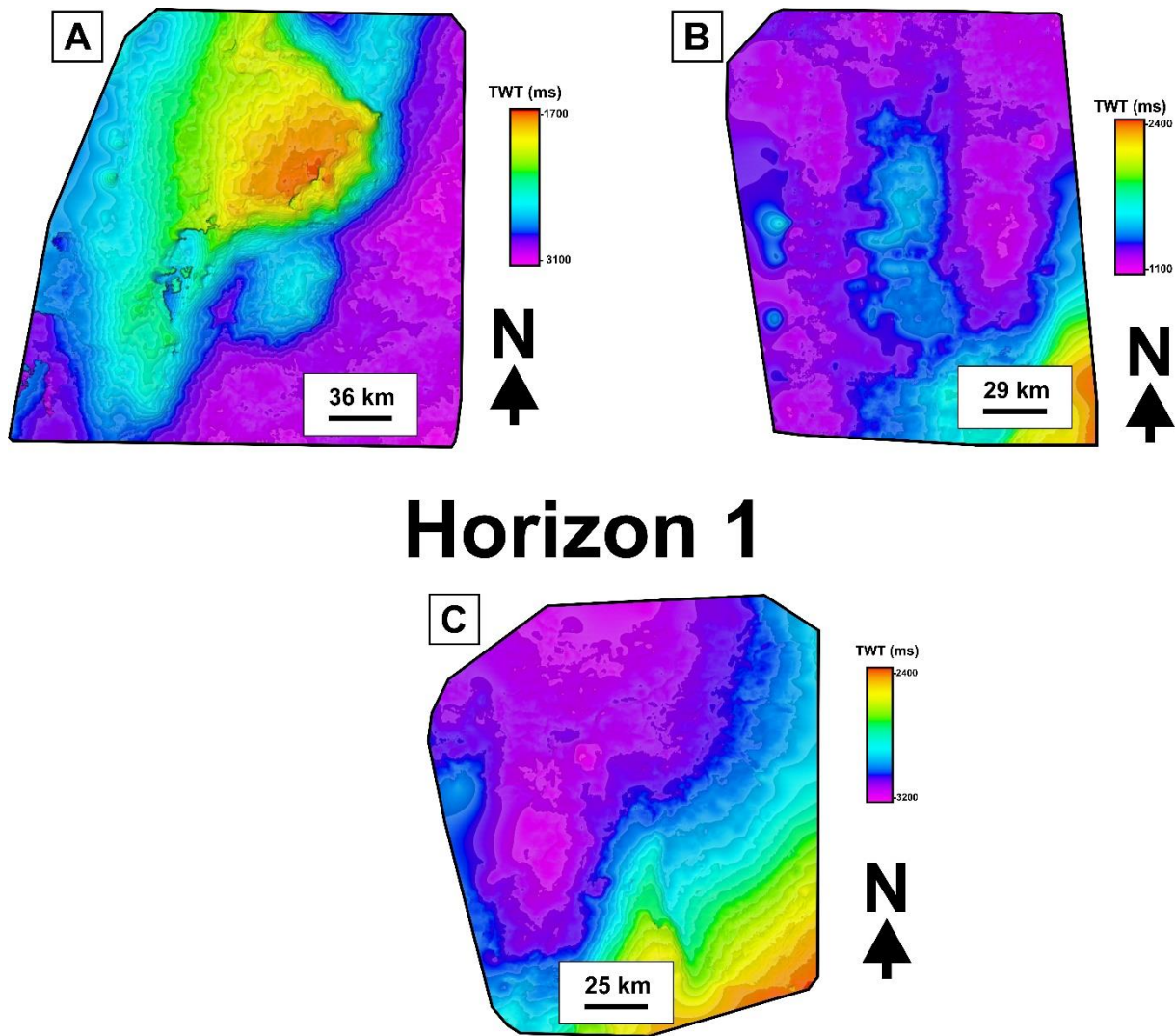


Figure 38: Time depth map of horizon pick one across A.) ST11MZ07 B.) ST98MZ C.) NX0802. (Vertical Exaggeration: 1)

Horizon 1 represents the time depth map (in two-way travel time) underlying a known event associated with the late Jurassic to early Cretaceous of the Mesozoic shown in Fig.38. See Fig.36 for associated seismic units. Hence, a distinct facies event and association.

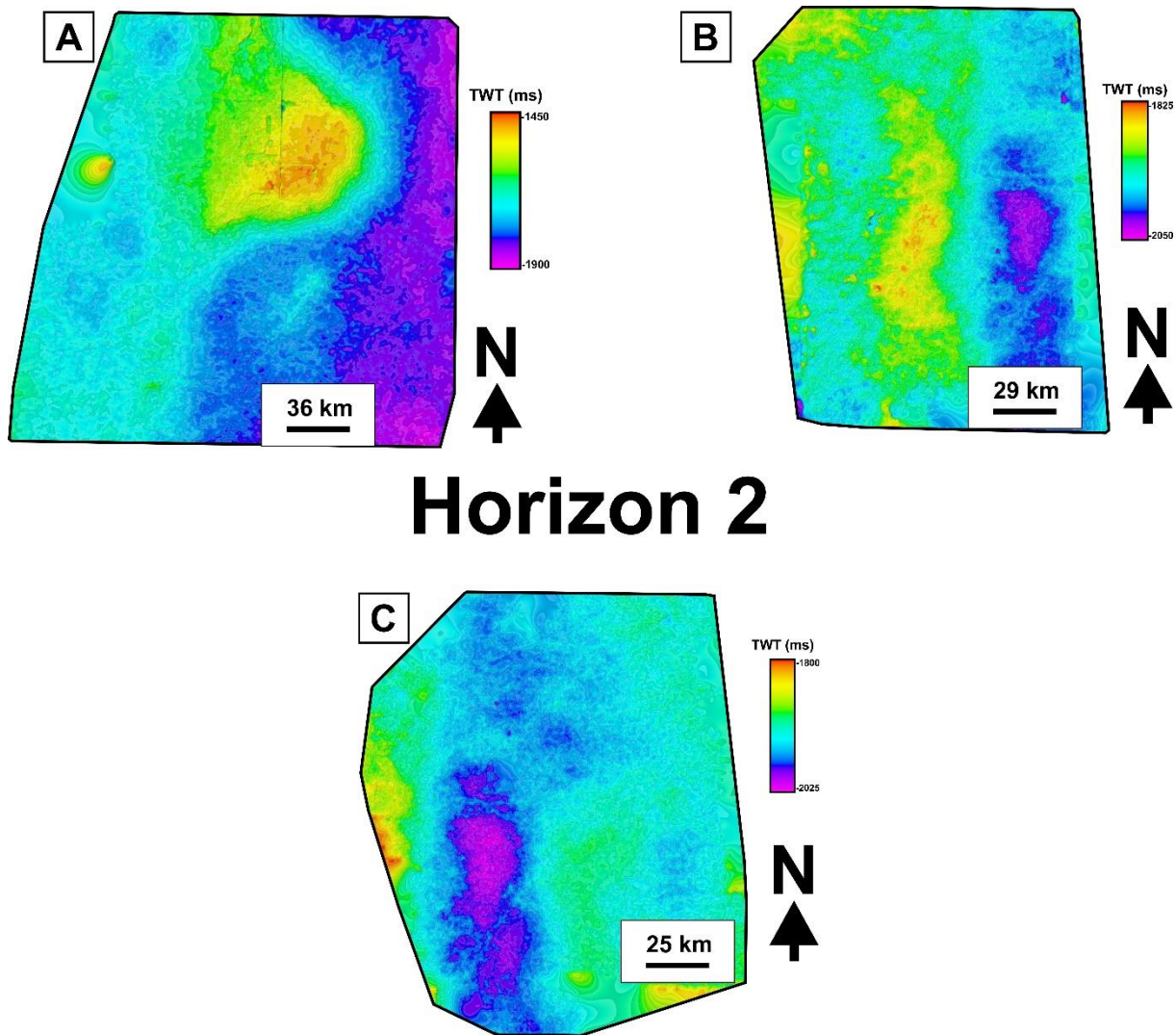


Figure 39: Time depth map of horizon pick two across A.) ST11MZ07 B).ST98MZ C).NX0802 (Vertical Exaggeration: 1)

Horizon 2 represents the time depth map (in two-way travel time) underlying a known event associated with the late Jurassic to early Cretaceous of the Mesozoic shown in Fig.39. See Fig.36 for associated seismic unit subdivision (this isn't easy to subdivide as there are chaotic reflections) Hence, a distinct facies event and subdivision association. It consists of the Cromer Knoll Group, Shetland Group, Hordaland Group and part of the Rogaland Group (section 4 describes this has been dominated by mudstone, siltstone and fine-grained sediment dominated).

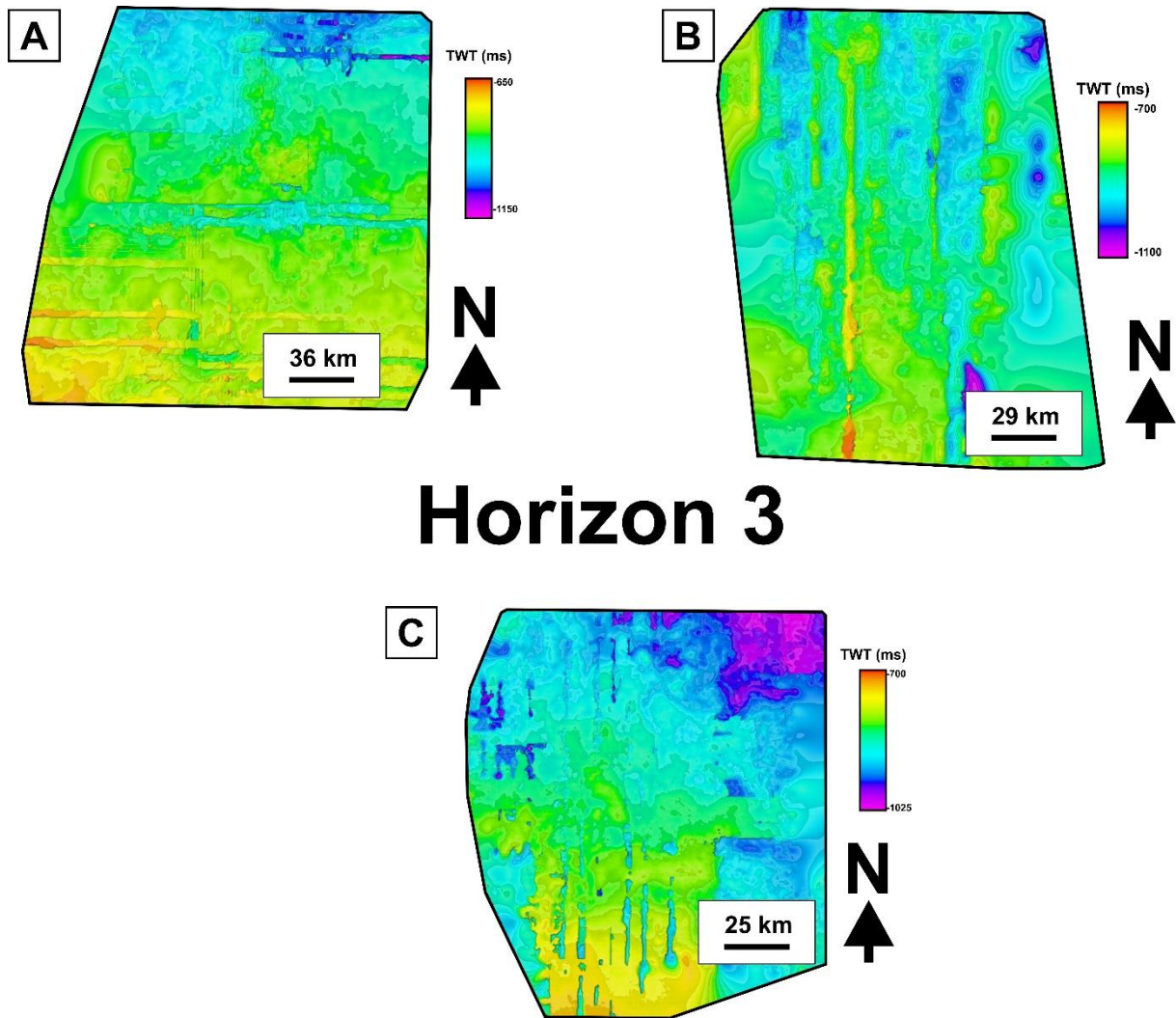


Figure 40: Time depth map of horizon pick 3 across A.) ST11MZ07 B).ST98MZ C).NX0802 (Vertical Exaggeration: 1)

Horizon 3 represents the time depth map (in two-way travel time) overlaying a known event associated with an unconformity within the Nordland group of Paleogene age of the Miocene to Pliocene epoch. shown in Fig.40. See Fig.37 for associated seismic units (this was a problematic horizon pick, hence manually adjusted within Corel draw). Hence, a distinct facies event and subdivide association. It was described as consisting of marine claystone (a reference to section 4.2 for underlying lithology)

## 10.2.1 Seismic Unit & Facies Descriptions

Table 6: showing examples of seismic units and seismic descriptions of their facies units obtained from a 3D seismic cube of Nx0802. Terminologies and reflection descriptions used were obtained from Løseth et al.(2009) and Badley (1985)

Nx0802- Examples		Description of reflections
<b>Cenozoic</b>	<p>XL- 15719 TWT (ms) Seafloor 2.6 km</p>	<p>Distinct seismic reflectors, parallel to subparallel, continuous reflection, with medium to high amplitudes and high frequency exhibited towards the seafloor of seismic cube NX0802</p>
	<p>XL- 15719 TWT (ms) Horizon 3 Mounded Jackup Discordant amplitude anomalies / chaotic reflections 5 km</p>	<p>Chaotic seismic reflections characterized by discontinuities in reflection, low amplitudes and low frequency. Underlying a continuous reflection above. It has faults and fractures initiated by the discontinuous amplitude anomaly.</p>
	<p>XL- 15719 TWT (ms) Cross cutting Reflections Dampened and Cross cutting Reflections Horizon 2 4.4 km</p>	<p>Low Dampened reflectors. Cross cutting and chaotic reflections sandwiched between interpreted Horizon 2 and Horizon 3.</p>
<b>Mesozoic</b>	<p>XL- 15719 TWT (ms) Horizon 1 Continuous Reflections Sagging Reflections 4.4 km</p>	<p>High amplitude reflectors, chaotic at different intervals. Reflectors are sagging to form synclines deeping downwards to the north of up to 50 ms. With an infilling of continous, reflections of high to medium amplitude and low frequency/spacing as seen below interpreted Horizon 1(base Cretaceous)</p>

Table 7: showing examples of seismic units and seismic descriptions of their facies units obtained from a 3D seismic cube of ST98M7. Terminologies and reflection descriptions used are obtained from Løseth et al.(2009) and Badley (1985)

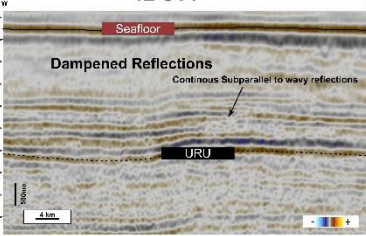
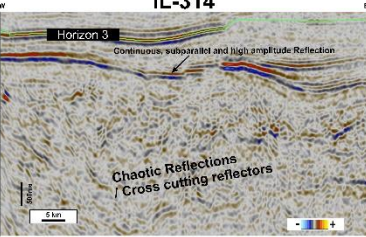
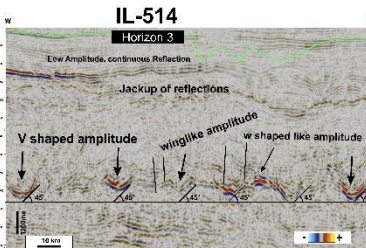
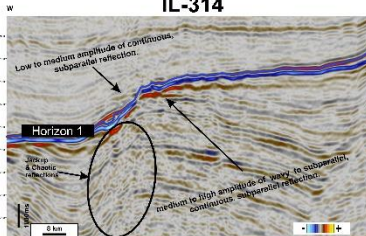
	ST98M7- (Examples)	Description of reflections
<b>Cenozoic</b>	<p style="text-align: center;">IL-314</p>  <p style="text-align: center;">TWT (ms)</p>	<p>Dampened reflections to the seafloor of seismic cube ST98M7, with continuous reflections of high amplitude about 150ms twt. Followed by discontinuous, low amplitude and low frequency reflectors.</p>
	<p style="text-align: center;">IL-314</p>  <p style="text-align: center;">TWT (ms)</p>	<p>Chaotic fills and discontinuous reflections at the base, overlain by continuous, subparallel and high amplitude reflections at the top</p>
	<p style="text-align: center;">IL-514</p>  <p style="text-align: center;">TWT (ms)</p>	<p>Low to medium amplitudes, of continuous, subparallel reflections at the top overlying chaotic reflections with distinct v, w, and winglike amplitude anomaly. Distinct v, w and winglike anomaly have a distinct angle of 45°. Sections of v and w amplitude anomaly have fractures between. V and w amplitude anomaly has a width measured to be at about 625ms in TWT.</p>
<b>Mesozoic</b>	<p style="text-align: center;">IL-314</p>  <p style="text-align: center;">TWT (ms)</p>	<p>Low to medium amplitudes, of continuous, subparallel reflections, overlying medium to high amplitude of wavy, to continuous, subparallel reflections with chaotic reflectors to the left.</p>



Table 8: showing examples of seismic units and seismic description of its facies unit obtained from 3D seismic cube of ST11MZ07. Terminologies and reflection descriptions used are obtained from Løseth et al.(2009) and Badley (1985)

ST11MZ07- (Examples)		Description of reflections
<b>Cenozoic</b>		<p>Subparallel reflections of high amplitude towards the seafloor with, charged very high amplitude anomaly close to the seafloor of 300ms in height at the top of reflections. Followed by masking of reflections and somewhat subparallel reflections with low amplitudes and contorted reflection and base of low amplitude.</p>
		<p>Continuous reflections of medium amplitude overlying, contorted reflections. Heavily faulted and with fractures ranging from 260ms to 70ms in two way travel time. Low amplitudes underlying continuous to contorted reflections with distinct, steeping v to w amplitude anomaly of width ranging from 280m to 660m.</p>
<b>Mesozoic</b>		<p>Low amplitude divergent reflection to the west and low amplitude overlying high amplitude divergent continuous, wavy reflection downwards located down throw of an interpreted fault line.</p>

## 10.4 Seafloor Morphology and Description of Seabeds Surface

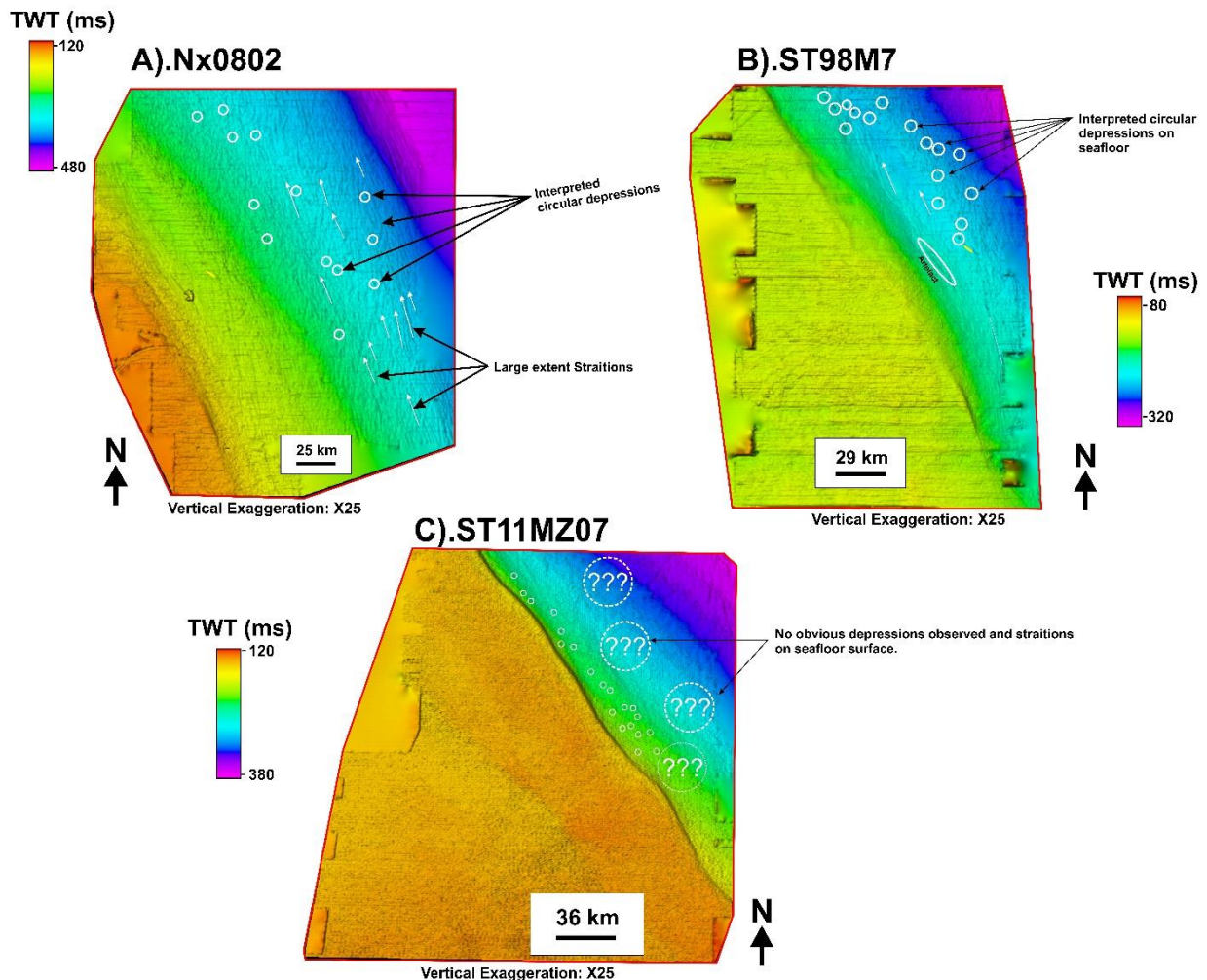


Figure 41: showing an interpreted seafloor surface of 3D seismic cubes corresponding to A). NX0802, B). ST98M7, and C). ST11MZ07 with a vertical exaggeration of 25.

Nx0802 interpreted seafloor surface, as shown in Fig. 41a, shows several circular depressions ranging from roughly 100m to 250 m in size from ruler tool on 2D. Depressions observed are highlighted with circles (re-described in Fig.43), showing distinct circular-shaped depressions visible on interpreted seafloor surfaces and seismic sections in Fig.43C. Circular depressions observed trend southeast to northwest on the seafloor. The lined arrows (referencing Fig.43) indicate somewhat extensive activities of elongated striations on the seafloor, trending similarly to the circular depressions identified on the seafloor.

Fig. 41b shows an interpreted seafloor surface from ST98M7 3D cube with distinctly noticeable depressions (redescribed Fig.42). Also, the sizes of circular depressions range from 110m to as large as roughly 300m from the interpreted seafloor surface from measurements obtained from ruler tool of the seafloor. Arrowhead direction shows likely interpreted striation directions observed on the interpreted seismic seafloor surface of the seismic cube, with distinct striations concentrated on the northeast section of the seafloor surface falling within the Norwegian trench. The southeast section lacks seismic data coverage to be considered part of the interpretation.

ST11MZ07 of the interpreted seafloor surface, shown in Fig.41c, seems to be lacking in these striations, which is very well identifiable on the interpreted seafloor surface both in NX0802 and ST98M7, indicated by the dashed circle with question mark symbols. Small circles of sizes 80 to 90m are identified but not as distinct as the pockmarks identified in NX0802 and ST98M7. Small depressions can be misinterpreted as depressions that might have resulted from the vertical exaggeration of 25 or as an artefact.

A further analysis, consisting of a zoomed-in interpretation, with an interpretation window of seismic with corresponding seafloor surface are shown in Fig. 42 (ST98M7), Fig.43 (NX0802), and Fig.44 (ST11MZ07).

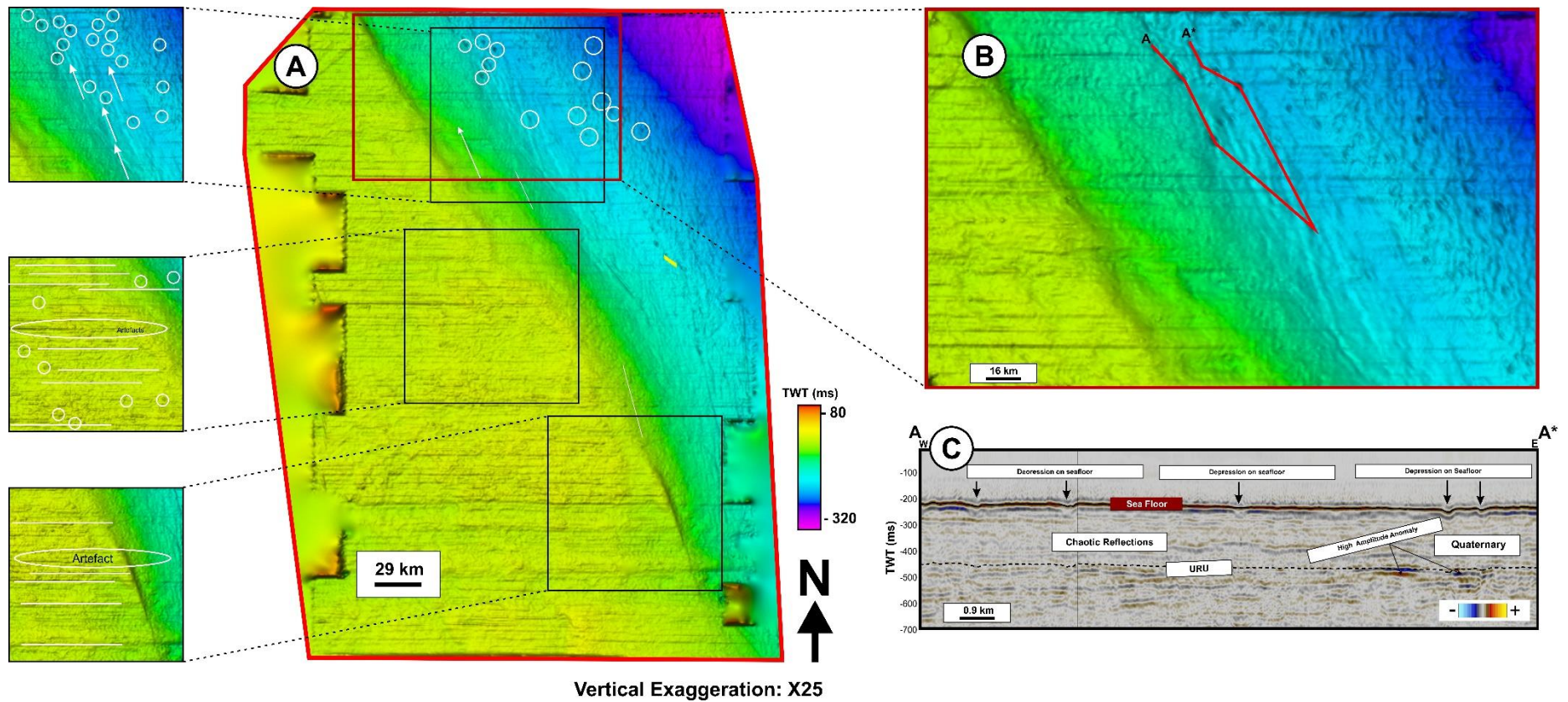


Figure 42: Showing an image of A). Corresponding to the interpreted seafloor surface of ST98M7 B). Zoomed in section of seafloor surface with a random line (A-A') C). A random line showing an interpretation window transecting depressions on seafloor surface at a vertical exaggeration of 25 with a dashed line indicating the URU (Upper Regional Unconformity) within the Quaternary.

Fig.42a shows an interpreted seafloor surface from a 3D seismic cube corresponding to ST98M7. Interpreted seafloor surface has a structural high in two-way travel time (twt) depth, towards the southwest and a structural low towards the northeast, as indicated by the time depth map. Depressions observed on seafloor surfaces are seen and observed towards the northeast section of the seafloor surface at a vertical exaggeration of 25. Circular depressions are observed on the structural low of the seafloor surface map in the northwest section, while the southeast section lacks data and has few to no circular depressions. The circular depression seen in the northeast could be an artefact created by extrapolating surface data from areas with poor seismic coverage.

Fig. 42b shows a zoomed section of ST98M7 capturing some of the circular depressions observed and highlighted with a dark circle. A random line of (A-A') in transecting circular depression is shown in Fig.42c. Each circular depression measures roughly 220m in width on the seafloor surface and about 270m in width from the interpreted window surface. A depression of about 15m was measured from the interpretation window ruler. This might be an artefact or a natural expression.

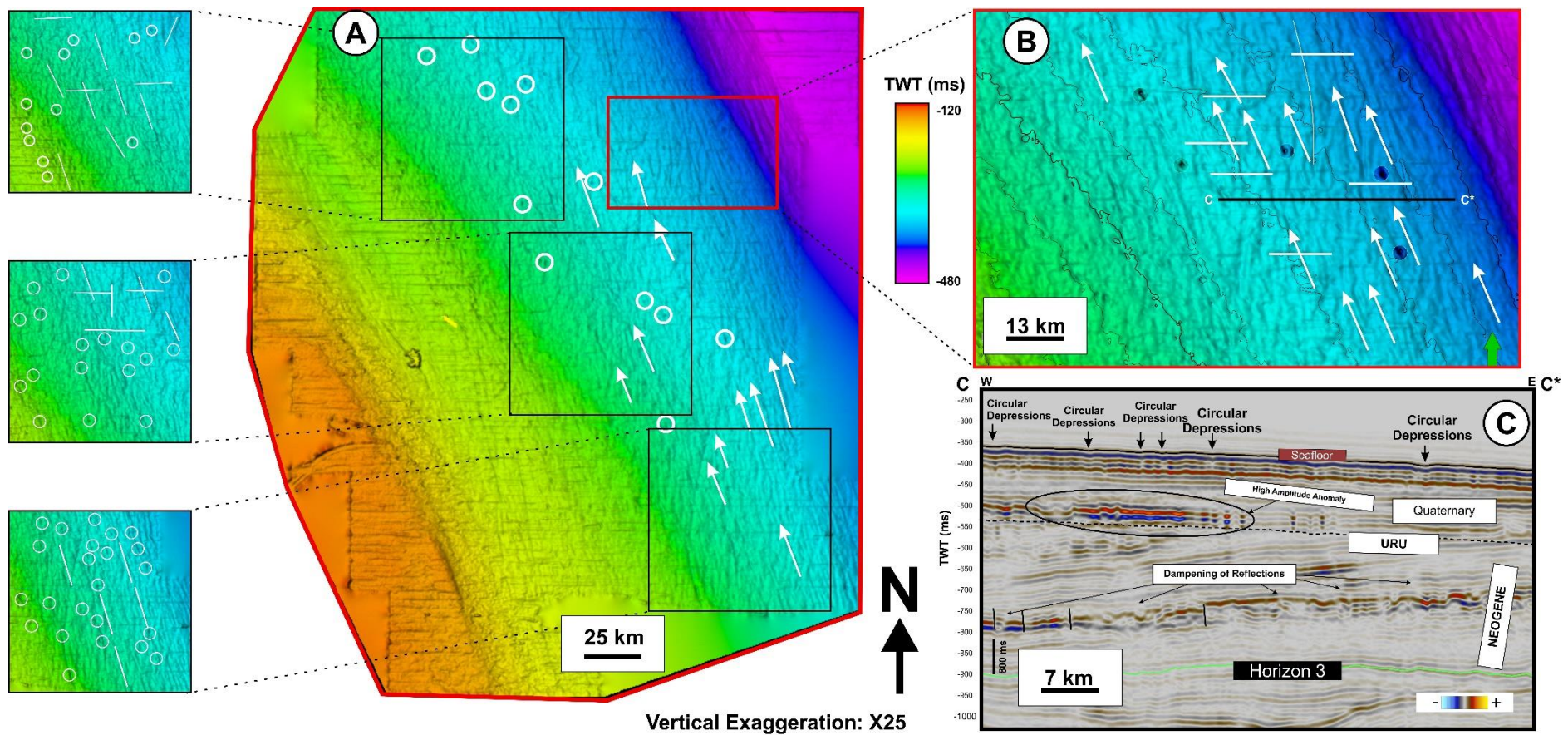


Figure 43: Showing an image of A). The corresponding surface of NX0802 B). Zoomed in section of seafloor surface with a random line (C- C\*) C). A random line obtained from (B) seafloor surface at a vertical exaggeration of 25 with a dashed line indicating the URU (Upper Regional Unconformity) within the Quaternary.

Fig.43a shows several circular depressions littered on the seafloor surface of NX0802, marked by several circles showing such depressions. The Arrowhead line shown indicates identified, long elongated lineation and striations observed on the interpreted seafloor surface. Circular depressions and striations are more intense towards the northeast than the southwest section. Circular depressions are also much smaller in size in comparison to depressions seen on the ST98M7 seafloor surface. Circular depressions are about 87 m to 170m in width measured from interpreted seafloor surface. The striations are trending northwest to southeast in directions.

Fig.43b shows an up-close, zoomed section of the interpreted seafloor surface, which shows parallel striations and striations cutting across the parallel marks, lines indicated by arrowhead. Striations can be due to artefacts or marks created by vertical exaggerations on the seafloor surface, especially in the direction in which the seismic vessel acquires the data.

Fig.43c shows an interpreted seismic line of (B- B\*) obtained from Fig.43b. The Interpreted seismic line of (B- B\*) shows a distinct circular depression reflecting on the seafloor with depth as little as 3m measured from the interpretation window. A closer look at Fig. 43b shows cross-cutting lines on the seafloor.

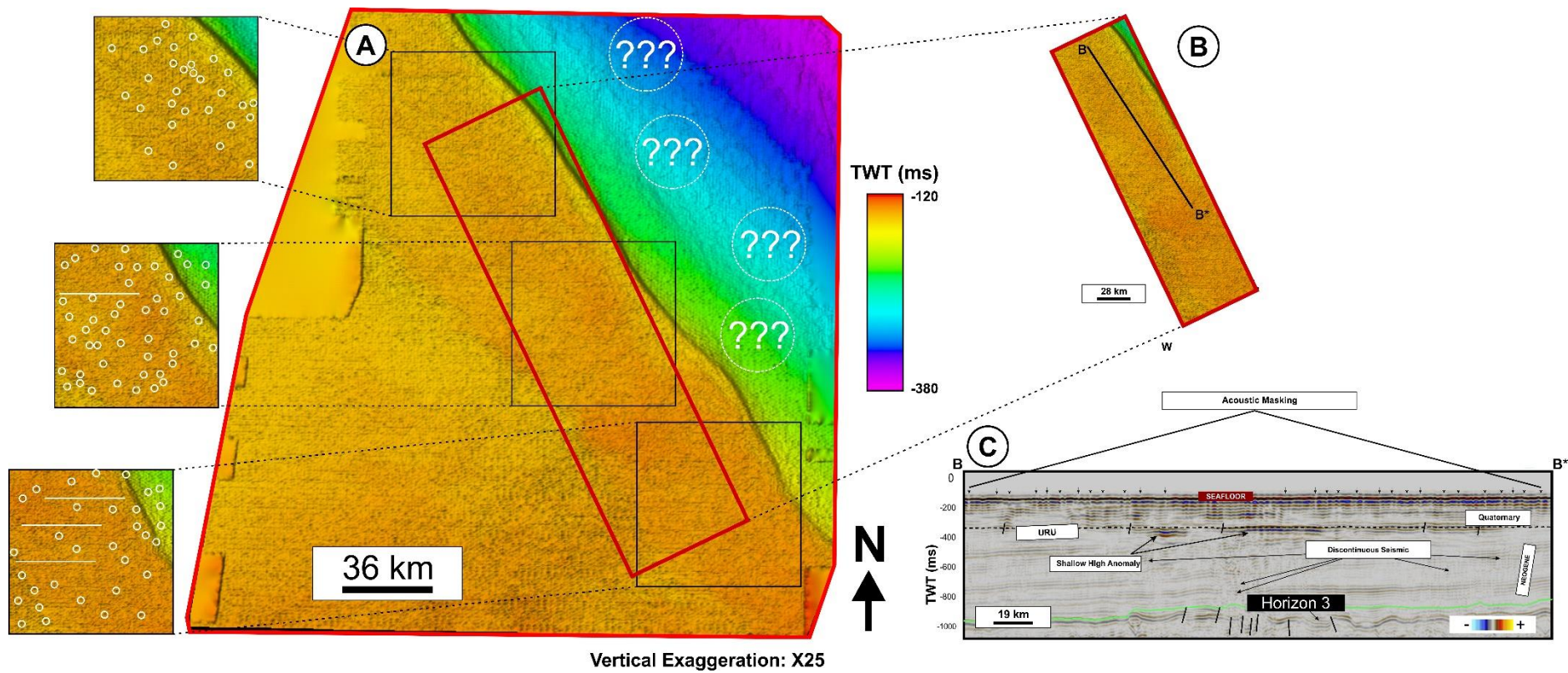


Figure 44: Showing an image of A). The corresponding surface of ST11MZ07 B). Zoomed in section of seafloor surface with a random line (B- B') C). A random line was obtained from B seafloor surface at a vertical exaggeration 25.



Fig. 44a shows the interpreted seafloor surface from a 3D seismic cube of ST11MZ07. The circle with question marks shows that the distinct depressive features observed on other 3D seismic cubes corresponding to ST98M7 and NX0802 are not noticeable on the interpreted seafloor surface. The time-depth map of the interpreted seafloor surface shows a distinct contrast between a structural high towards the southwest and a structural low towards the northeast part of the seafloor map.

Fig. 44b shows a zoomed section of a seafloor map containing an intersecting random line (B-B') obtained from the seafloor. Fig. 44c of the line shows depressions marked by circles, but they are not distinct enough concerning depression and width compared to the two previous 3D cubes. These tiny depressions are noticeable and more persistent in contrast to depressions on previous seismic cubes with much more frequent spacing between depressions.

## 10.5 Fluid Indicators on Seismic Sections (High Anomaly)

### 10.5.1 Shallow amplitude anomalies towards the seafloor.

Shallow distinct and high amplitude anomalies were observed towards the interpreted seafloor surface on all 3D seismic cubes corresponding to ST11MZ07, NX0802, and ST98M7. The seismic attribute root mean square amplitude (RMSA) was used along time-shifted surfaces with Search windows above this surface. The surface generated and utilised with the corresponding search window is seen on interpreted window on the left, near high amplitude anomalies, as shown in some examples;

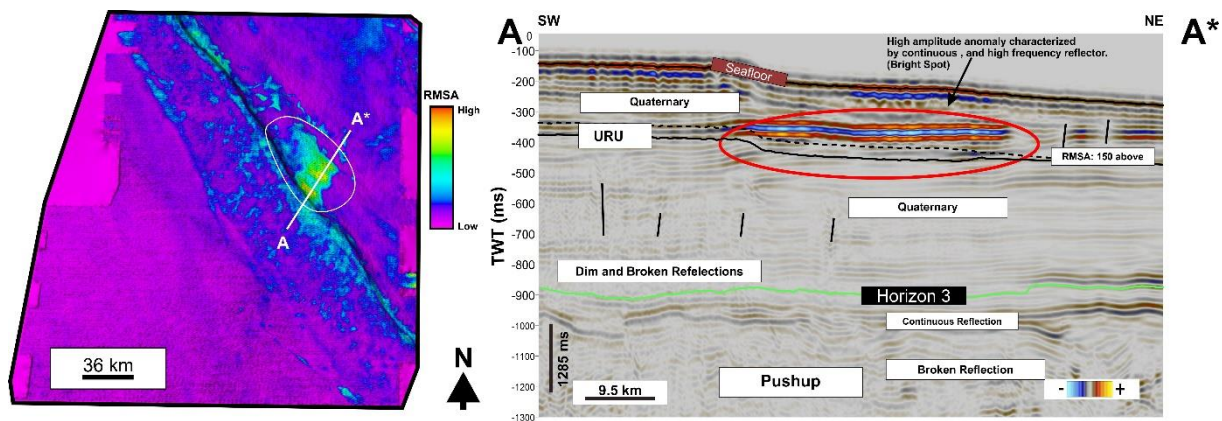


Figure 45: showing shallow amplitude anomaly from a seismic 3D cube of ST11MZ07 mapped with a search window of 150ms (twt) above surface interval to map out shallow anomalies towards the seafloor. Line A-A\* represents an arbitrary line transecting shallow anomaly indicated by a red circle. (Note: the vertical exaggeration of the RMSA map is 7.5.)

Fig.45 shows a root mean square amplitude (rmsa) to the left attribute ran along a time-shifted surface indicated on the interpretation window to the right. Search window values were determined using a horizon probe to capture areas of high amplitude interval above the surface to the seafloor. High amplitude anomalies are concentrated towards the northeast of the RMSA map to the left, separated by a line separating a structural high (southwest) from a structural low (northeast). High amplitude anomalies are marked by a circle on the RMSA map, and to the left shows the high amplitude anomaly mapped to be at a height interval of 300 to 350ms in twt (two-way travel time) from two-way travel time.

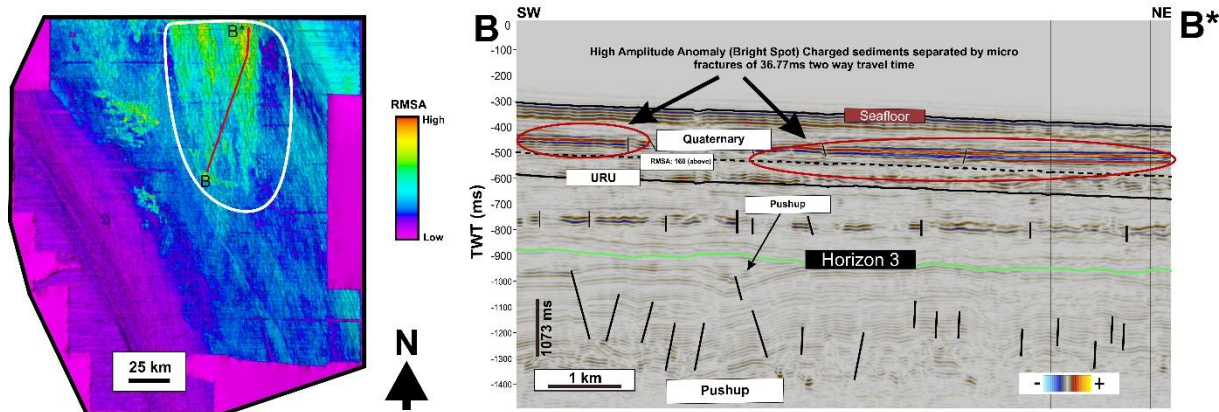


Figure 46: showing shallow amplitude anomaly from a seismic 3D cube of NX0802 mapped with RMSA with a search window of 160ms (twt) above to map out shallow anomalies towards the seafloor. Line (B-B\*) represents an arbitrary line transecting shallow anomaly indicated by a red circle. (Note: the vertical exaggeration of the RMSA map is 7.5).

Fig.46, similarly, from a 3D seismic cube of NX0802, shows an RMSA attribute map to the left indicating high and low amplitude anomaly, with an arbitrary line (B-B\*) showing an interpretation window (160ms) capturing areas of high amplitude anomaly to the right. The Shallow amplitude anomaly indicated using a white circle on the RMSA map to the left is separated by observed measured microfractures (manually) of roughly 36.77ms in TWT (ms) with no noticeable displacement in reflections separating shallow amplitude anomalies. The anomalies occur at an interval of between 400ms and 500ms in two-way travel time towards the seafloor. A 160ms (twt time) search window was used from the time-shifted horizon to map such high amplitude anomaly from the dashed surface indicated on the interpretation window to the left.

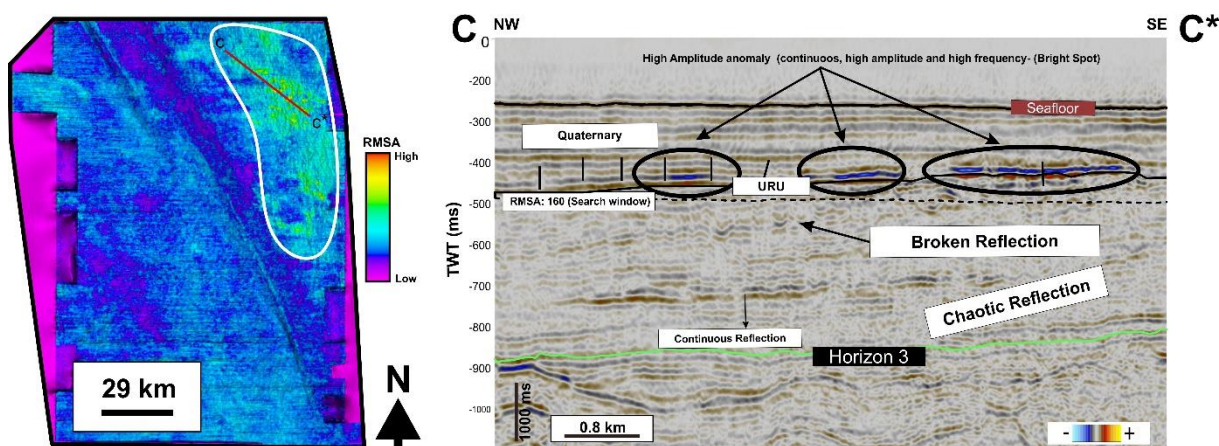


Figure 47: showing shallow amplitude anomaly from a seismic 3D cube of ST98M7 mapped with RMSA with a search window of 160ms (twt) to map out shallow anomalies towards the seafloor. Line (C-C\*) represents an arbitrary line transecting areas of shallow anomaly from one of the 3D seismic cubes. (Note: the vertical exaggeration of RMSA map is 7.5).

Fig.47, similarly, an RMSA attribute map to the left, showing amplitude anomalies indicating both high and low amplitude anomalies. Interpretation to the right was generated using an

arbitrary line (C-C\*) to intersect areas of high amplitude anomalies. This given example has a micro-fracture of about 60ms in TWT (two-way travel time) with no noticeable displacement. Shallow amplitude anomaly occurs at an interval of between 400ms to 500ms TWT. Amplitude anomaly in this section is concentrated towards the northeast section, as seen on the RMSA map to the left. Also, the amplitude anomaly is not as high as the shallow amplitude anomaly mapped on previous 3D seismic cubes of ST11MZ07 and NX0802. A dampening in amplitude anomaly is observed on the interpretation window of the ST98M7 but is still distinct on the interpretation window to the right.

In general, the intensity of these observed shallow high amplitude anomalies is concentrated and limited to the downslope of ST11MZ07 cube, and more spread out and concentrated towards the northeastern sides of the NX0802 cubes.

10.5.2 Occurrence of V, W, and winglike amplitude anomalies with associated structures.

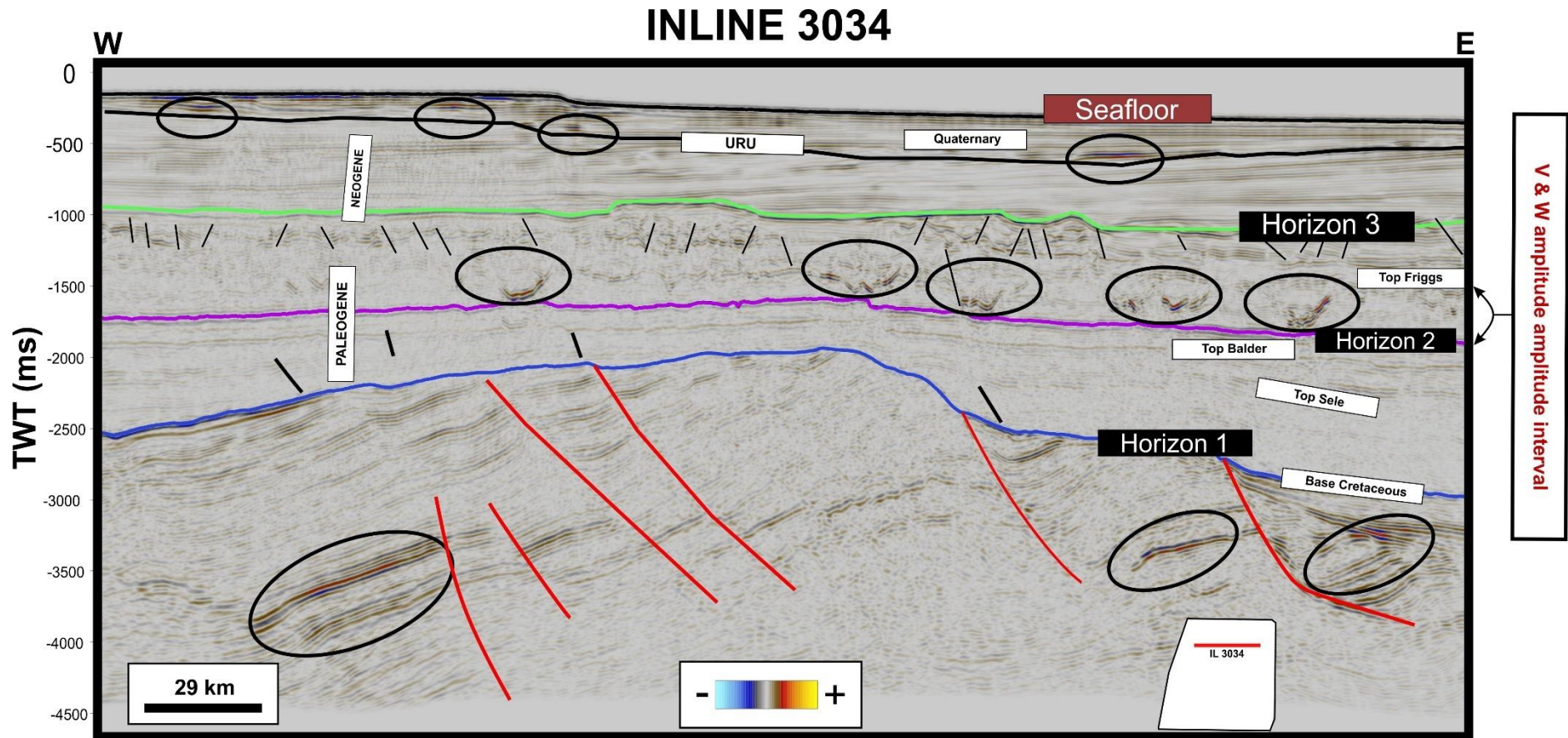


Figure 48: showing an interpretation window of inline 3034 from a 3D cube corresponding to ST11MZ07 showing amplitude anomalies, with horizon subdivisions and major (Large faults) faults and minor faults (basis as been previously established)

Fig.48 shows an inline of 3034 obtained from seismic cube ST11MZ07. With major seismic subdivisions of stratigraphy from existing works of literature. Elliptical circles map out areas of high amplitude anomalies occurring towards the seafloor, between Horizon 2 and Horizon 3, with a v, w, and a winglike structure of high amplitude anomalies. High amplitude anomalies at the bottom of seismic below horizon 1 are associated with more considerable faults. Seismic units between horizon 2 and horizon 1 are much quieter with little to no structure, which are areas somewhat inferred roughly to as Top Balder and Top-Sele formations. However, some parts of cubes are characterized by faults in areas with intense uplift.

Fig.48 also shows manually interpreted faults and fractures associated with different events. Red lines indicate the major/ Large faults occurring below. In contrast, the black lines represent a summation of minor faults and possible fractures occurring at the top of v, w, and winglike-shaped amplitude anomalies.

A particular focus on the v, w and winglike anomaly has shown in intervals of v, w and winglike amplitude anomaly of Fig.48, between Top Frigg's and Top Balder formation shows this high amplitude anomaly to be increasing eastwards and more pervasive in occurrence on the eastern section of interpretation window shown in Fig.48. A further analysis of the occurrence of this v, w, and winglike amplitude anomaly is shown in Fig. 49, 50 and 51, regarding timeslices obtained across subdivisions of inline 3034. V, w, and winglike type amplitude anomaly are bound to around 1400ms to 1650ms of seismic subdivisions for ST11MZ07, not factoring other cubes whose occurrence varies. They occur in width sizes ranging from as low as about 500m to as high as 1500m measured from the ruler tool of the interpretation window.

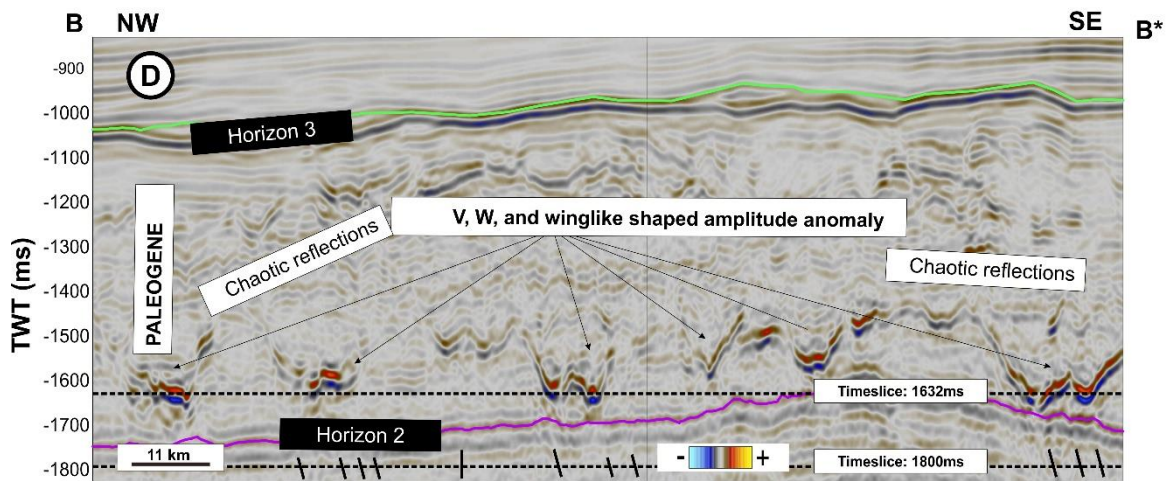
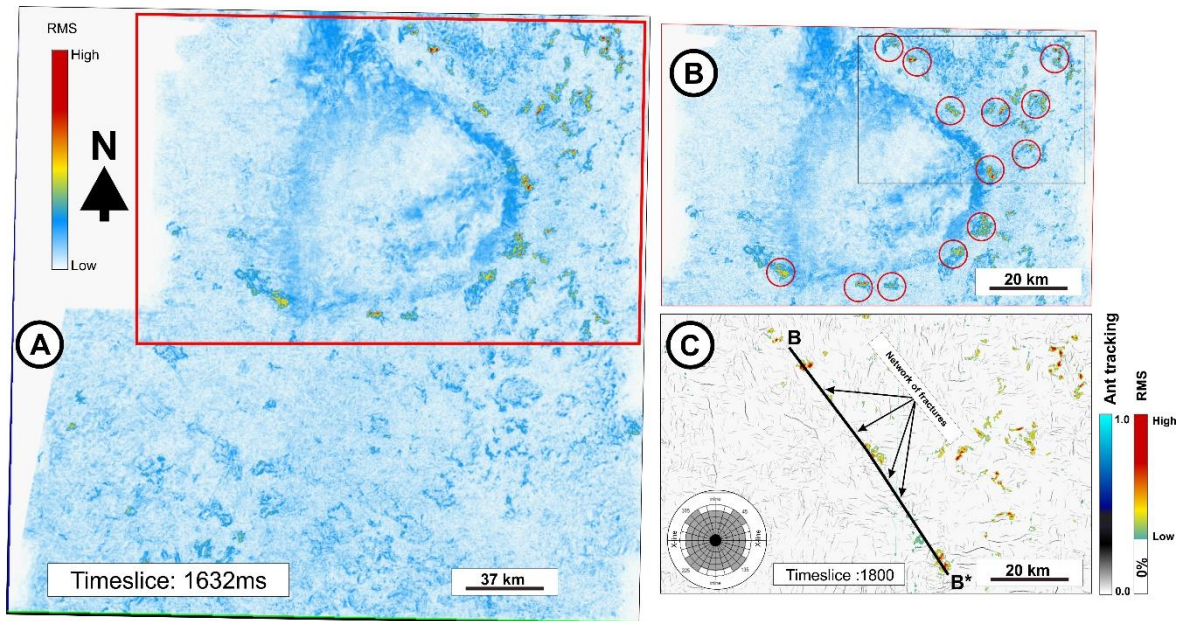


Figure 49: showing A). Distribution of v, w and winged-shaped anomaly with an RMSA time slice of 1632 from ST11MZ07 B). Zoomed in section of this anomaly on a RMSA at 1632 C). An ant tracking timeslice at 1800 with an adjusted RMSA opacity. D). An interpretation window showing an example of these anomalies with corresponding fractures beneath.

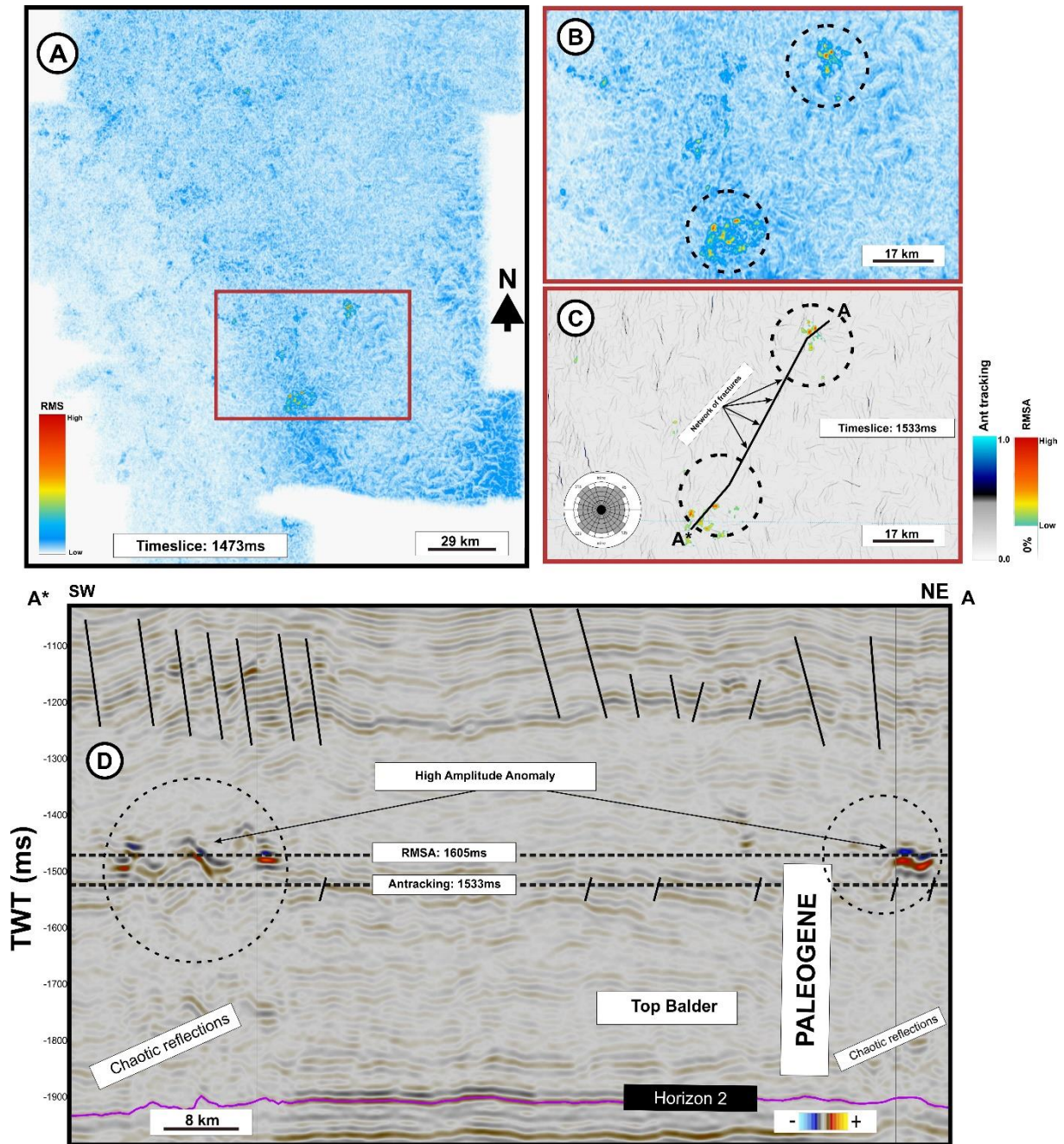


Figure 50: showing A). Distribution of  $v$ ,  $w$  and winged-shaped anomaly with an RMSA time slice of 1473 from NX0802 B). inset image of this anomaly from RMSA at 1473ms C). An ant tracking attribute time slice was obtained at 1533ms with an adjusted RMSA opacity. D). An interpretation window showing an example of these anomalies with corresponding fractures highlighted beneath NX0802



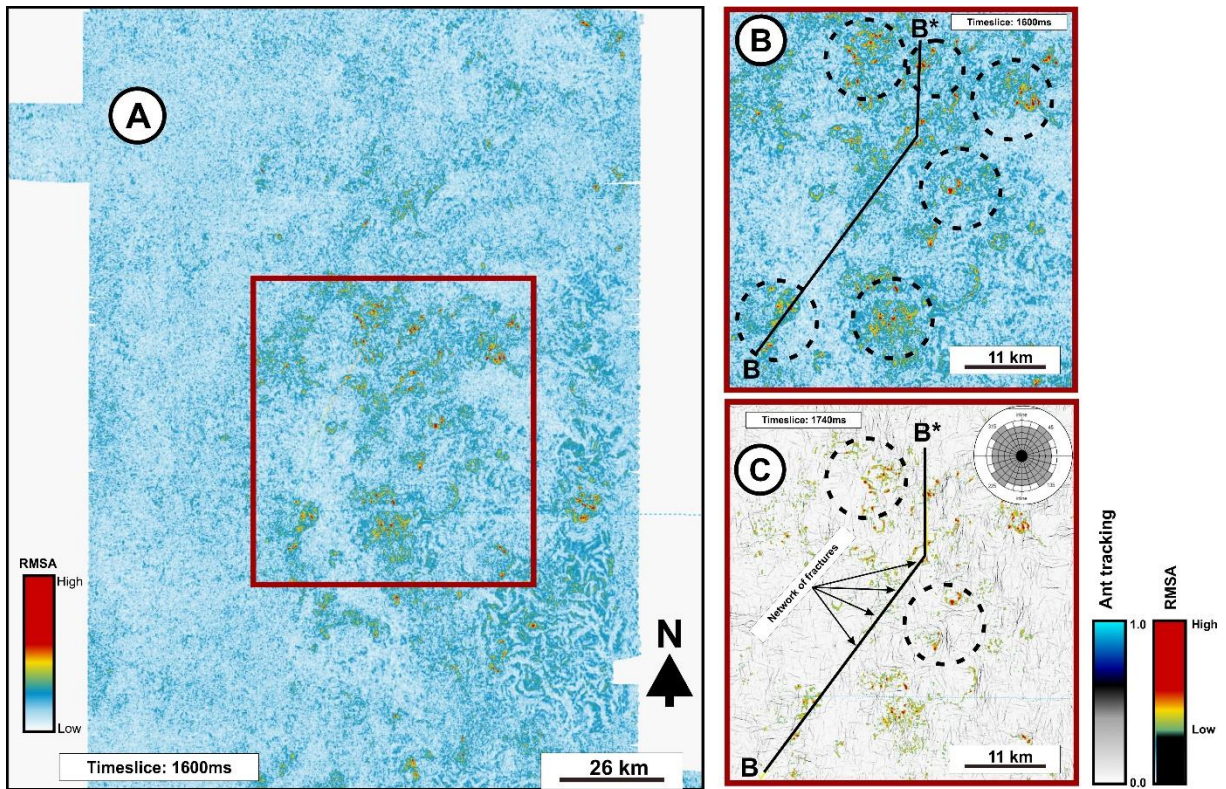


Figure 51: showing A). Distribution of  $v$ ,  $w$  and winged-shaped anomaly with an RMSA time slice of 1600ms from ST98M7 B). Inset image of this anomaly on an RMSA at a time slice of 1600ms C). An ant tracking attribute time slice obtained at 1740ms with adjusted RMSA opacity D). An interpretation window showing an example of these anomalies with corresponding fractures beneath.

Fig. 49, Fig. 50, and Fig.51 shows the distribution of this pervasive high anomaly across the interpreted seismic cubes and its occurrence using time slices above this structure and across the structure itself to highlight potential structures such as fractures that might be associated with the formation of this structure as seen in the composite images. Note that the event that occurred above interpreted Horizon 2, which was earlier defined facies-wise.

The formation of these structures is underlain by some fractures, as shown in Fig. 49c, 50c, and Fig. 51c. These were intended to be picked up with ant-tracking variance attributes using the aggressive and stereo net parameters experimentally (inset and crossline dips might be wrong). Fig. 49 shows a higher occurrence of this v, w, and winglike anomaly in comparison with other seismic cubes in both Fig. 50 and Fig. 51. Also, there is an increase in fracture occurrence probably associated with an intense uplifted reflection seen more to the northwest in seismic cube ST11MZ07 and described in terms of facies and distinct events. These anomalies have almost similar characteristics, such that they are characterized by chaotic reflections underlying them and overlying them slightly in some cases below the Top Balder formation (subjective no well log basis or distinct boundary for this) and interpreted Horizon 2.

The pervasiveness of this distinct anomaly in Fig. 49 is more established and higher than that of Fig.50 and Fig.51, as shown by composite seismic transecting this high amplitude anomaly distribution.

Orientation-wise, high amplitude anomaly occurs more to the northeast in Fig.49, while in Fig. 50, this anomaly occurs sparsely to the south. In Fig.51, the distribution of this high anomaly occurs more to the northwest.

### 10.5.3 Deeper amplitude anomalies

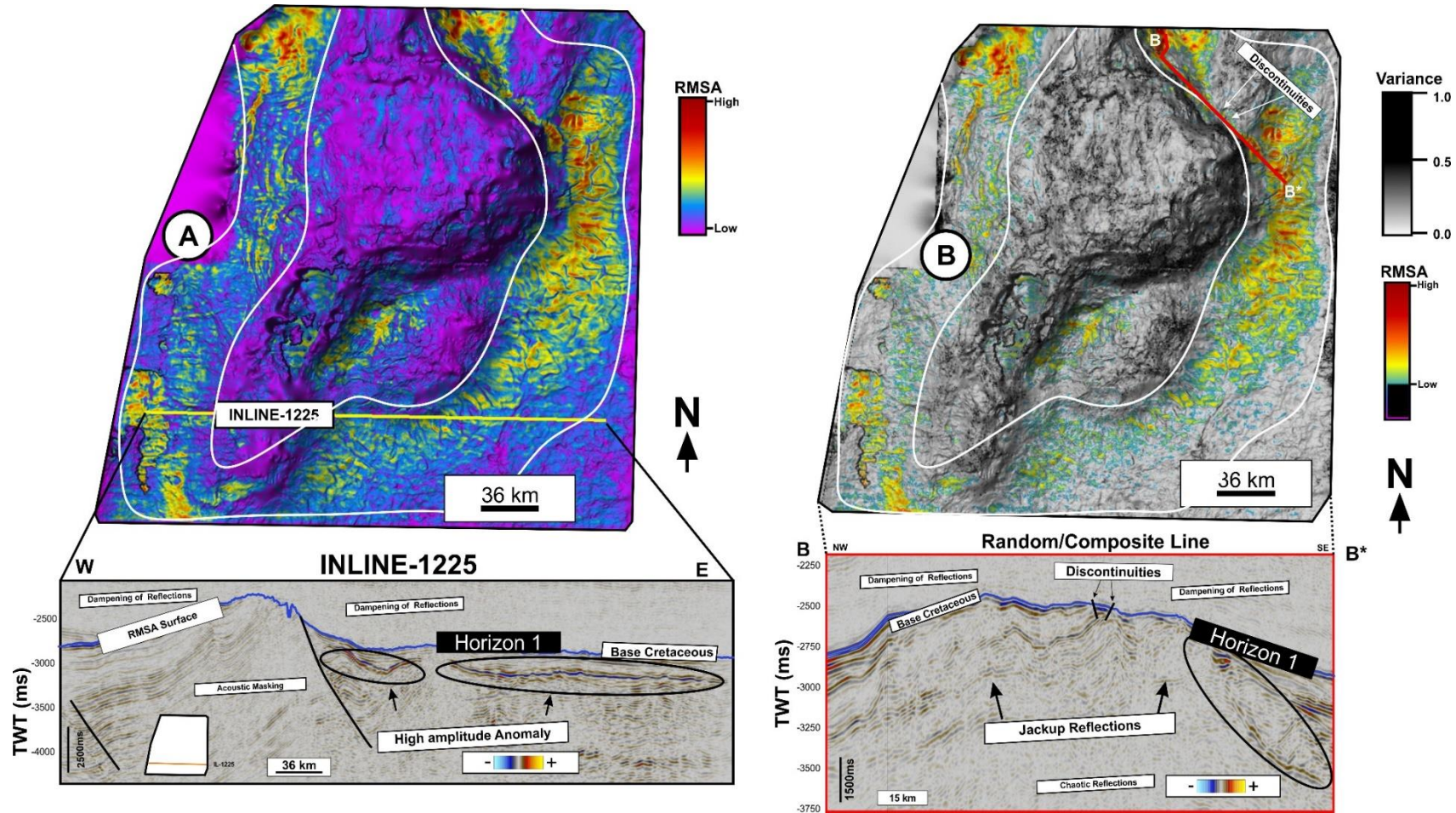


Figure 52: shows a composite image of A). An RMSA attribute along interpreted surface (Horizon 1) of an uplifted structure located at a depth of -2250ms in two-way travel time, showing high amplitude anomalies along the interpreted horizon from ST11MZ07- 3D cube (note that no search window was used and concentric circles highlights brightened amplitude beneath) B). A combination of adjusted RMSA opacity and variance along this surface with discontinuities with a corresponding arbitrary line of (B-B\* on the interpretation window) and horizons/ surface are at a vertical exaggeration of 7.5).

Fig.52 shows a deep-seated structure characterised by an intense uplift on the northeast section of ST11MZ07. In two-way travel time, the surface was generated overlapping uplifted regions at depths below 2500ms along Horizon 1. This was done to map high anomalies located at depth below, characterised by high amplitude anomalies and deep-seated structures identified on seismic profiles.

Fig.52a shows an RMSA map generated across horizon 1, noted by the blue line seated at a depth below 2500ms in the two-way travel time of ST11MZ07. The highest amplitude anomaly extends at the trough of this structure and is more intensely associated with this uplifted folding and probable fractures induced around this uplifted structure. An identified decollement surface was associated with this intense uplifted structure with a high amplitude anomaly terminating on such surface, as shown on the seismic interpretation line in Fig.52a manually

Fig.52b combines the variance map and an opaque adjusted RMSA map, to show induced fractures and discontinuities. Most representations on the surface might be artefacts due to chaotic reflections across uplifted folds of the 3D cube on which the surface was interpreted (Fig.52). A somewhat identified discontinuity was observed on the variance map, projected by a random line of (B-B\*). These discontinuities reveal fractures cutting interpreted surface upon which RMSA and variance were taken from Fig. 52b (see image)

## 10.6 Fault Description and Orientation

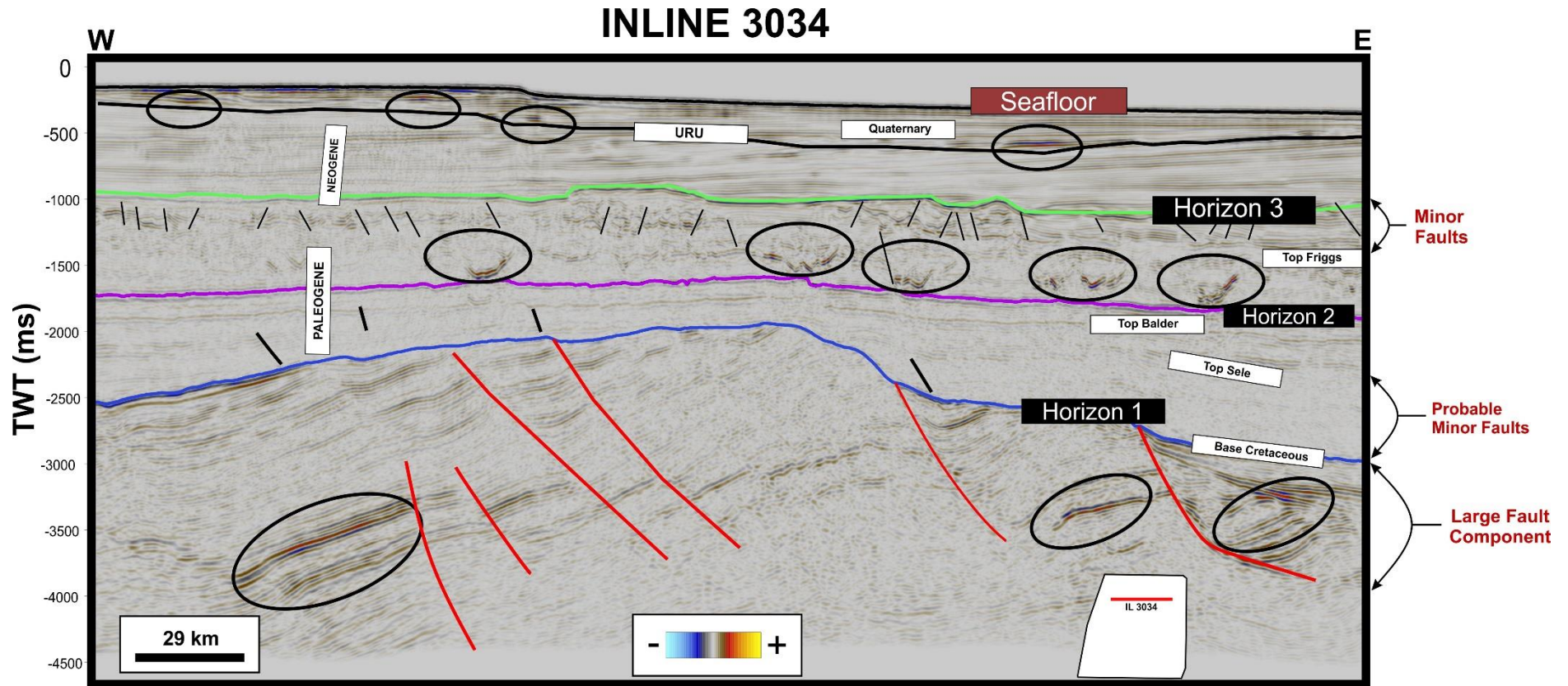


Figure 53: showing Inline 3034 from T11MZ07, with manually picked fractures/faults. Classified into minor faults, probable minor faults and large fault components observed at the base..

### 10.5.1 Small and Large Fault Components

Small fault components shown in a seismic subdivision in Fig. 53 as a basis occurring at the top between 1000ms and 1250ms. Some seemingly mistaken faults can be fractures with no noticeable displacement in reflection to be termed faults. Minor/small faults from 120m to 150m were measured at this interval overlying the top Balder's v, w and winglike anomaly in TWT. Also, observed are minor faults and fractures which develops at the base of the Top Balder but not as distinct as the ones above the Top Balder formation which are intense and reoccurring as faults and fractures. Minor faults, which are observed not to be distinct occurs at the crest of the intense fold of example in Fig.53 (for basis) within the 2000ms to 2500ms in two-way travel time. Similar measurements in thickness from 120m to 150m, such as minor faults at the top of the balder, were found.

Large fault component develops at the base of roughly 2500ms to 4500ms in two-way travel time, which are large faults with rolled surfaces as illustrated using variance and time slice in Fig.54. This large fault component is observed to thicken in reflections against the downthrow of this large fault component. The large fault component measures roughly 3500m in length on the fault surface measured from with interpretations window ruler. Also, very high amplitude anomaly terminates towards or along the large fault component of the seismic example in Fig. 53.

These observations are also peculiar to other 3-D seismic cube, not being described, in this case, referring to 3D seismic cubes NX0802 and ST98M7.

Fig.54 perfectly images a variance obtained across NX0802 – 3D seismic cube. Fig.54a shows a variance obtained at a two-way travel time of 1001ms. Focus is placed on inline 13871, indicated in Fig. 54c, with distinct, identifiable minor faults, as previously explained and interpreted manually in Fig. 53 (For basis). Fig.54c shows that these faults have discontinuities that crosscut each other towards the southeastern area of the 3D cube as imaged by Fig. 54c from the red colour

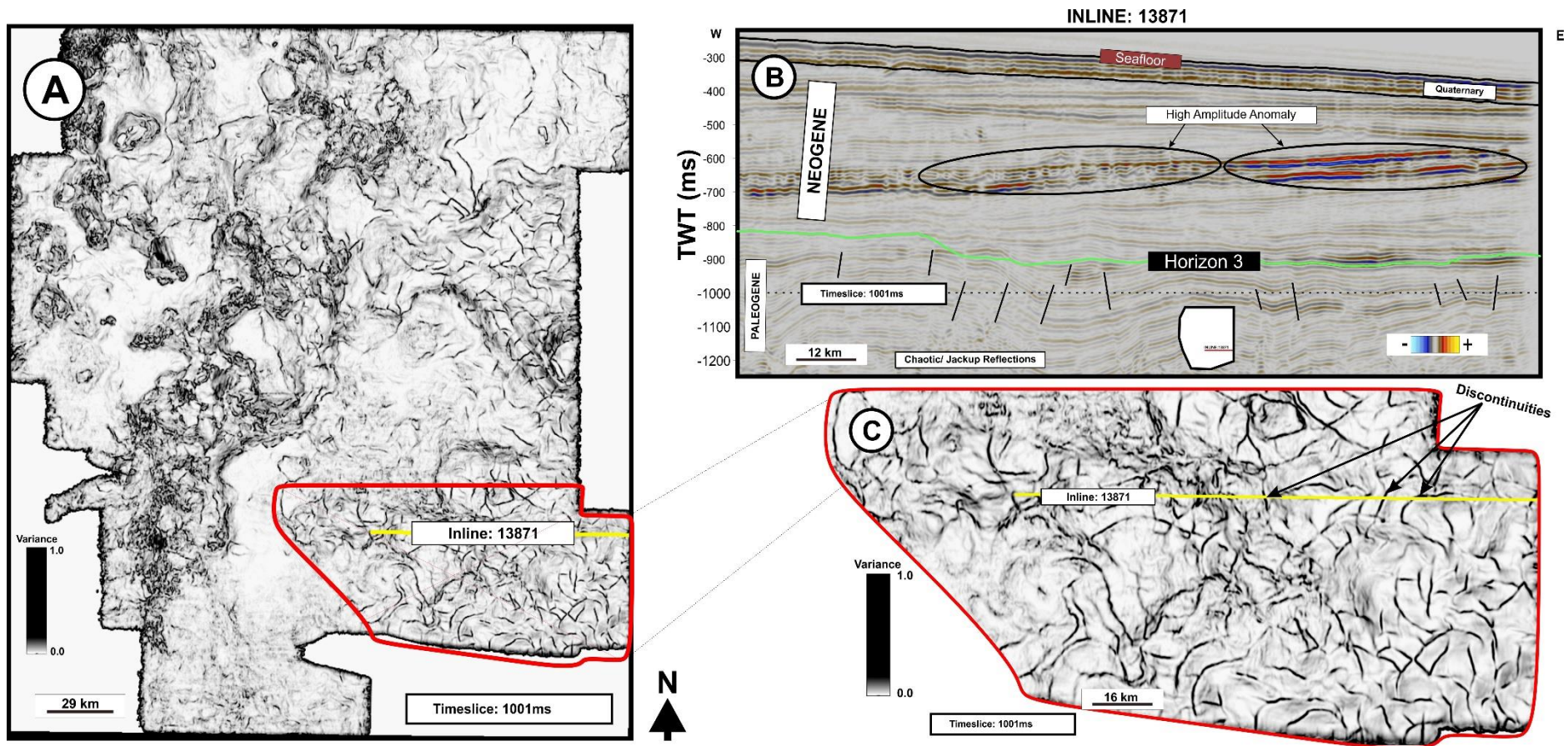


Figure 54: showing A). variance of -1001ms taken across the 3D cube (NX0802) B). showing a seismic sample with an inline 13871 (marked by the yellow line) with some examples of faulting imaged by the variance time slice. C). A close-up view of the variance time slice with several cross-cutting discontinuities imaged by the variance time slice.

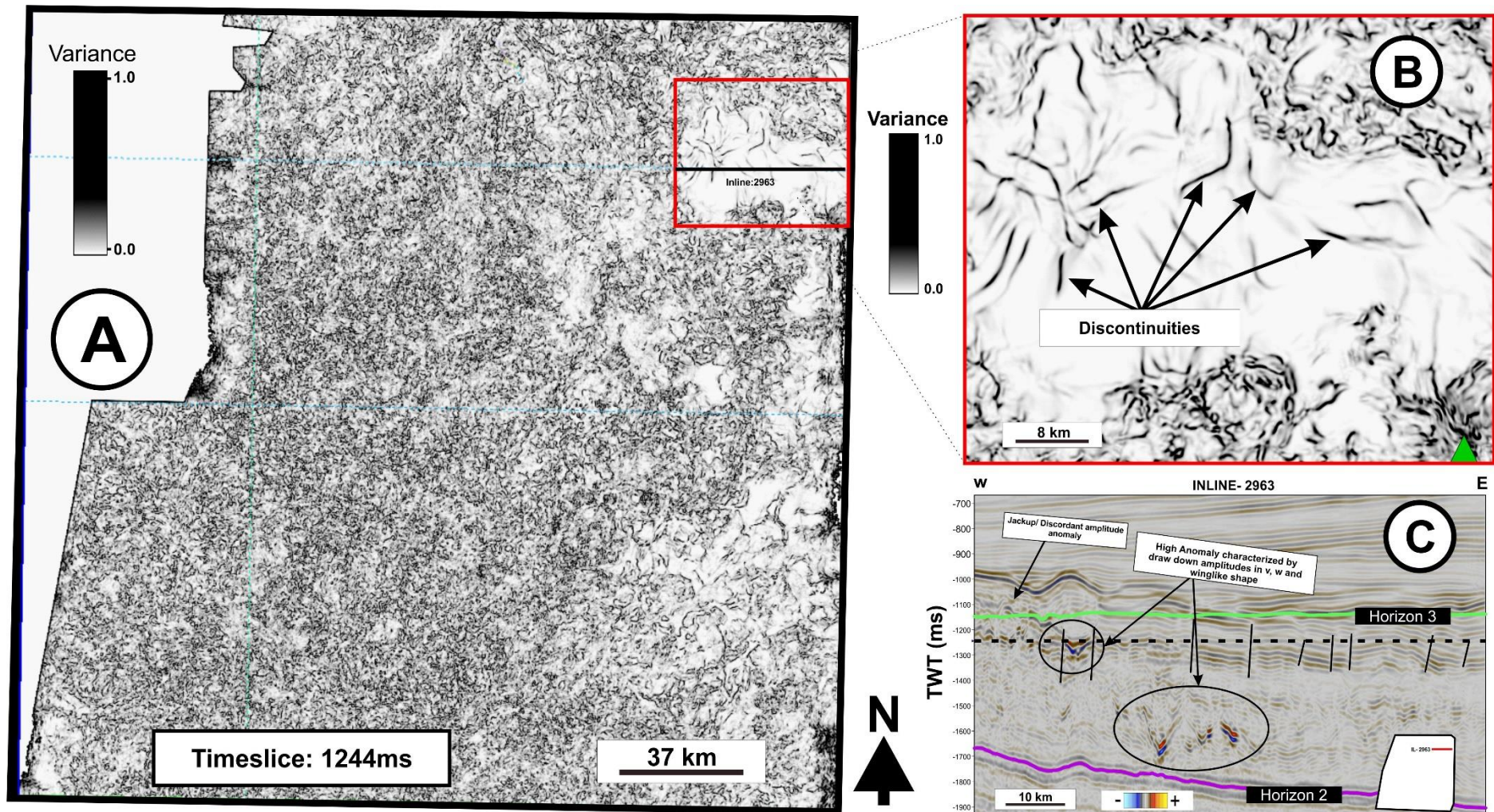


Figure 55: showing A). variance of -1244ms taken across the 3D cube (ST11MZ07) B). A close-up view of the variance time slice at 1244ms in two-way travel time with cross-cutting discontinuities and discontinuities imaged by the variance time slice. C). showing a seismic sample with an inline 2963 with some examples of faulting imaged by the variance time slice.



On an interpretation window with the ruler tool, these faults range from 29 to 60 ms in two-way travel time, regarding Fig.53 subdivision. Also, some faults do not have a distinct displacement to be termed faults due to their lack of distinct displacement of continuous reflectors. Another word that could replace the word fault is fractures, which were also observed on the southeastern side of the area. A culmination of faults and fractures must have resulted in the cross-cutting discontinuities imaged by the time slice variance map in Fig. 54c and 55b. These observations are somewhat bounded to Horizon 3(see Fig .53 for subdivision); this structure is noticed below the interpreted Horizon 3. This example was selected because it was observed to be distinct across most seismic cubes. It is important to note that this also occurs on other 3D seismic cube as shown in Fig.55.

Fig. 55 similarly shows a variance obtained along 1244ms along the ST11MZ07 3D seismic cube. This crosscutting relationship observed on NX0802 is also observed in ST11MZ07, as shown in Fig.55b, and is more localised towards the northeastern section of the 3D seismic coverage. A seismic section in Fig. 53 (subdivisions established previously) shows these faults overlying some high amplitude discussed previously as v, w and winglike shapes in Fig. 54 & 55. No coverage of this cross-cutting relationship was seen on ST98M7 (Hence not documented).

Orientation of these observed cross-cutting faults/ fractures trends on the variance time slice map in the northeast to southwest direction and from west to east opposite directions in two 3-D seismic cubes of both NX0802 and ST11MZ07.

10.5.2 Large Fault Component

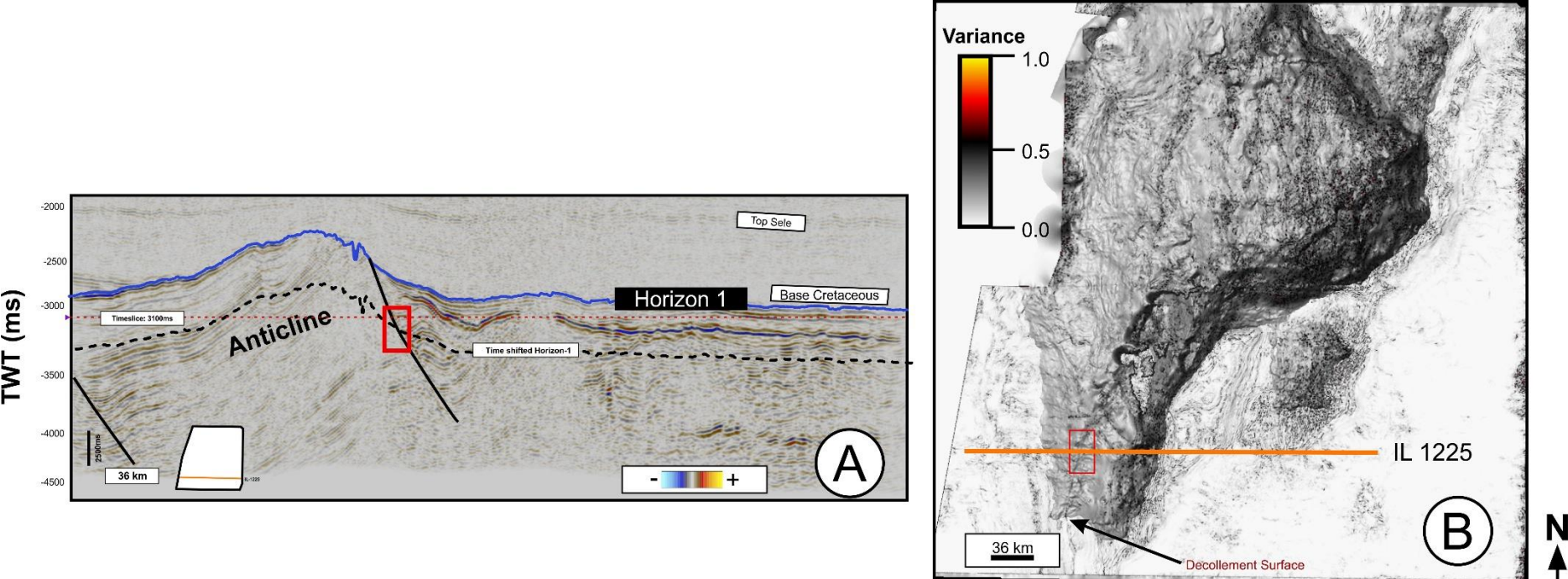


Figure 56: showing A). Uplifted area with a decollement surface, interpreted fault with time-shifted surfaces and time slice B). A variance map along a time-shifted horizon (vertical exaggeration of 7.5) and a time slice of 3100ms to image significant fault components. Vertical Exaggeration:7.5)

Large fault component observed on seismic were associated with the base Cretaceous of the seismic, marked by the intense uplift most noticeable in the 3D seismic cube ST11MZ07. Fig.56a shows an interpreted horizon 1 and a variance obtained along horizon 1 shown in Fig. 56b in combination with a time slice obtained along -3100ms in two-way travel time imaging, an example of a significant fault component upon which high amplitude seismic reflections terminating against a supposed fault in the red . This example from an inline of 1225 is marked with a red box to show the structure revealed with a time slice and a horizon variance. This structure is just an example and was obtained at the lower crest of the intense folding observed at the base Cretaceous of the ST11MZ07 3D cube.

The equivalent of this structure on other 3D seismic cubes, such as NX0802 and ST98M7, are seen to be represented by reflection troughs, synclines, and some of what looks like a sagging structure reflections. It is observed that this structure seems to have several high anomalies

#### 10.5.3 Large Structures Underlying Base Cretaceous.

As previously described, this large fault component section. These significant fault components underlie the base Cretaceous, measured from 190 to over 3000 meters from the interpretation window. Fig. 57 shows this significant fault component, the most extensive set of faults observed on this seismic. This fault is repetitive and particularly associated with the folded structure of ST11MZ07. With high anomalies terminating on this large fault structure. This fault surface is seen to be more curled towards the downthrow. It is also observed that there is a thickening of reflection towards the east of Fig.57 of the seismic example, where the anomaly is intense. The variance map of Fig. 57 shows a line separating the time slice high anomaly region lying at a structural low compared to the structural high, intense folded region to the northwest lacking these anomalies as part of the composite image, suggesting a movement from east to east to west.

Similarly, Fig.58 is a composite image of an inline towards the east of the Norwegian Trench, characterised by an intense basin sag and slight uplift). The anomaly also observed in this seismic example is seen to be intense. It terminates on discordant reflections that are swollen. To the West of this sample is a corresponding sag of reflections with increasing steepness in reflection.

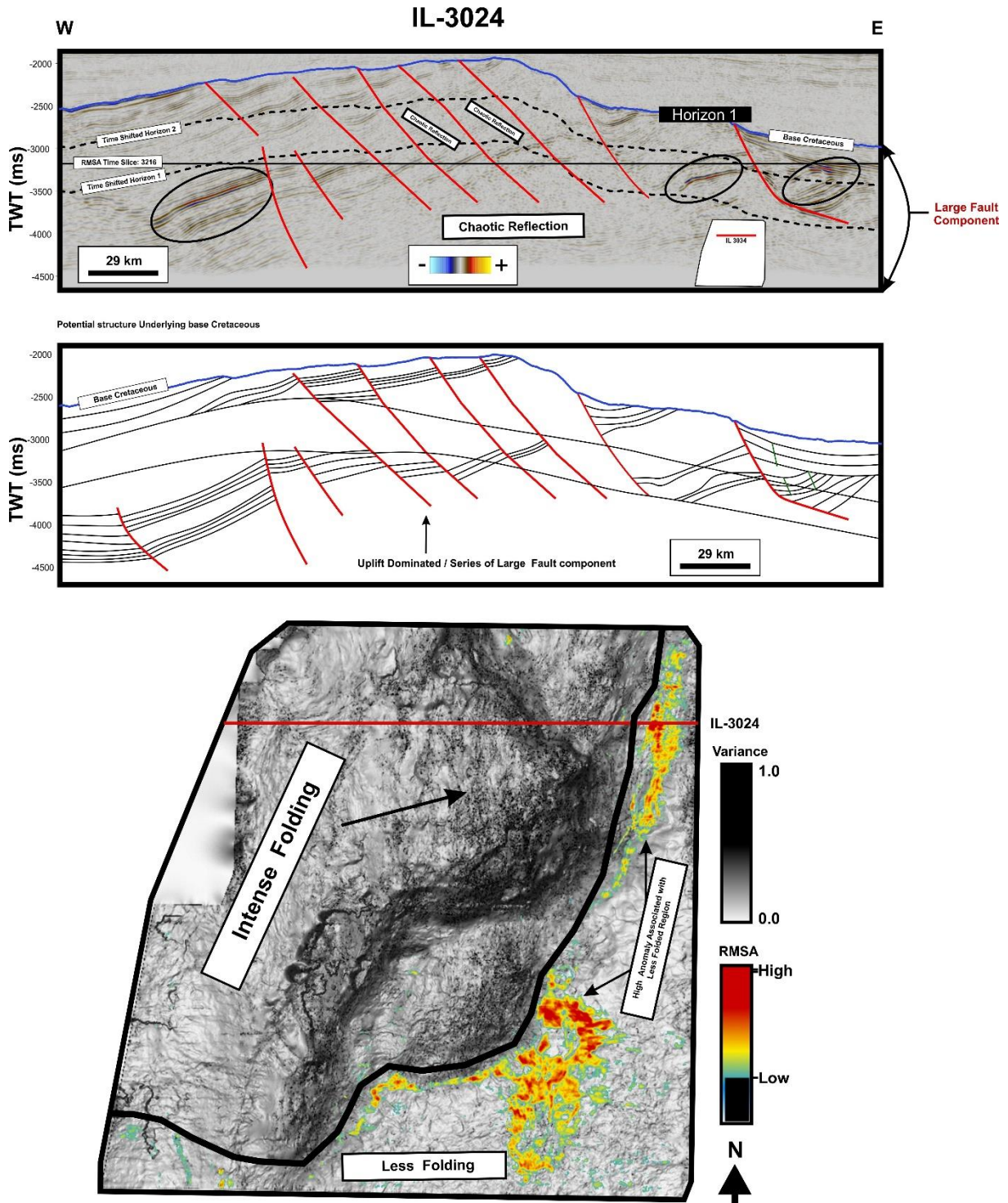


Figure 57: A composite image showing an example of potential structures underlying the base Cretaceous of ST11MZ07. A variance map across horizon (Vertical exaggeration:7.5) superimposed on an adjusted RMSA timeslice indicated on image showing an uplifted structure with several large fault components below the base Cretaceous. Note: Time-shifted horizon surface attributes was not shown, but added of boundary used in showing profile.

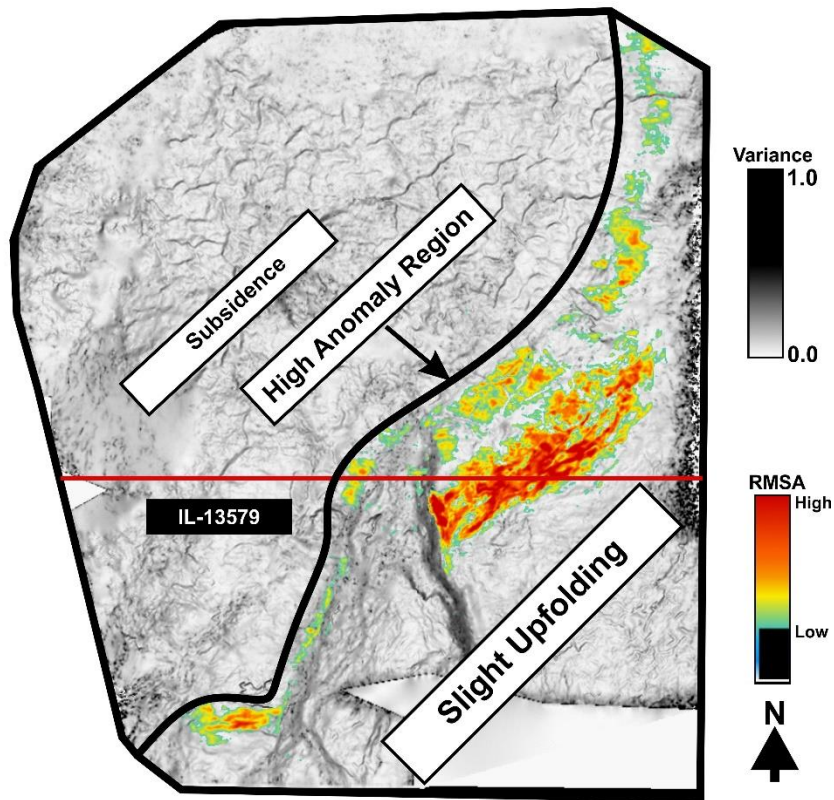
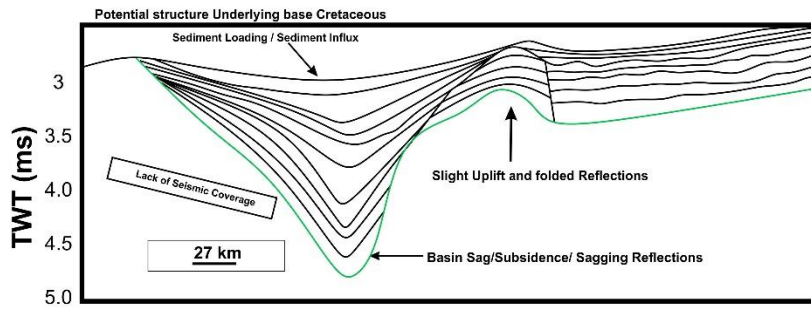
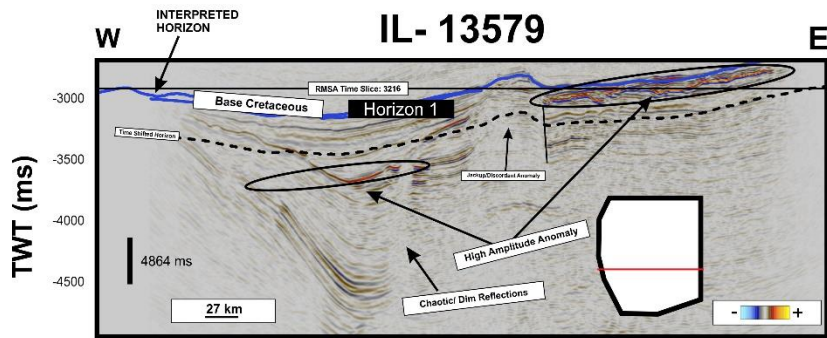


Figure 58: A composite image showing an example of potential structures underlying base Cretaceous of NX0802. A variance map (Vertical exaggeration: 7.5) horizon 1 with an adjusted RMSA opacity map showing a sagging structure with dipped reflections. The time-shifted surfaces are just used in generating a profile showing a sag and loading.

10.6 Possible Pathways / Fluid Flow related Structures

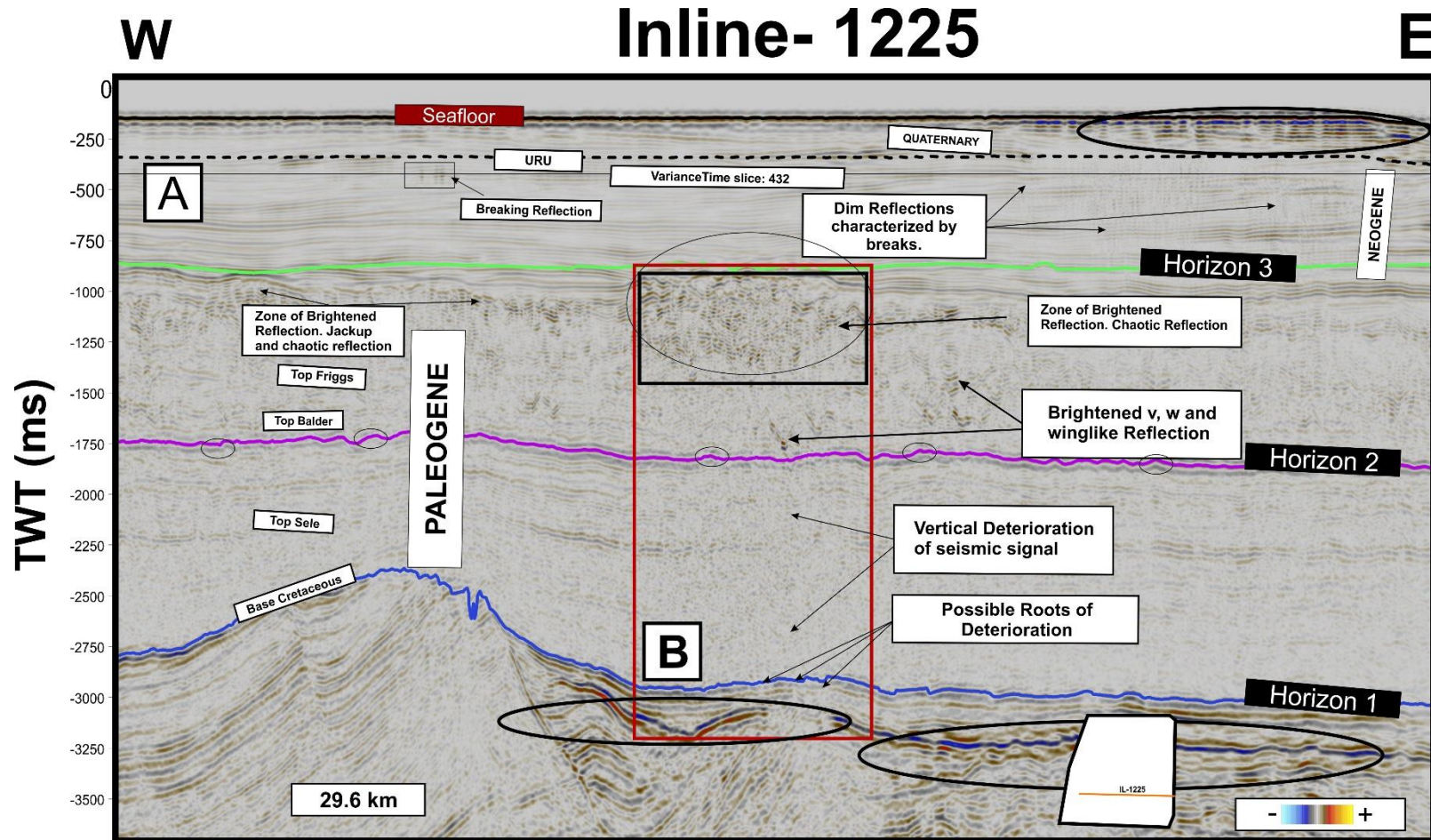
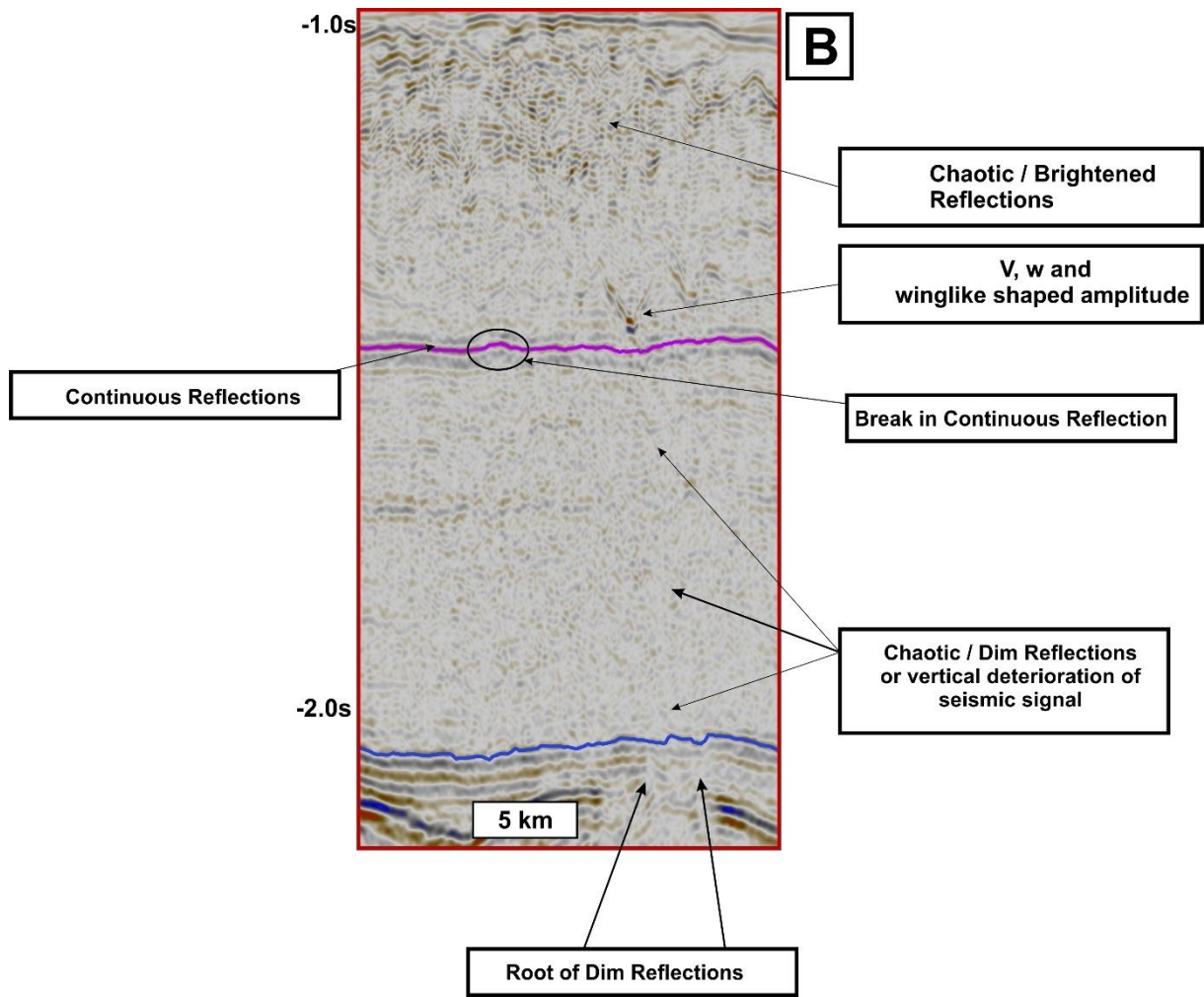


Figure 59: showing A). An image from ST11MZ07 of inline-1225 with distinct seismic descriptions and an inset image (B). Terminologies used are from Loseth et al. (2009)

Fig. 59a shows an example of inline-1225 associated with ST11MZ07 from West to East and areas with distinct seismic activities (anomalies). Summarily, Fig.59a presents a vertical deterioration of seismic signal from the base Cretaceous from Horizon 1 and possible root source of this deterioration towards Horizon 2, characterised by a jack-up noticed and marked in thin circles along Horizon 2 and into its chaotic zone beneath Horizon 3 also dim, chaotic reflections described eastwards within the Neogene aged reflection, sloping eastwards towards the trench and charging the Quaternary reflections eastwards on slope.

An inset of Fig.59 b with a clear description, from Fig. 59a with described features identifying the root of this deterioration reflection as occurring from the base Cretaceous (Horizon 1), vertically upwards with chaotic reflections and a continuous reflection tending to be jacked up at Horizon 2 and brightening into a V-shaped anomaly charging and brightening up into Horizon 3 but capped by continuous reflection above.

Fig. 60 shows a variance time slice obtained at 432ms (two-way travel time) from Fig.59. revealing several distinct discontinuities and breaks beneath the URU (Upper Regional Unconformity) within the Quaternary /Neogene reflection associated with several breaks in reflection, imaged as discontinuities on the variance timeslice





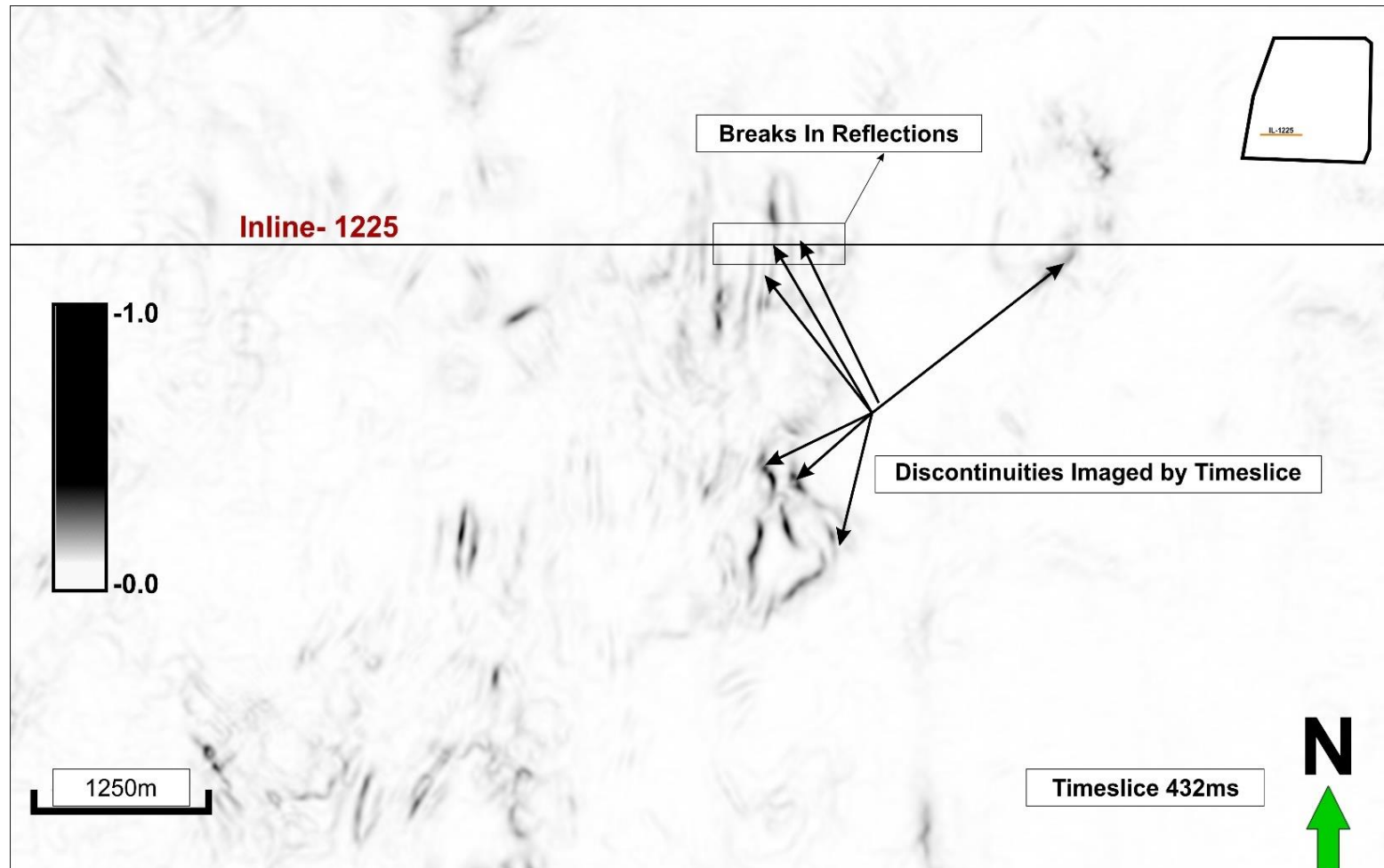


Figure 60: Timeslice 432 from Fig.59 imaging several discontinuities and breaks in reflections.

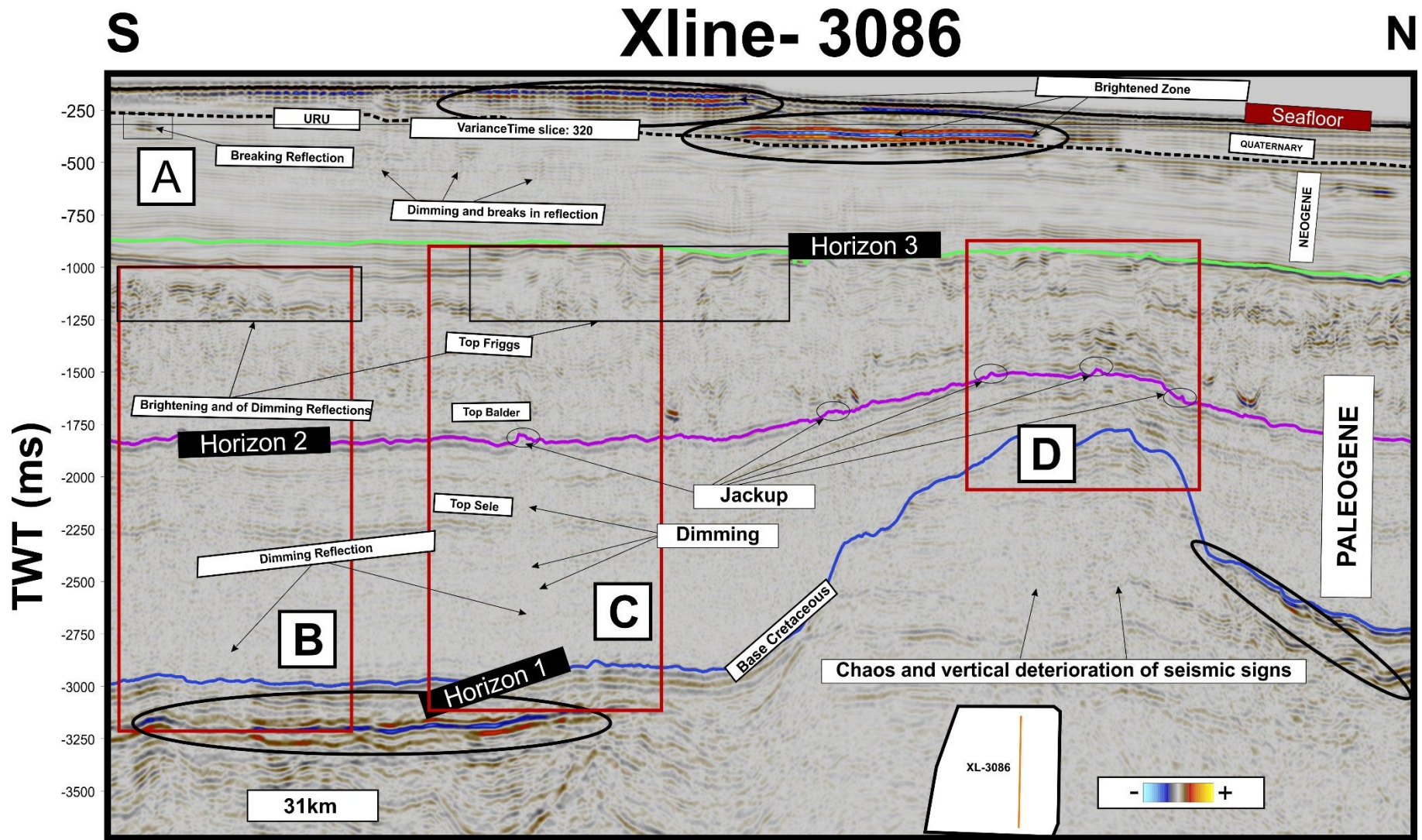


Figure 61: showing A). Image from ST11MZ07 OF INLINE -3086 with associated seismic descriptions and an inset image (B, C and D)

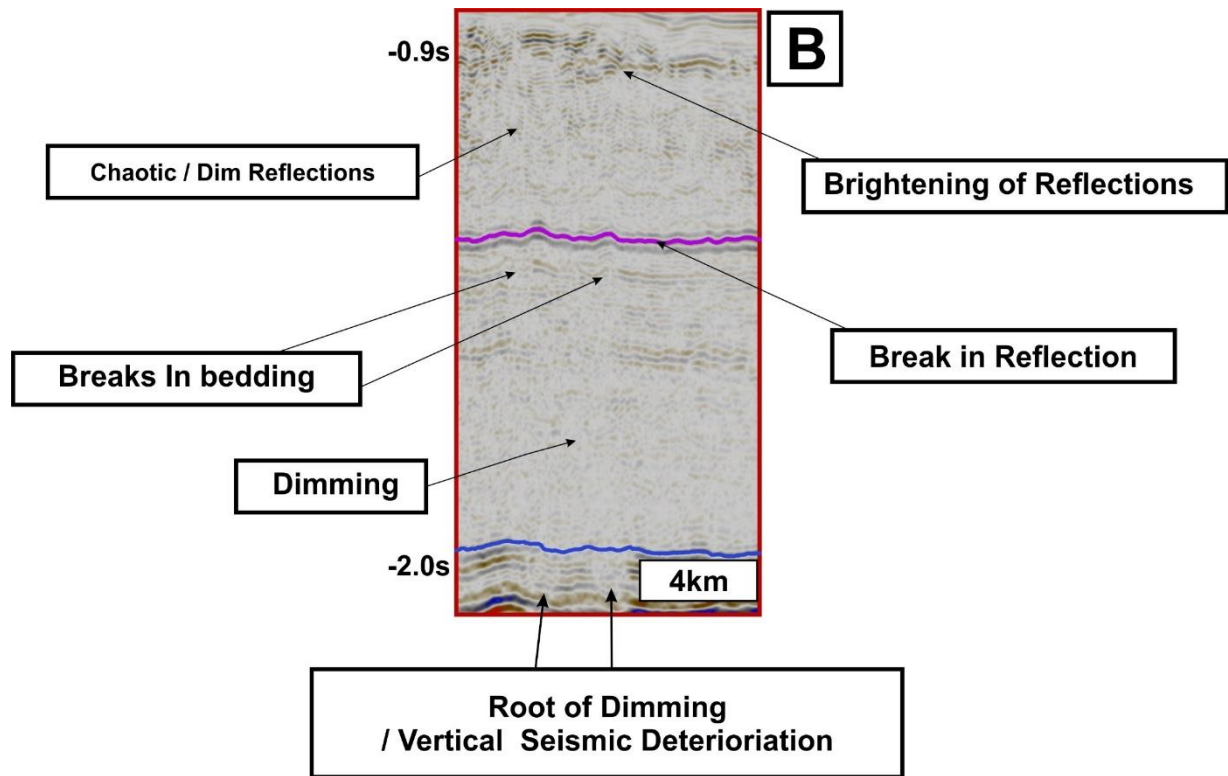
Fig.61a generally describes crossline-3086 associated with ST11MZ07 South to North with distinct and unique seismic activities (anomalies). Areas of seafloor sloping downwards towards the Norwegian Trench are charged with high anomaly and highlighted in deep oval circles towards the North and within the Quaternary reflection. Beneath are seismic reflections described as dimming and breaks in the reflection within the Quaternary and Neogene reflections, slightly across the URU to the seafloor. A detailed description of insets B, C and D is presented from Fig.61.

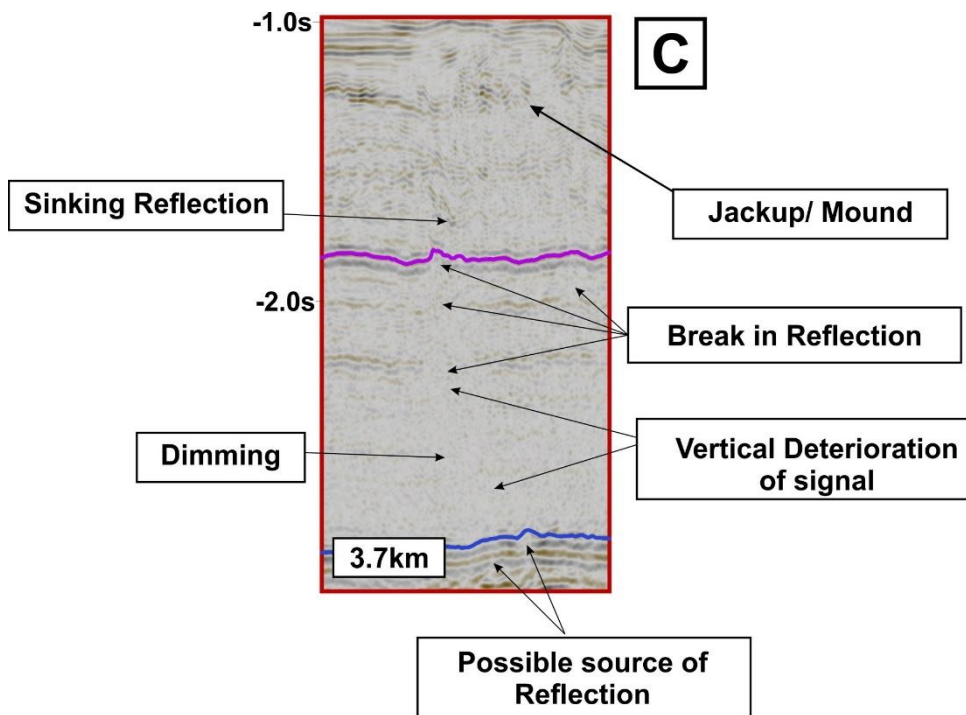
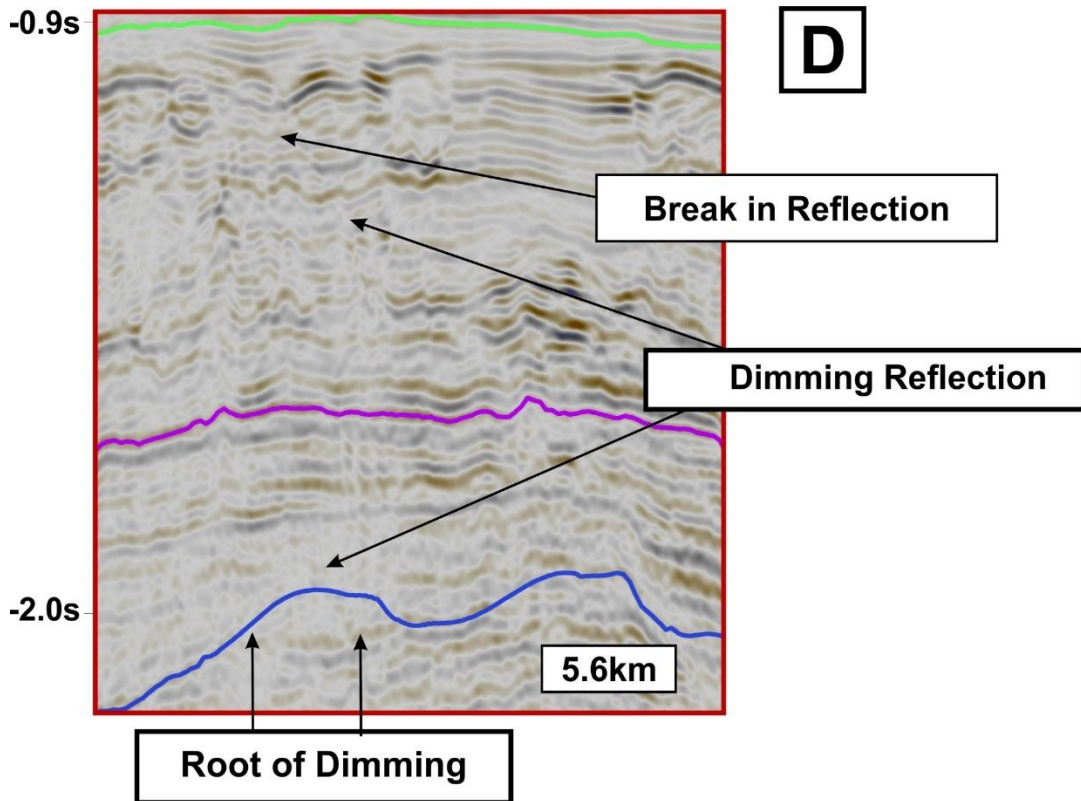
Fig. 61b (inset) from Fig.61a shows roots of dim reflections from below the base Cretaceous with vertical dimming and deterioration of reflections towards horizon 2 within the Paleogene reflections with horizon1 characterised back a break in reflections and jack up or bulge.

Fig. 61c (inset) from Fig.61a shows something similar: a root from base Cretaceous towards Horizon 2 of the Paleogene aged unit and a brightening and chaotic reflection towards Horizon 3 capped by continuous reflections.

Fig. 61d (inset) from Fig.61a shows an inset but associated with an uplifted structure interpreted to be associated as the base Cretaceous with roots of dimming towards Horizon 2 within the Paleogene and a dimming event characterized by chaos and breaks in reflection towards the low amplitude continuous Neogene.

Fig.62. Shows a variance time slice of 320ms (TWT) from Fig.61 obtained cutting across the Quaternary- Neogene reflections, imaging several discontinuities within the Quaternary and Neogene reflections.





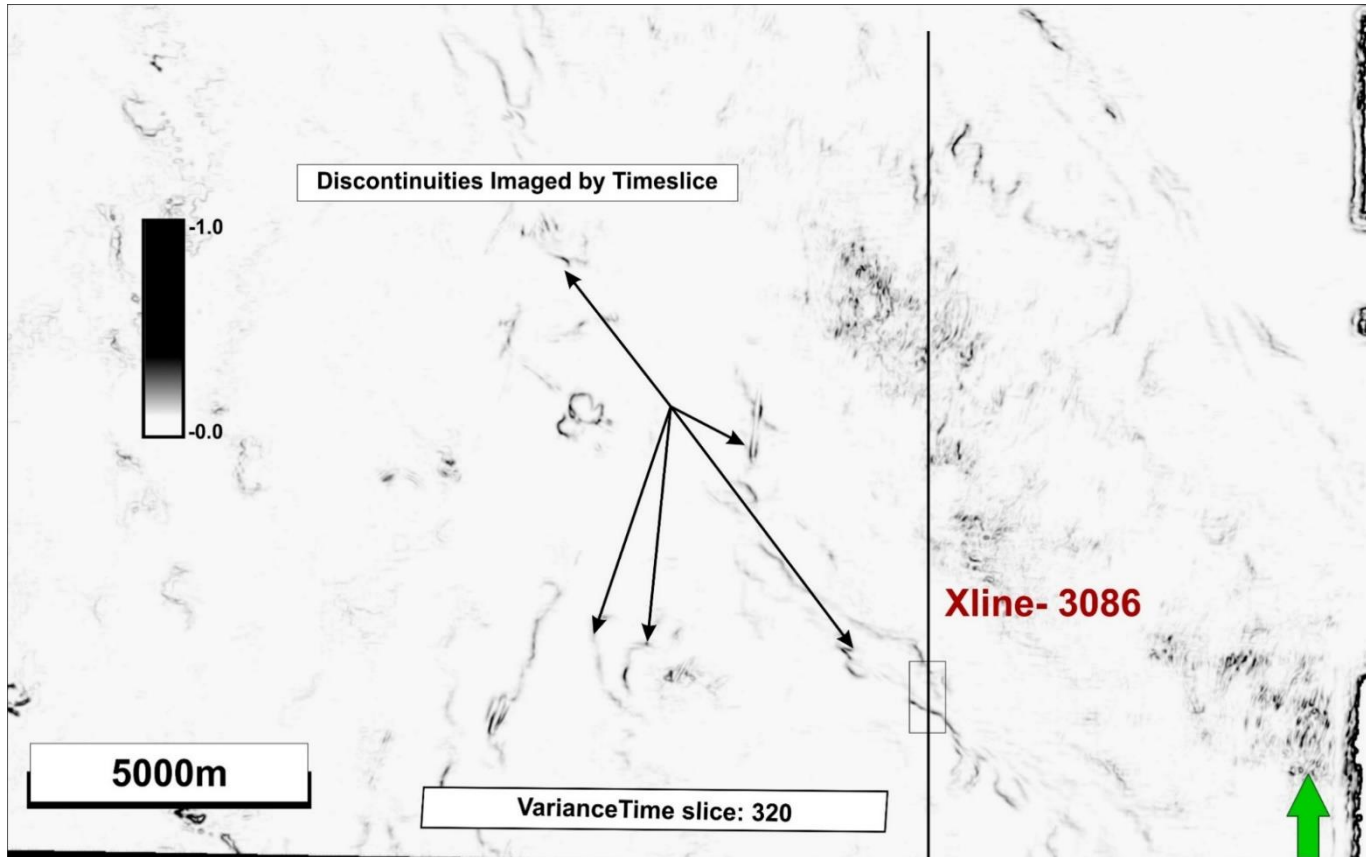


Figure 62: A time slice of 320 from Fig.61.

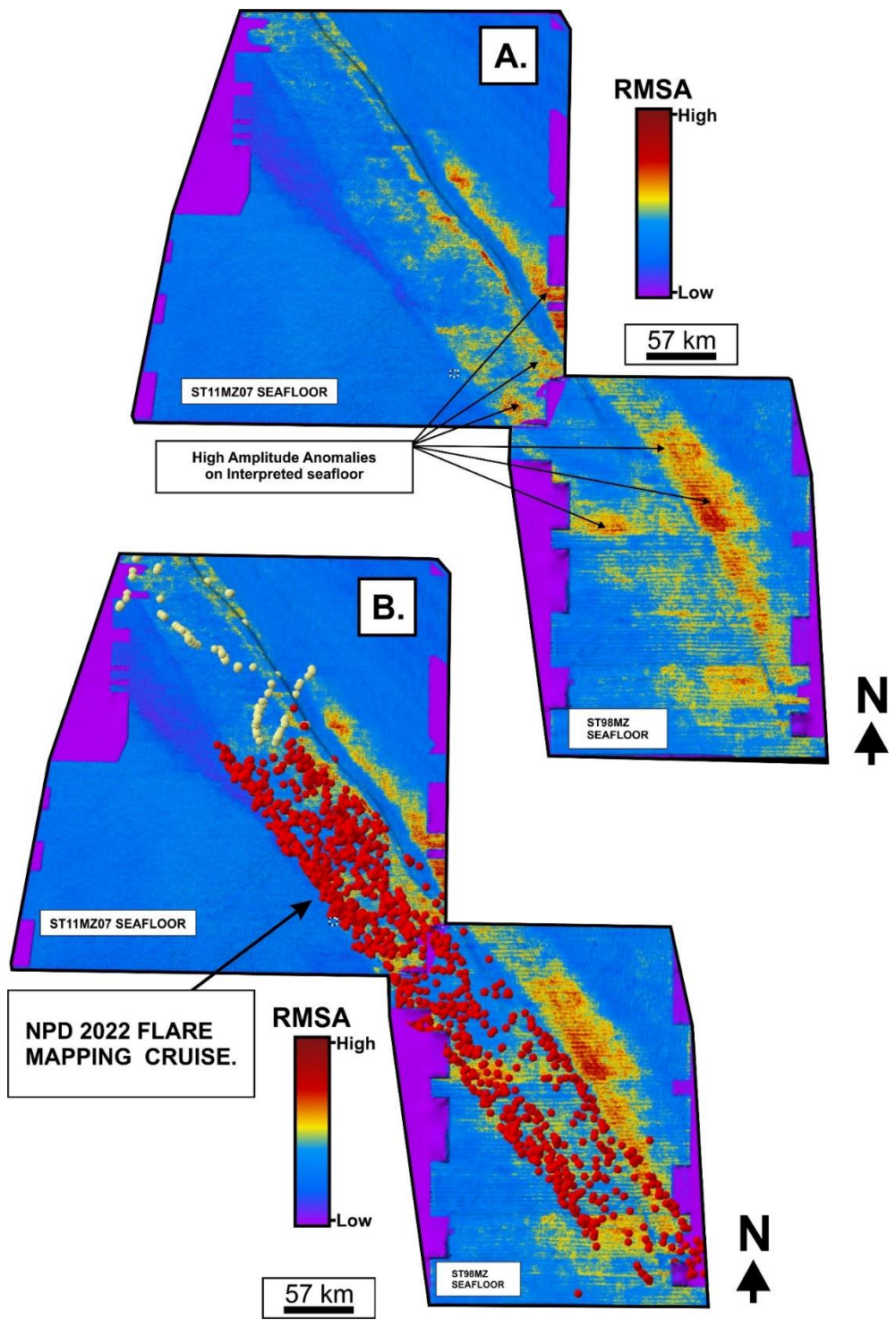


Figure 63: Showing an A). RMSA map obtained of the seafloor showing high anomaly against slope from the east B).RMSA map of interpreted seafloor superimposed with flare data from NPD cruise, mapping out flares from the water column across an embankment north of the Northern Sea from a 2D window.

Fig .63a shows an RMSA map where the embankment falls towards the west, along with flares obtained during a cruise by the NPD (Norwegian Petroleum Directorate) in 2022. Fig. 63b falls on the embankment of some part of 3D seismic interpreted within a 3D seismic cube of ST11MZ07 and ST98MZ. Note that more flares might have occurred around the areas associated with the Norwegian Trench. Still, the cruise was focused on a specific area that falls along the embankment (sloping downwards) which intersects primarily ST11MZ07 and ST98M7. Flares fall along high amplitude area imaged with an RMSA from the seafloor with associated small holes previously described, as shown on the time depth map (TWT)



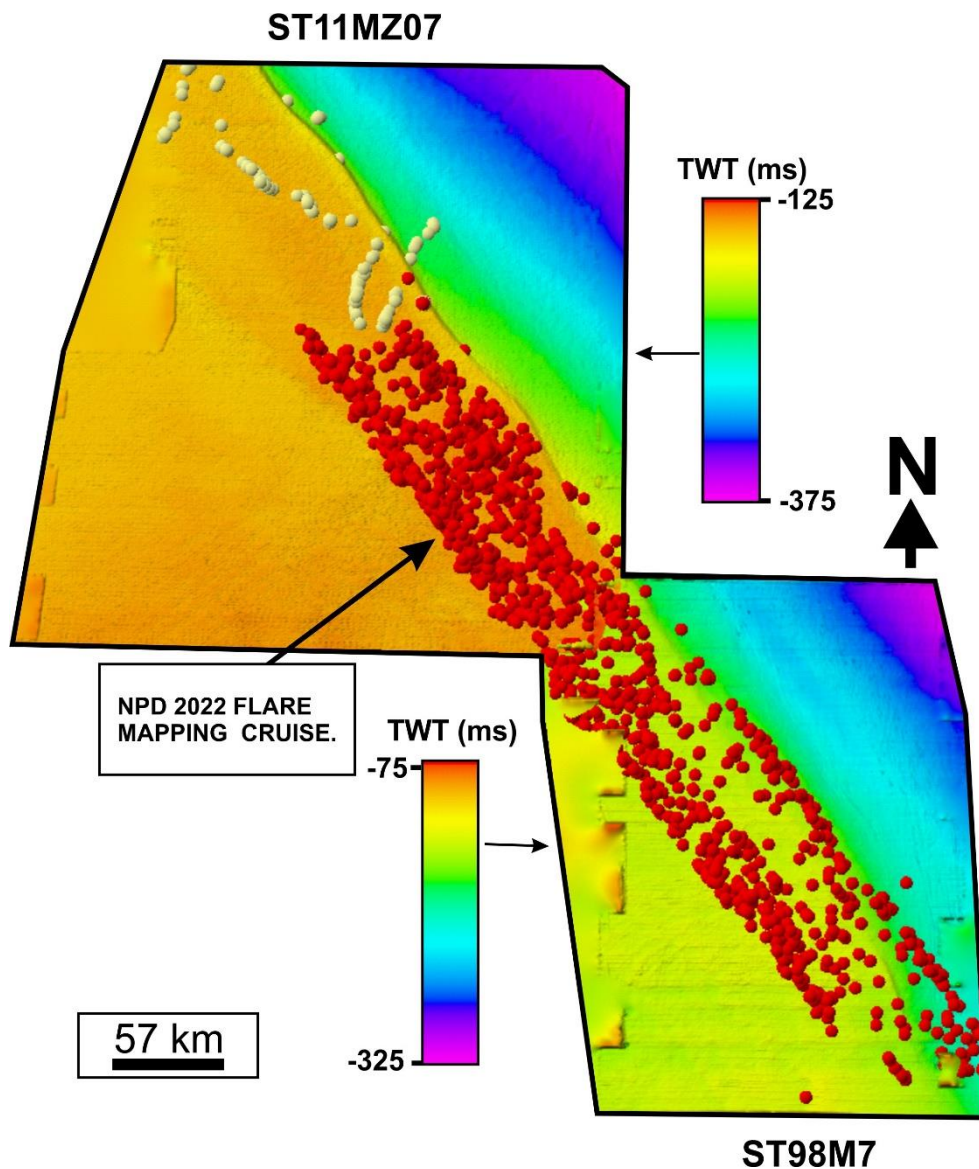


Figure 64: Showing an A). RMSA map obtained of the seafloor B). RMSA map of interpreted seafloor along with a cruise by NPD mapping out flares from the water column across an embankment north of the Northern Sea from a 2D window

Fig.64 shows a time depth map from the interpreted seafloor with available flare data for ST98M7 and ST11MZ07. Note the exemption of NX0802 from the sample above because flares weren't mapped along the Norwegian Trench, in which NX0802 falls primarily.

## 11. Discussions

### 11.1 Seismic Unit & Facies Descriptions

According to (Badley, 1985), seismic reflections and seismic units can be described in terms of depositional environment. Upon which depositional environment and the type of reflections can be made to suggest/ infer the type of depositional environment of a seismic reflection. A continuous reflection can imply a deep marine environment with lithology corresponding to finer and more uniform sediment than fluvial grain sizes, which have coarser grain and differential grain sizes. Discontinuous reflections and chaotic reflections much more reflects differential fluvial grain sizes. Hence, a reliance on this approach is somewhat unreliable and subject to further data such as well logs, cores, and better seismic imaging (Badley, 1985). This approach is also limited to seismic resolution, seismic data processing, other processing factors effects such as tuning and steeping beds (Badley, 1985).

### 11.2 Glacier-induced Marks / Morphology and Glacier Expressions on Seabed.

The observed results above strongly support the presence of elliptical and circular depressions obtained from the interpreted seabed on different 3D seismic. The most important observation is the differential occurrence of these structures in size and shape. Ottesen et al. (2016) confirms that areas corresponding to the north of the North Sea are composed of glacier-dominated processes, as attested to by the Norwegian channel characterised by fast-flowing ice streams. So, it makes reasonable sense to infer that the seabed morphology and structures observed on seafloor are linked to the previous Fennoscandia- BIIS (British Irish ) ice sheet (see section: 3), which forms during the Weichselian glaciation attested to by several studies such as; (Becker et al., 2018; Nygård et al., 2005; Ottesen et al., 2016, 2018; Patton et al., 2022). It is important to note that these features observed on the seafloor are not necessarily induced totally by the ice sheet covering, especially as is the case of the 3D cubes in ST11MZ07, which falls partially on the Norwegian channel to the West represented by a structural high. Lithology on this structural high/ embankment has lots of depressed circular holes on its embankment that might have consist of eroding gravels and influx of sediments washed from the east Shetland to the West area capable of fluid expulsion, which was seen in Fig.41 and 42 with samples and littering of several concentric circles, which does not have a resemblance to pockmarks or seafloor mounds described in several literature describing seafloor morphology (i.e. Andreia Plaza et al., 2011.; Bünz et al., 2012; Løseth et al., 2009, 2011). Fluvial progradation of east Shetland could somewhat explain this observation on the embankment and lithology, infilling

the study area (especially ST11MZ07 that falls outside of the Norwegian Trench) corresponding to a timescale of the earliest Quaternary (Ottesen et al., 2018). The East Shetland platform has been highlighted as an essential sediment source throughout the Cenozoic period (Eidvin & Rundberg). This lithology has been noted by Ottesen et al. (2018) to be composed of silty and gravelly material.

Long lengths of striations and elongated lineation's clearly shown in Fig.43b are testaments to the mega-scale glacial lineation by the formation of the Norwegian channel ice stream, which was described by Ottesen et al. (2018) to have developed around 1.1ma to about 0.8ma as a remarkable feature of the Eurasian Icesheet during the middle to late Quaternary (Ottesen et al., 2014, 2016, 2018). This extended elongation seen on the paleo shelf and results are interpreted to be a mega-scale lineation that has resulted from the Norwegian channel ice stream that flowed initially across the Måløy plateau and migrated around 60km to the west during the middle to late Quaternary (Batchelor et al., 2017; Nygård et al., 2005; Ottesen et al., 2016; Rise, 2004).

Generally, Quaternary sediment sequence and infilling into the Northern Sea are poorly constrained. This is acknowledged by Ottesen et al. (2014) when discussing the infilling of Quaternary sediment in the north section of the Norwegian North Sea basin. It is often doubtful to rely on the North Sea's Dutch, German, and UK sectors, which are different in lithology and are of shallower waters than the norwegian North Sea (Ottesen et al., 2014). Identifying Quaternary URU (Upper Regional Unconformity) in the western section of the Northern basin was difficult from seismic examples from seafloor morphology because the URU is conformable with sediment influx from the west region (ST11MZ07 seismic cube), in comparison to the eastern ward section (NX0802) which is cut by the Norwegian channel ice stream, making the URU more noticeable, shown in given random line in examples which shows clear, distinct separation with base unit separating it from pre Quaternary sediments (Ottesen et al., 2014). Assumptions were made regarding this boundary, and an inference was made based on the remarkable work of Ottesen et al. (2018). This was inserted with corel draw as explained initially.

Unique depressions of obviously large sizes were observed, as shown in Fig. 42b and 43b, and they look more like cave-ins or deformations on the seafloor with distinct sizes resembling deformations and cave-in characterising soft sediment bodies, as Løseth et al. (2009) described when studying hydrocarbon leakage deformation structures. This structure is entirely different from the one recognised in Fig. 44, which looks like a smaller tiny hole and is much smaller in sizes, most likely owing to progradation from east shetland. This feature has been described

as a **pockmark** instead of a mound that looks more like a swell (Løseth et al., 2009). These pockmarks might be permanent deformation following fluid (gas) expulsion from the seafloor. The features described as a pockmark might be releasing fluid, or might not, but in examples of seismic given in Fig.43c and 44c, there are strong indications of high anomalies (interpreted as shallow gas infilling semi-permeable sediments) underneath these interpreted pockmarks, which can deform the seafloor which are often made up of glaciogenic input, debris flow and very fine sediments (see section 4 for stratigraphy descriptions) within the Quaternary (Løseth et al., 2009b; Sejrup et al., 2003).

An attempted schematic diagram showing the formation of this iceberg and its impact on the seafloor north of the Northern Sea, along with penetrating literature (i.e. (Batchelor et al., 2017; Ottesen et al., 2018; Sejrup et al., 2003, 2016)) and an understanding of the landscape of the Northern Sea is shown in Fig .63. This factors the mega-scale lineation/ Elongated features on the Paleo shelf observed on interpreted seafloor from 3D cubes of NX0802 and ST98M7.

Fig. 65 considers the covering of the northern North Sea by the Fennoscandian ice sheet during the Weichselian period. Deglaciation and retreat of the ice sheet reveal structures that might be scour marks and striations described previously, with a zoomed feature section showing the feature. The mega-scale lineation might have been initiated by a fast-moving stream of ice carving out long elongated features on the sea floor towards the Norwegian Trench (Ottesen et al., 2014). The implication of this ice sheet and the carving out of the Norwegian Trench is the erosive impact along the trench area, which might, in turn, strip overburden sediments to expulse fluid that might be trapped downslope from on embankment from the east Shetland platform. Circular depressions observed on the west embankment's seafloor might probably have little to do with the Norwegian Channel Trench drainage but with the influx of unconsolidated sediment from the east Shetland platform source area and probably climatic stripping (erosion from high relief to low relief). No BSR was analysed, as there are no clear-cut bases for that. Hence, a reference to facies describes what might be going on from the dataset, suggesting that glacial covering might have had little impact on the Norwegian section of the North Sea despite having several glacier-induced processes and input of sediment (subjective).

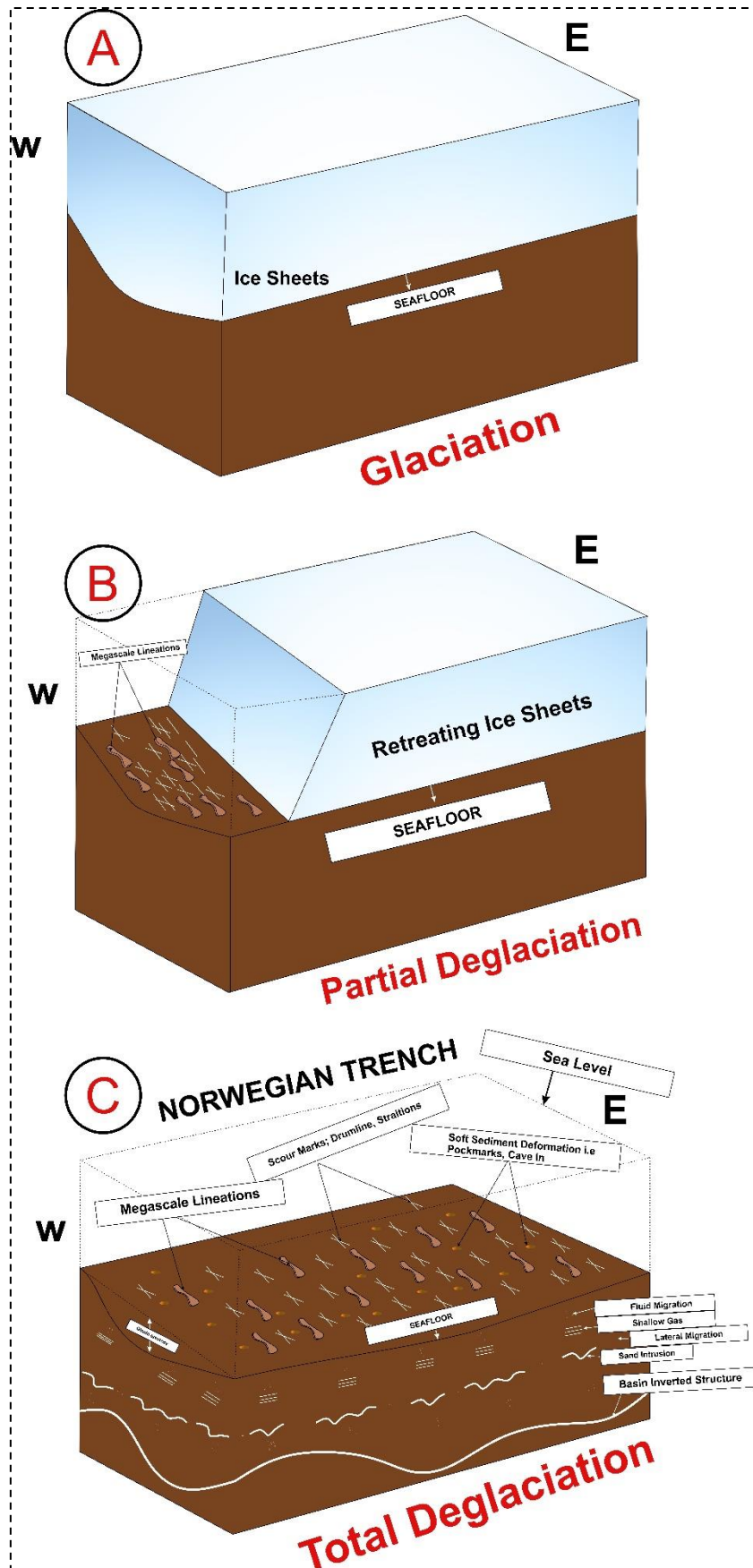


Figure 65: Shows an image of the impact of glaciers on the seafloor with A). Full glaciation of the Fennoscandian ice sheet B) Receding Glacier and Fast-moving ice streams C). A complete deglaciation showing the impact and action of glaciers.

### 11.3 Shallow Amplitude Anomaly towards the Seafloor

Fig.45, Fig.46, and Fig. 47 are peculiar observations of shallow high amplitude anomalies observed on all seismic cubes charged towards the seafloor within the Quaternary. To capture anomalies, it was essential to map this distinct anomaly trapped within the Quaternary sediment packages with a time-shifted horizon from the seafloor. It was challenging to distinguish and establish unconformities within the seismic concerning Quaternary sedimentary infilling due to the absence of 2D seismic and chronostratigraphic data (age markers) controls. The issue of chronostratigraphic controls of the infilling of Quaternary sediment infilling was highlighted by (Ottesen et al., 2018). However, an extensive database of 2D seismic was available in studies characterising the Quaternary, which was inferred from the description (Ottesen et al., 2018). Studies were used to identify and discuss succinctly the Quaternary infilling of the North Sea. An approximate inference to this study was used to establish the URU characterizing the onset of Quaternary infill and in which most shallow amplitude anomaly was trapped. This was a failed attempt on 3D- seismic of ST11MZ07, primarily influenced by fluvial input of East Shetland, and described as conformable to sediment beneath the Quaternary URU (Upper regional Unconformity) and the common URU noted to be carved out because of the Norwegian Channel development, which is well developed on 3D seismic cube of NX0802.

Approximate boundaries were made using existing literature and Quaternary sediment infilling. It is described as composed of fine sediments and uniform sediments. However, looking at the continuity seismic reflection data, we see that such sediment types are typical of deep-water sediments because they are continuous and might include glacier deposits (Badley, 1985). A term describing this occurrence towards the seafloor is a gas-charged, slightly porous layer in a comprehensive work and fluid-related description characterising hydrocarbon leakage (Løseth et al., 2009a). It spans several lengths in height on seismic to about 350ms two-way travel time. Acting as an indicator that something might be charging this anomaly from below.

#### 11.4 V, w, and winglike shaped Anomaly

The Norwegian section of the North Sea has undergone several explorations in the past, and it is still undergoing present exploration that falls within the APA (awarded predefined areas), according to the NPD (Norwegian Petroleum Directorate). This implies that a lot is known about its geology, and it has facilities to ensure continual exploration efforts. Despite that, the basin's complex tectonic history and several geological models are still a subject of contention and arguments. (Evans, 2003; Fossen, 1989; Fossen & Hesthammer, 1998). One of these probable structures that has gained much attention due to its pervasiveness in the North Sea and is poorly understood form is the v, w and winglike structure. (Huuse et al., 2012; Huuse & Mickelson, 2004). Several unique reflections were encountered on all seismic sections, proving their vastness and occurrence, as shown in Fig. 49, Fig.50 and Fig. 51 of the given interpreted seismic.

Using time slices at a certain depth of observation was an attempt to quickly screen out these features, which are associated with the high anomaly observed, along with RMSA and Ant tracking variance attribute to investigate the bottom of this structure and along the structure. Figures 49, 50, and 51 report this occurrence from interpreted seismic, with examples of seismic showing the formation of this structure. The main observation is the pervasiveness of this structure from the west to the east. This structure's apparent pervasiveness and well-developed occurrences are inferred from the description to be more associated with the uplifted structure observed mostly in the west close to the east Shetland platform than examples noticeable to the east. A reasonable correlation can be made to suggest that this structure formation might be prominent and associated with the basin's complex tectonic history that somewhat gave rise to the uplifted structure is seen to be distinct to the west and is variable in occurrence. This structure tectonics is noted comprehensively by Evans (2003) in various authors' accounts.

This intrusive structure has been worked on primarily and represents a post-depositional structure that develops during the Northern basin's rifting stage. From observation from interpreted seismic, the implication is to show that the distribution is not without reason in the seismic area observed and that this structure is possibly also connected to the several shallow anomalies observed towards the sea floor through visible fractures and faults. Hence, it might act as a conduit to the high anomaly that might have contributed to the release of fluids to the seafloor and into the water column observed in the Northern Sea (Jackson et al., 2009).

Several authors have worked on this complex structure to understand its occurrence, geometry, and triggering mechanism of formation. ( i.e. Faeroe-Shetland. (Cartwright et al., 2008); Alba Field (Huuse et al., 2003, 2007); Tampen Spurr (Huuse & Mickelson, 2004); Volund (Huuse et al., 2009); Maløy slope (Jackson et al., 2009) ; Gamma Field; (Huuse et al., 2007) ). While its triggering mechanisms remain unsolved. Proposed triggering mechanisms have been highlighted, and it is described that for this structure to occur, three ingredients might have facilitated its formation.

- A deep-water system consisting of an unconsolidated sandstone encased in a low permeable sealing mudstone presence (Cartwright et al., 2008, 2008; Hurst et al., 2007; Huuse & Mickelson, 2004).
- The presence of an over-pressured condition caused by disequilibrium conditions (see section 6 for theoretical background with figures explain different pressure type), caused by rapid sediment loading resulting in differential compaction (Berndt, 2005; Cartwright et al., 2008; Huuse et al., 2007, 2007; Li et al., 2022).
- An occurrence of large-scale earthquakes, volcanic activity, intrusions, meteorites, landslides and faulting episodes capable of inducing this structure through Liquefaction processes (Huuse et al., 2009; Huuse & Mickelson, 2004).

It is also important to note that this structure has recently been associated with economic discoveries, as announced by NPD (Norwegian Petroleum Directorate). But argument still ensues about its formation and might be linked to the basin's complex tectonics (see section 2 with regards to some notable tectonic events and some ensuing arguments). This intervals are structures that are difficult to explain, and inferred not to be associated with a petroleum system.

#### 11.5 Fault, fractures, and Structures Encountered Probably Associated with Fluid Flow

As proof of the complexity of these tectonic episodes and the complex geology of the North Sea, there are subdivisions of two types of faults, fractures along with a sagging structure in which differential compaction could have occurred (Fig.58) as previously described:

1. **Small Faults:** These faults are classified as forming above the base Cretaceous, making a significant boundary associated with the late Jurassic-early Cretaceous. Above interpreted Horizon 1. This classification is not necessarily rigid. As fractures can be misidentified as a fault due to low image resolution (posing as a limitation), they might



not be imaged correctly due to seismic resolution. So, this resulted in some manual visual interpretation with a noticeable displacement of a previous continuous horizon that might not be imaged correctly using seismic attributes. Tectonics and complex basin inversion might have induced these fractures, from the crustal thickening and shortening crust following the main rifting events below the base Cretaceous (Evans, 2003). Another possible episode of event as an explanation for some of this structure and induced minor faults and fractures might be associated with the late Paleocene to early Eocene uplift, referred to as a marginal uplift following the breakup of the NE Atlantic during the Cenozoic (Faleide et al., 2002). These are described collectively as post-depositional structures that might have formed following the main rifting event below the base Cretaceous corresponding to the Mesozoic (main rifting stage) (Evans, 2003). Faulting imaged with variance time slice, having a cross-cutting relationship in Fig.54 and 55, are termed polygonal faulting, which forms at the top of the v, w and winglike amplitudes which have been previously described and documented by several literatures also falls within this category (see section.5 on some theoretical frameworks set initially this type of faults found on the North Sea). This type of faulting system is strata-bound and forms in mica-rich lithology, typical of clayey sediments (Berndt et al., 2003; Cartwright & Lonergan, 1996). The implication of this structure encountered in the result can also be part ways/conduits of fluids trapped in the v, w, and wing-like intrusion into the shallow anomalies seen towards the seafloor.

2. Large Fault components: These significant fault components are distinct features strictly underlying the interpreted base Cretaceous from the seismic image. A geo-profile image was attempted to show this large fault in Fig. 57. This composite figure was produced to show this fault system's occurrence, which was discussed previously as the main event characterising the Northern Sea basin and well covered in the tectonic history covered in section 2 briefly (Evans, 2003; Fossen & Hesthammer, 1998). This fault exists and is linked with several high amplitude anomalies terminating at depth along these structures, as shown in the composite image of Fig.57 and marked by dark oval circles at depth highlighting such high amplitude anomaly. These structures are most likely testament to the basin inversion, which might be the primary tectonic control during the Mesozoic which was covered in section 2 also Fig.12 of section 5 regarding a fault system called a Domino fault system (Evans, 2003; Fossen, 2016; Ziegler & Van, 1989). The implication of this fault might be somewhat linked to the source of the fluid

and complex tectonic history migrating the fluid in the v, w, and winglike shape anomaly into shallower areas (this is discussed later on).

3. Differential Compaction: Fig.58 presents an excellent example of structures found below the base Cretaceous structures beneath interpreted Horizon 1 (basis as been established). This structure is presented as a result, highlighting its significance and being somewhat pivotal in the remobilization of fluids. These structures are called out to highlight differential compactions of sediment formed from crustal thickening. These are described as both syndepositional and post-depositional features, which might prove pivotal in fluid movement from high to low-pressured areas accompanying its deformation. Hence, the Fig.56, 57 and 58 beneath the base Cretaceous emphasis.

However, it is very difficult to distinguish what might be fault or fracture which poses as a limitation.

#### 11.6 Fluid Flow Structures and Leakages on Tampen Spurr.

Concerning fluid flow structures, which have been discussed in previous chapters, giving some examples in section 8 Berndt (2005) on the theoretical framework of fluid flow. Fig. 59 and 61. Fig.63 and 64 show an RMSA map of the seafloor merged with a research cruise by NPD in 2022 and a time-depth map of the seafloor in two-way travel time to map out flare data showing the area of seeps along the embankment of the area study, which is the key objective of this study. This might often be a buoyancy-driven migration process from highly pressurised areas of natural gases from deeper source into shallower and overlying layers. Some likely mechanisms that might have formed these processes, according to existing literature ( i.e. (Arntsen et al., 2007; Løseth et al., 2009a, 2009b) are ;

1. Tectonic activity/ tectonic forces, such as faulting and fractures, can create pathways for natural gas to migrate vertically through and across formation/Lithology. These fractures and faults might have acted as conduits for gas to ascend to the seafloor into the water column in the study area, which can be linked to the formation of vertical deteriorated seismic signals observe in Fig. 59 and 61
2. Diagenetic Processes: Strong evidence for the gas chimneys observed on given examples of what looks like acoustic masking are diagenetic processes altering the physical and chemical changes in a sedimentary rock during burial and compaction, creating impermeable formations capable of migrating gas from depth vertically to the

shallower surface. This is the case with structures seen at the interpreted base Cretaceous on all 3D seismic cubes. Significant fault components, folding, growth fault, and differential compaction were seen at the base Cretaceous following the basin inversion and crustal thickening as attested to by Evans (2003).

3. Capillary Effects: Differential pressure might have been experienced during the uplift (basin inversion / Crustal Thickening), documented by (Evans, 2003; Fossen, 2016), which was more intense to the west of the study area, as witnessed by the differential folding and subducted base of the Cretaceous. This differential pressure might have migrated fluids, which includes natural gas, mobilised at the base Cretaceous. A theoretical framework for Capillarity effects and pressure was established in Section 6.

The geometry of this chimney that has formed within the study area varies in size, ranging from narrow conduits to broader, funnel-shaped structures, possibly due to lithology types and structural control of the Chimney.

#### 11.7 Potential Geological Model, rootpoint and Triggers for the North Northern Sea gas seepage.

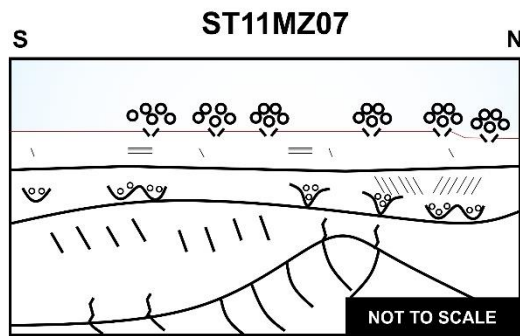
The schematic model attempts to interpret observed seismic data results based on DHIs (see section 9), high anomalies, identifiable structures, and other available geological assumptions and datasets covered in previous chapters. This model seeks to explain the trigger and root from the known petroleum system below the base Cretaceous of the seafloor using a simplified approach, as shown in Fig.66.

The proposed model attempts to explain that fluid release into the seafloor might be of a thermogenic source of origin (a known petroleum system), released from below the base of the Cretaceous fueled by an existing petroleum system (see section 6 for a theoretical framework) at a depth beyond the base of Cretaceous, with a source of fluid that spans to the base Cretaceous. This statement with attempted examples from Fig.59 and 61 is based on assumptions following the main rifting event of the late Cretaceous and early Jurassic rifting stages, which is complex. Furthermore, this main event might be a controlling factor that induced stress on the basin and shaped it with fractures and faults that might have carved the V, W, and wing-like sandstone intrusion and charged it with fluids within the Paleogene sequence ( Fossen, 1989; Ziegler, 1992; Ziegler & Van, 1989).

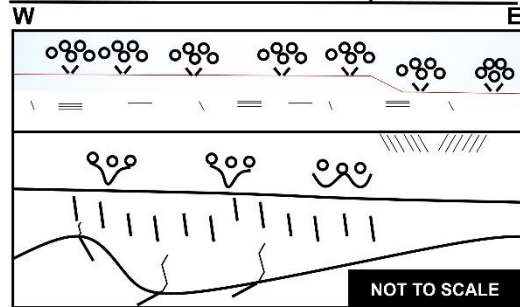
In summary, the model in Fig.66 attempts to explain the source of fluid to the West embankment rather than to the eastern sides of banks falling on the Norwegian Trench—an account of the

holes seen are somewhat resulting from prograding fluvial input from east Shetland platform of the UK sector onto the embankment.(Ottesen et al., 2018). Other accounts that might have influenced this fluid seep seen might include (i.e. climatic factors, eustatic changes and weather conditions capable of eroding unconsolidated material brought from the west bank input of east Shetland, but they are also another possible explanation that can account for driving these seeps on the banks, close to the east Shetland platform (Gołędowski et al., 2012). In summary, the source of fluids is from a known event associated with an active source of fluid from the base Cretaceous fueling the seeps above through various migrations through faults and fractures initiated by the complex tectonics (Fig.66).

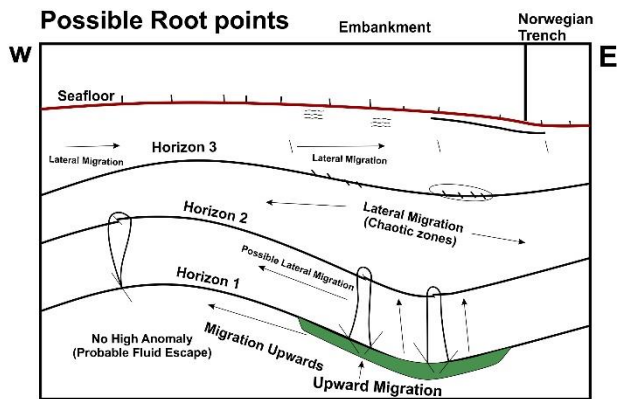
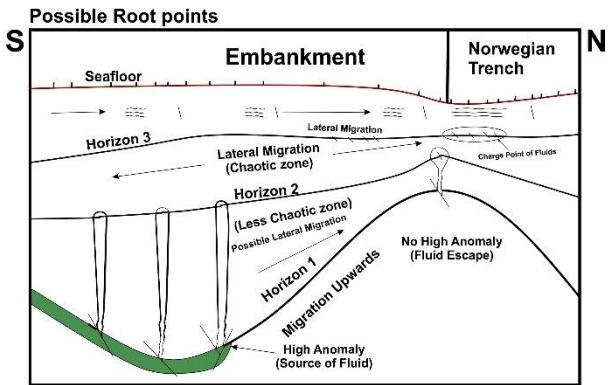
East Shetland Platform **Sloping Downwards** Norwegian Trench



East Shetland Platform **Sloping Downwards** Norwegian Trench



- Large Fault Component (Fossen, 1989, 2016; Fossen & Hesthammer Ziegler 1990)
- Polygonal Fault Component (Berndt et al., 2003; Cartwright & Lonergan, 1996)
- Fluid
- Charged Shallow Gas in semi permeable layer (Løseth et al., 2009)
- Fault/ Fracture Component
- Variation of Intruded Sandstone (Huse and Mickelson (2009))
- Sea Floor
- Source of Fluids
  - base Cretaceous petroleum systems (Horstad et al. (1995))



- Shallow Gas
- Gas Seeps
- Faults and Fractures
- Migration Pathways
- Dying Anomaly/ Leaks
- Source of Fluids (Sagging anticlinal structure associated with)

Inspired by: (Løseth et al., 2009)

Figure 66: Proposed Model and root points of possible fluid and migration pathways (Not to scale and not generalized)

## 12. Conclusion

Based on the short stint of studies conducted in this research, three 3D-seismic cubes were obtained along the North Sea, with bathymetry data and flare data from NPD. This has led to the following observations and conclusions that can be made. This includes:

- The North Sea is a peculiar basin in which the long and complex tectonic activity is a primary driver for structures encountered on the seismic, such as the large growth fault, normal faults observed at the base Cretaceous of the seismic, and more minor faults observed at the shallower part of the Cenozoic region of the basin which comprises of smaller faults components and fractures dominating upper regions. This brings about the classification of the faults observed in the following groups:
  - Prerifted structures: These structures are deep-seated as growth faults, normal faults of several lengths, as discussed, representing the significant fault components observed.
  - Synrifted structures: These are initiated by the more minor fractures and faults initiated after the rifting episode of the basin. This is picked up by the ant tracking and variance attributes shown.
  - Post-rifted structures: These are structures such as the polygonal faulting that might have reactivated by another episode of tectonic stress. And, after the main rifting effect. It can also be induced by fluids trapped and finding itself towards the seafloor.
- The fluid and high anomaly observed from the base Cretaceous to Quaternary sediment package are tectonically controlled and trapped due to the complex nature of tectonic history, attested to by various features observed on the seismic.
- The gas fluid expulsion prevalent on the seafloor and into the water column is aided primarily by the fast-flowing streams of ice characterized by the Norwegian Channel, stripping away/ eroding sediments, and thereby lowering overburden pressure capable of keeping fluids at bay, to be released into the water column. This holds for a 3D-seismic cube corresponding to NX0802 and ST98M7, which falls on the Norwegian Channel based on observation.
- The severity of the tectonic setting has been imaged on the variance map at the base Cretaceous of the ST11MZ07 might somewhat have induced stresses and triggers that

might have had large-scale implications on fluid expulsion to the west embankment and the structural high to the west of the study area sloping into the Trench.

- Fluids are most likely to have a thermogenic origin from strong root points/source points from the base Cretaceous of 3D seismic cubes, which seem persistent in all seismic cubes. This is not generalized but assumed from the given example.
- The source of fluids is somewhat likely of Thermogenic origin. However, it is not generalised; it is only hinted at and might be wrong if isotopic analysis is carried out on seeps.
- Causes of seeps at the embankment are most likely from erosion and stripping of sediments downslope processes associated with the Norwegian Trench to the east and the south of the Norwegian Trench. Charging the slope.

### 13. Further Works

The most common thoughts are:

- Carrying out geochemical and isotopic analysis on fluid seep to determine the fluid source for other forms of source of fluid.
- A proper characterization of cross-cutting relationships of faults, fracture and structural analysis wasn't adequately covered due to a lack of imaging resolution.
- A proper chronostratigraphic marker, well data calibration and 2D seismic integration to properly characterise Quaternary stratigraphy with shallow gas hinting at unique seismic reflections and possible fluid movement.

# REFERENCES

- Andreia Plaza, F., Stefan, B., & Jürgen, M. (n.d.). Repeated fluid expulsion through sub-seabed chimneys offshore Norway in response to glacial cycles. *Department of Geology, Dramsveien 201, University of Tromsø, Norway*, 33.
- Arntsen, B., Wensaas, L., Løseth, H., & Hermanrud, C. (2007). Seismic modeling of gas chimneys. *GEOPHYSICS*, 72(5), SM251–SM259. <https://doi.org/10.1190/1.2749570>
- Badley, M. E. (1985). *Practical seismic interpretation*. Internat. Human Resources Development Corp. [u.a.].
- Batchelor, C. L., Ottesen, D., & Dowdeswell, J. A. (2017). Quaternary evolution of the northern North Sea margin through glacial debris-flow and contourite deposition. *Journal of Quaternary Science*, 32(3), 416–426. <https://doi.org/10.1002/jqs.2934>
- Becker, L. W. M., Sejrup, H. P., Hjelstuen, B. O., Haflidason, H., & Dokken, T. M. (2018). Ocean-ice sheet interaction along the SE Nordic Seas margin from 35 to 15 ka BP. *Marine Geology*, 402, 99–117. <https://doi.org/10.1016/j.margeo.2017.09.003>
- Berndt, C. (2005). Focused fluid flow in passive continental margins. *Philosophical Transactions of the Royal Society A: Mathematical, Physical and Engineering Sciences*, 363(1837), 2855–2871. <https://doi.org/10.1098/rsta.2005.1666>
- Berndt, C., Büinz, S., & Mienert, J. (2003). Polygonal fault systems on the mid-Norwegian margin: A long-term source for fluid flow. *Geological Society, London, Special Publications*, 216(1), 283–290. <https://doi.org/10.1144/GSL.SP.2003.216.01.18>
- Böttner, C., Haeckel, M., Schmidt, M., Berndt, C., Vielstädte, L., Kutsch, J. A., Karstens, J., & Weiß, T. (2020). Greenhouse gas emissions from marine decommissioned hydrocarbon wells: Leakage detection, monitoring and mitigation strategies.



*International Journal of Greenhouse Gas Control*, 100, 103119.

<https://doi.org/10.1016/j.ijggc.2020.103119>

Bradwell, T., Small, D., Fabel, D., Clark, C. D., Chiverrell, R. C., Saher, M. H., Dove, D., Callard, S. L., Burke, M. J., Moreton, S. G., Medialdea, A., Bateman, M. D., Roberts, D. H., Golledge, N. R., Finlayson, A., Morgan, S., & Cofaigh, C. Ó. (2021). Pattern, style and timing of British–Irish Ice Sheet retreat: Shetland and northern North Sea sector. *Journal of Quaternary Science*, 36(5), 681–722.

<https://doi.org/10.1002/jqs.3163>

Bradwell, T., Stoker, M. S., Golledge, N. R., Wilson, C. K., Merritt, J. W., Long, D., Everest, J. D., Hestvik, O. B., Stevenson, A. G., Hubbard, A. L., Finlayson, A. G., & Mathers, H. E. (2008). The northern sector of the last British Ice Sheet: Maximum extent and demise. *Earth-Science Reviews*, 88(3–4), 207–226.

<https://doi.org/10.1016/j.earscirev.2008.01.008>

Bünz, S., Polyanov, S., Vadakkepuliambatta, S., Consolaro, C., & Mienert, J. (2012). Active gas venting through hydrate-bearing sediments on the Vestnesa Ridge, offshore W-Svalbard. *Marine Geology*, 332–334, 189–197.

<https://doi.org/10.1016/j.margeo.2012.09.012>

Caillet, G. (1993). The caprock of the Snorre Field, Norway: A possible leakage by hydraulic fracturing. *Marine and Petroleum Geology*, 10(1), 42–50.

[https://doi.org/10.1016/0264-8172\(93\)90098-D](https://doi.org/10.1016/0264-8172(93)90098-D)

Cartwright, J., James, D., Huuse, M., Vetel, W., & Hurst, A. (2008). The geometry and emplacement of conical sandstone intrusions. *Journal of Structural Geology*, 30(7), 854–867. <https://doi.org/10.1016/j.jsg.2008.03.012>

- Cartwright, & Lonergan. (1996). Volumetric contraction during the compaction of mudrocks: A mechanism for the development of regional-scale polygonal fault systems. *Basin Research*, 8(2), 183–193. <https://doi.org/10.1046/j.1365-2117.1996.01536.x>
- Clark, C. D., Hughes, A. L. C., Greenwood, S. L., Jordan, C., & Sejrup, H. P. (2012). Pattern and timing of retreat of the last British-Irish Ice Sheet. *Quaternary Science Reviews*, 44, 112–146. <https://doi.org/10.1016/j.quascirev.2010.07.019>
- Clemmensen, L. B., JACOBSEN, V., & STEEL, R. (1980). *Some aspects of Triassic sedimentation and basin development: East Greenland, North Scotland and North Sea. Norsk Petroleumsforening.*
- Cloetingh, S., & Kooi, H. (1992). *Intraplate stresses and dynamical aspects of rift basins.* (Vol. 3).
- De Schepper, S., & Mangerud, G. (2018). Age and palaeoenvironment of the Utsira Formation in the northern North Sea based on marine palynology. *Norwegian Journal of Geology*. <https://doi.org/10.17850/njg97-4-04>
- Deegan, C. E., & Scull, B. J. (1977). A proposed standard lithostratigraphic nomenclature for the central and Northern North Sea. *Bull. Norw. Petrol. Direct., No. 1, HMSO, London.*
- Dimitrov, L. (2002). Contribution to atmospheric methane by natural seepages on the Bulgarian continental shelf. *Continental Shelf Research*, 22(16), 2429–2442. [https://doi.org/10.1016/S0278-4343\(02\)00055-9](https://doi.org/10.1016/S0278-4343(02)00055-9)
- Eidvin, T., Jansen, E., Rundberg, Y., Brekke, H., & Grogan, P. (2000). *The upper Cenozoic of the Norwegian continental shelf correlated with the deep sea record of the Norwegian Sea and the North Atlantic* (pp. 579–600). *Marine and Petroleum Geology*.
- Eidvin, T., & Rundberg, Y. (2007). Post-Eocene strata of the southern Viking Graben, northern North Sea; integrated biostratigraphic, strontium isotopic and

- lithostratigraphic study. In *Post-Eocene strata of the southern Viking Graben, northern North Sea; integrated biostratigraphic, strontium isotopic and lithostratigraphic study* (Vol. 87, pp. 391–450).
- Evans, D. (2003). *The millennium atlas: Petroleum geology of the central and northern North Sea*. The Geological Society of London.
- Faleide, J. I., Kyrkjebø, R., Kjennerud, T., Gabrielsen, R. H., Jordt, H., Fanavoll, S., & Bjerke, M. D. (2002). Tectonic impact on sedimentary processes during Cenozoic evolution of the northern North Sea and surrounding areas. *Geological Society, London, Special Publications*, 196(1), 235–269.  
<https://doi.org/10.1144/GSL.SP.2002.196.01.14>
- Fossen, H. (1989). *Indication of transpressional tectonics in the Gullfaks oilfield, northern North Sea* (pp. 22–30).
- Fossen, H. (2016). *Structural geology* (Second edition). Cambridge University Press.
- Fossen, H., & Hesthammer, J. (1998). Structural geology of the Gullfaks Field, northern North Sea. *Geological Society, London, Special Publications*, 127(1), 231–261.  
<https://doi.org/10.1144/GSL.SP.1998.127.01.16>
- Fyfe, J. A., Gregersen, U., Jordt, H., Runderg, Y., Eidvin, T., Evans, D., & Andresen, P. (2003). *Oligocene to holocene. The Millennium Atlas: Petroleum geology of the central and northern North Sea* (pp. 279–287).
- Galloway, W. E. (2002). Paleogeographic Setting and Depositional Architecture of a Sand-Dominated Shelf Depositional System, Miocene Utsira Formation, North Sea Basin. *Journal of Sedimentary Research*, 72(4), 476–490.  
<https://doi.org/10.1306/110801720476>
- Gandy, N., Gregoire, L. J., Ely, J. C., Cornford, S. L., Clark, C. D., & Hodgson, D. M. (2021). Collapse of the Last Eurasian Ice Sheet in the North Sea Modulated by Combined

- Processes of Ice Flow, Surface Melt, and Marine Ice Sheet Instabilities. *Journal of Geophysical Research: Earth Surface*, 126(4), e2020JF005755.  
<https://doi.org/10.1029/2020JF005755>
- Gołędowski, B., Nielsen, S. B., & Clausen, O. R. (2012). Patterns of Cenozoic sediment flux from western Scandinavia. *Basin Research*, 24(4), 377–400.  
<https://doi.org/10.1111/j.1365-2117.2011.00530.x>
- Gregersen, U., & Johannessen, P. N. (2007). Distribution of the Neogene Utsira Sand and the succeeding deposits in the Viking Graben area, North Sea. *Marine and Petroleum Geology*, 24(10), 591–606. <https://doi.org/10.1016/j.marpetgeo.2007.04.006>
- Hald, M., & Vorren, T. O. (1984). *Modern and Holocene Foraminifera and sediments on the continental shelf off, North Norway* (pp. 133–154). *Boreas* 13,.
- Hedberg, H. D. (1976). International Stratigraphic Guide: A guide to stratigraphic classification, terminology and procedure. *International Subcommission on Stratigraphic Classification of IUGS Commission on Stratigraphy*. Wiley-Interscience, New York.
- Hjelstuen, B. O., Nygård, A., Sejrup, H. P., & Haflidason, H. (2012). Quaternary denudation of southern Fennoscandia – evidence from the marine realm. *Boreas*, 41(3), 379–390.  
<https://doi.org/10.1111/j.1502-3885.2011.00239.x>
- Holder, G. D., Katz, D. L., & Hand, J. H. (1976). *Hydrate Formation in Subsurface Environments*. (pp. 981–988). AAPG.
- Hornafius, J. S., Quigley, D., & Luyendyk, B. P. (1999). The world's most spectacular marine hydrocarbon seeps (Coal Oil Point, Santa Barbara Channel, California): Quantification of emissions. *Journal of Geophysical Research: Oceans*, 104(C9), 20703–20711.  
<https://doi.org/10.1029/1999JC900148>

- Horstad, I., Larter, S. R., & Mills, N. (1995). Migration of hydrocarbons in the Tampen Spur area, Norwegian North Sea: A reservoir geochemical evaluation. *Geological Society, London, Special Publications*, 86(1), 159–183.  
<https://doi.org/10.1144/GSL.SP.1995.086.01.12>
- Hovland, M. (2002). On the self-sealing nature of marine seeps. *Continental Shelf Research*, 22(16), 2387–2394. [https://doi.org/10.1016/S0278-4343\(02\)00063-8](https://doi.org/10.1016/S0278-4343(02)00063-8)
- Hubbert, M. K., & Rubey, W. W. (1959). Role of fluid pressure in mechanics of overthrusting faulting. In *Role of fluid pressure in mechanics of overthrusting faulting* (pp. 115–166). AAPG Bulletin.70. [https://doi.org/10.1130/0016-7606\(1959\)70\[115:ROFPIM\]2.0.CO;2](https://doi.org/10.1130/0016-7606(1959)70[115:ROFPIM]2.0.CO;2)
- Hughes, A. L. C., Gyllencreutz, R., Lohne, Ø. S., Mangerud, J., & Svendsen, J. I. (2016). The last Eurasian ice sheets – a chronological database and time-slice reconstruction, DATED-1. *Boreas*, 45(1), 1–45. <https://doi.org/10.1111/bor.12142>
- Hurst, A., Cartwright, J. A., & American Association of Petroleum Geologists (Eds.). (2007). *Sand injectites: Implications for hydrocarbon exploration and production*. American Association of Petroleum Geologists.
- Huuse, M., A. L. Jackson, C., Olobayo, O., Dmitrieva, E., & J. Andresen, K. (2012, June 4). A *sand injectite stratigraphy for the North Sea*. 74th EAGE Conference and Exhibition incorporating EUROPEC 2012, Copenhagen, Denmark. <https://doi.org/10.3997/2214-4609.20148702>
- Huuse, M., Cartwright, J., Hurst, A., & Steinsland, N. (2007). Seismic Characterization of Large-scale Sandstone Intrusions. In *Sand Injectites* (pp. 21–35). American Association of Petroleum Geologists. <https://doi.org/10.1306/1209847M873253>
- Huuse, M., Duranti, D., Guargena, C. G., Prat, P., Holm 1, K., Steinsland 1, N., Cronin 1, B. T., & Hurst, N. (2003). Sandstone intrusions: Detection and significance for

- exploration and production. *First Break*, 21(9). <https://doi.org/10.3997/1365-2397.2003014>
- Huuse, M., Jackson, C., Cartwright, J., & Hurst, A. (2009). *Large-Scale Sand Injectites in the North Sea: Seismic and Event Stratigraphy and Implications for Hydrocarbon Exploration*.
- Huuse, M., & Mickelson, M. (2004). Eocene sandstone intrusions in the Tampen Spur area (Norwegian North Sea Quad 34) imaged by 3D seismic data. *Marine and Petroleum Geology*, 21(2), 141–155. <https://doi.org/10.1016/j.marpetgeo.2003.11.018>
- Isaksen, D., & Tonstad, K. (1989). A revised Cretaceous and Tertiary lithostratigraphic nomenclature for the Norwegian North Sea. In *A revised Cretaceous and Tertiary lithostratigraphic nomenclature for the Norwegian North Sea* (p. 59). NPD Bulletin 5,.
- Jackson, C., Barber, G., & Huuse, M. (2009). Geometric Characterisation of Clastic Intrusion Complexes Adjacent to a Deep-Water Slope Channel: A 3D Seismic Case Study from Offshore Norway. *AAPG*.
- Judd, A., Davies, G., Wilson, J., Holmes, R., Baron, G., & Bryden, I. (1997). Contributions to atmospheric methane by natural seepages on the UK continental shelf. *Marine Geology*, 137(1–2), 165–189. [https://doi.org/10.1016/S0025-3227\(96\)00087-4](https://doi.org/10.1016/S0025-3227(96)00087-4)
- Judd, A. G. (2004). Natural seabed gas seeps as sources of atmospheric methane. *Environmental Geology*, 46(8), 988–996. <https://doi.org/10.1007/s00254-004-1083-3>
- Judd, A., & Hovland, M. (2009). *Seabed Fluid Flow: The Impact on Geology, Biology and the Marine Environment*. Cambridge University Press.  
<https://books.google.no/books?id=RhFfigXasLQC>

- King, E. L., Haflidason, H., Sejrup, H. P., & Løvlie, R. (1998). *Glacigenic debris flows on the North Sea Trough Mouth Fan during icestream maxima* (pp. 217–246). *Marine Geology* 152.
- King, E. L., Sejrup, H. P., Haflidason, H., Elverhøi, A., & Aarseth, I. (1996). Quaternary seismic stratigraphy of the North Sea Fan: Glacially-fed gravity flow aprons, hemipelagic sediments, and large submarine slides. *Marine Geology*, 130(3–4), 293–315. [https://doi.org/10.1016/0025-3227\(95\)00168-9](https://doi.org/10.1016/0025-3227(95)00168-9)
- Kvenvolden, K. A., & McMennamin, M. A. (1980). *Hydrates of natural gas: A review of their geological occurrence* (pp. 1–11).
- Li, C., Zhan, L., & Lu, H. (2022). Mechanisms for Overpressure Development in Marine Sediments. *Journal of Marine Science and Engineering*, 10(4), 490. <https://doi.org/10.3390/jmse10040490>
- Løseth, H., Gading, M., & Wensaas, L. (2009a). Hydrocarbon leakage interpreted on seismic data. *Marine and Petroleum Geology*, 26(7), 1304–1319. <https://doi.org/10.1016/j.marpetgeo.2008.09.008>
- Løseth, H., Gading, M., & Wensaas, L. (2009b). Hydrocarbon leakage interpreted on seismic data. *Marine and Petroleum Geology*, 26(7), 1304–1319. <https://doi.org/10.1016/j.marpetgeo.2008.09.008>
- Løseth, H., Nygård, A., Batchelor, C. L., & Fayzullaev, T. (2022). A regionally consistent 3D seismic-stratigraphic framework and age model for the Quaternary sediments of the northern North Sea. *Marine and Petroleum Geology*, 142, 105766. <https://doi.org/10.1016/j.marpetgeo.2022.105766>
- Løseth, H., Wensaas, L., Arntsen, B., Hanken, N.-M., Basire, C., & Graue, K. (2011). 1000 m long gas blow-out pipes. *Marine and Petroleum Geology*, 28(5), 1047–1060. <https://doi.org/10.1016/j.marpetgeo.2010.10.001>

- Magoon, L. B., & Dow, W. G. (1994). *The Petroleum System- from source to trap*. AAPG Memoir 60.
- Makogon, Y. F. (1981). *Hydrates of Natural Gas*. Penn Well Publ.Co.
- Makogon, Y. F., Trebin, F. A., Trofimuk, A. A., Tsarev, V. P., & Cherskiy, N. V. (1971). *Detection of a pool of natural gas in a solid (hydrated gas) state* (pp. 197–200). Dokl. Akad Nauk SSSR 196.
- Mørk, M. B. E., & Duncan, R. A. (1993). Late Pliocene basaltic volcanism on the Western Barents Shelf margin: Implications from petrology and Ar-Ar dating of volcanoclastic debris from a shallow drill core. In *Late Pliocene basaltic volcanism on the Western Barents Shelf margin: Implications from petrology and Ar-Ar dating of volcanoclastic debris from a shallow drill core*. (pp. 209–225). Norsk Geologisk Tidsskrift 73.
- Mueller, B., Wehrle, V., & Fuchs, K. (1997). *Release of the World Stress Map*. <http://www-wsm.physik.uni-karlsruhe.de/>
- Nygård, A., Sejrup, H. P., Hafliðason, H., & Bryn, P. (2005). The glacial North Sea Fan, southern Norwegian Margin: Architecture and evolution from the upper continental slope to the deep-sea basin. *Marine and Petroleum Geology*, 22(1–2), 71–84. <https://doi.org/10.1016/j.marpetgeo.2004.12.001>
- Ottesen, D., Batchelor, C. L., Dowdeswell, J. A., & Løseth, H. (2018). Morphology and pattern of Quaternary sedimentation in the North Sea Basin (52–62°N). *Marine and Petroleum Geology*, 98, 836–859. <https://doi.org/10.1016/j.marpetgeo.2018.08.022>
- Ottesen, D., Dowdeswell, J. A., & Bugge, T. (2014). Morphology, sedimentary infill and depositional environments of the Early Quaternary North Sea Basin (56°–62°N). *Marine and Petroleum Geology*, 56, 123–146. <https://doi.org/10.1016/j.marpetgeo.2014.04.007>



- Ottesen, D., Stewart, M., Brønner, M., & Batchelor, C. L. (2020). Tunnel valleys of the central and northern North Sea (56°N to 62°N): Distribution and characteristics. *Marine Geology*, 425, 106199. <https://doi.org/10.1016/j.margeo.2020.106199>
- Ottesen, D., Stokes, C. R., Bøe, R., Rise, L., Longva, O., Thorsnes, T., Olesen, O., Bugge, T., Lepland, A., & Hestvik, O. B. (2016). Landform assemblages and sedimentary processes along the Norwegian Channel Ice Stream. *Sedimentary Geology*, 338, 115–137. <https://doi.org/10.1016/j.sedgeo.2016.01.024>
- Patton, H., Hubbard, A., Heyman, J., Alexandropoulou, N., Lasabuda, A. P. E., Stroeven, A. P., Hall, A. M., Winsborrow, M., Sugden, D. E., Kleman, J., & Andreassen, K. (2022). The extreme yet transient nature of glacial erosion. *Nature Communications*, 13(1), 7377. <https://doi.org/10.1038/s41467-022-35072-0>
- Pettersen, O., Storli, A., Ljosland, E., & Nyaard, O. (1990). The Gullfaks Field. In *The Gullfaks Field* (pp. 429–446).
- Phillips, E., Hodgson, D. M., & Emery, A. R. (2017). The Quaternary geology of the North Sea basin. *Journal of Quaternary Science*, 32(2), 117–126. <https://doi.org/10.1002/jqs.2932>
- Plaza-Faverola, A., Bünz, S., Johnson, J. E., Chand, S., Knies, J., Mienert, J., & Franek, P. (2015). Role of tectonic stress in seepage evolution along the gas hydrate-charged Vestnesa Ridge, Fram Strait. *Geophysical Research Letters*, 42(3), 733–742. <https://doi.org/10.1002/2014GL062474>
- Rasmussen, E. S., Dybkjær, K., & Piasecki, S. (2010). *Lithostratigraphy of the Upper Oligocene-Miocene succession of Denmark*. Geological Survey of Denmark and Greenland, Ministry of Climate and Energy.

- Rise, L. (2004). Mid-Pleistocene ice drainage pattern in the Norwegian Channel imaged by 3D seismic. *Quaternary Science Reviews*, 23(23–24), 2323–2335.  
<https://doi.org/10.1016/j.quascirev.2004.04.005>
- Schulte, B. (2024). *Seismic Acquisition*.
- Sebastian, N. (2022). *Sand Injectites in the northern North Sea Basin*. The University of Manchester.
- Sejrup, H. P., Aarseth, I., Haflidason, H., Løvlie, R., Tien, Å. B., Tjøstheim, G., Forsberg, C. F., & Ellingsen, K. L. (1995). *Quaternary of the Norwegian Channel: Glaciation history and palaeoceanography*. <https://api.semanticscholar.org/CorpusID:131584449>
- Sejrup, H. P., Clark, C. D., & Hjelstuen, B. O. (2016). Rapid ice sheet retreat triggered by ice stream debuttrressing: Evidence from the North Sea. *Geology*, 44(5), 355–358.  
<https://doi.org/10.1130/G37652.1>
- Sejrup, H. P., Hjelstuen, B. O., Nygård, A., Haflidason, H., & Mardal, I. (2015). Late DEVENSIAN ice-marginal features in the central North Sea – processes and chronology. *Boreas*, 44(1), 1–13. <https://doi.org/10.1111/bor.12090>
- Sejrup, H. P., Larsen, E., Haflidason, H., Berstad, I. M., Hjelstuen, B. O., Jonsdottir, H. E., King, E. L., Landvik, J., Longva, O., Nygård, A., Ottesen, D., Raunholm, S., Rise, L., & Stalsberg, K. (2003). Configuration, history and impact of the Norwegian Channel Ice Stream. *Boreas*, 32(1), 18–36. <https://doi.org/10.1080/03009480310001029>
- Selley, R. C., & Sonnenberg, S. A. (2015). *Elements of petroleum geology* (Third edition). Elsevier, Academic Press.
- Sloan, E. D. (1990). Clathrate Hydrates of Natural Gases. *Marcel Decker New York*.
- Stoker, M. S., Balson, P. S., Long, D., & Tappin, D. R. (2011). *An overview of the lithostratigraphical framework for the Quaternary deposits on the United Kingdom continental shelf* (p. 48). British Geological Survey Research Report RR/11/03.

- Svensen, H., Planke, S., Jamtveit, B., & Pedersen, T. (2003). Seep carbonate formation controlled by hydrothermal vent complexes: A case study from the Vøring Basin, the Norwegian Sea. *Geo-Marine Letters*, 23(3–4), 351–358.  
<https://doi.org/10.1007/s00367-003-0141-2>
- Terzaghi, K. (1936). *The shearing resistance of saturated soils* (Vol. 1, pp. 54–56).
- Thöle, H., Gaedicke, C., Kuhlmann, G., & Reinhardt, L. (2014). *Late Cenozoic sedimentary evolution of the German North Sea—A seismic stratigraphic approach*. (pp. 299-329.). Newsletters on Stratigraphy,.
- Vollset, J., & Dore, A. G. (1984). *A revised Triassic and Jurassic Lithostratigraphic nomenclature for the Norwegian North Sea*. Oljedirektoratet.
- Ziegler, P. A. (1990). *Geological atlas of western and central Europe 1990* (2nd. ed). Shell Internationale Petroleum Maatschappij BV.
- Ziegler, P. A. (1992). North Sea rift system. *Tectonophysics*, 208(1–3), 55–75.  
[https://doi.org/10.1016/0040-1951\(92\)90336-5](https://doi.org/10.1016/0040-1951(92)90336-5)
- Ziegler, P. A., & Van, H. (1989). *Evolution of the North Sea Rift* (pp. 471–500). AAPG Memoir 46.

## **List of Tables**

Table 1: 3D seismic Data Acquisition and Processing Information .....	64
Table 2 shows the vertical and resolution of the 3D seismic data used. Frequencies used are selected from spectral analysis and inspecting of 3D data (See Fig.29 for dominating frequencies used ). ....	64
Table 3: shows Vertical Resolution based on chronostratigraphic age concerning dominant frequencies used in estimating seismic cubes ( See Fig.29 for dominating frequencies used ).	
Information obtained from previous studies in the area with well logs (Sebastian, 2022).....	65
Table 4: Seismic attributes are used in interpretation, and what are they measured. ....	69

Table 5: Parameters Inputted for both Volume and surface attribute. (Most are default settings except that of the antracking).....	69
Table 6: showing examples of seismic units and seismic descriptions of their facies units obtained from a 3D seismic cube of Nx0802. Terminologies used are obtained from Løseth et al.(2009).....	78
Table 7: showing examples of seismic units and seismic descriptions of their facies units obtained from a 3D seismic cube of ST98M7. Terminologies used are obtained from Løseth et al. (2009). .....	79
Table 8: showing examples of seismic units and seismic description of its facies unit obtained from 3D seismic cube of ST11MZ07. Terminologies used are obtained from Løseth et al. (2009). .....	80

# List of Figures

Figure 1: Possible origins of CH <sub>4</sub> from the lithosphere to the hydrosphere and the fate of fluids and natural gas seepage need to be explained. Inspired by ( Judd, 2004). .....	11
Figure 2: A bathymetry map showing the study area marked in red and corresponding seismic cubes (ST11MZ07, ST98M7 and NX0802) analysed with major subbasins. Where NVG is North Viken Graben, SVG is South Viken Graben.....	12
Figure 3: showing the structural map of the Northern Sea and its basins. Where alphabets A to H represents cleavage zones previously identified and mapped out. Modified from fig 4.2 Evans (2003) .....	14
Figure 4: Extension of the North Sea basin during the late Jurassic to early Cretaceous rifting stage. Modified from Evans (2003).....	16
Figure 5: Tectonic History of the North Sea Basin and corresponding lithologies, showing the 3 main rifting episodes (Highly generalized for the North sea). Modified from Evans (2003). .....	18
Figure 6: Stratigraphic column of the Quaternary with timescale, palaeomagnetic column, marine isotope stages, and regional stage divisions from diverse authors for the North Sea basin. Image modified from figure 2 of Phillips et al. (2017). .....	23
Figure 7: showing a map of possible maximum glaciation scenarios of the Nordic Sea cutting across Northern Sea. Figure from Sejrup et al. (2003) .....	25
Figure 8: showing the extent, collapse of the Eurasian sheets attested to by several authors. Modified from Gandy et al. (2021) .....	26
Figure 9: Lithological Nomenclature using the Gullfaks field. The Green area in Inspired by Figure 15 Pettersen et al.(1990).....	28
Figure 10. General stratigraphy cutting across Tampen Spurr. Inspired by Fig. 3. Horstad et al.( 1995) .....	35
Figure 11: The basic type of faults with corresponding stress regimes. A). Normal fault caused by extensional stress B). Reverse Faults caused by compressional stress C). Strike- Slip fault accompanied by shear stress. ....	38
Figure 12: Domino/ Structural Type Model accompanying extension of north Northern Sea. A). shows the lithology prior to deformation B). Dipping of fault following rotation at an angle 30° C). Further dips of 10° due to shearing and realignment of grains. Inspired by Fossen (2016), Pettersen et al. (1990) & Ziegler (1992).....	39
Figure 13: A simple cross section of a Petroleum system. Inspired by figure 7.1 (Selley & Sonnenberg, 2015).....	40
Figure 14: A simplistic illustration of Darcy's Experiment. ....	41
Figure 15: Showing fluid replacement due to capillary pressure and wettability of different fluids. Figure 6.14 of (Selley & Sonnenberg, 2015).....	42
Figure 16: showing the entry of petroleum into a water filled reservoir. ....	42
Figure 17: Van Krevelen diagram. Inspired by Selley & Sonnenberg (2015).....	43
Figure 18: Depth and Pressure relationship illustrating hydrostatic and lithostatic (geostatic) pressures and concepts inspired by (Selley & Sonnenberg, 2015) & (Li et al., 2022).....	46
Figure 19: Pressure and Depth relationship of Marine sediments and corresponding stress. modified from fig 1 of (Li et al., 2022) .....	47
Figure 20: shows a.) compressional stress applied to a strata b.) A shear stress applied to a strata. Both result in the overpressure of fluids. Modified from figure 6 of (Li et al., 2022).....	48

Figure 21: showing a compaction fluid-controlled system and pressure regime in a marine sediment. Modified from figure 2 of (Li et al., 2022).	49
Figure 22: Compaction controlled fluids and related seismic structures and its expressions as a pockmark on seafloor. Image from Berndt (2005).	49
Figure 23: Seismic expressions in a volcanic controlled fluid system. Modified from Berndt (2005)	50
Figure 24: Loseth et al. (2001) natural gas-controlled fluid system from Niger delta. Modified from Berndt (2005)	51
Figure 25: Pressure and Temperature Graph showing the stability field of gas hydrates. Inspired by Hunt (1996) & Selley & Sonnenberg, (2015).	52
Figure 26: A Model showing different fluid-controlled systems and its equivalent surface expressions on seabed for a passive continental margin. Image from Berndt (2005)	54
Figure 27 showing a marine towed streamer seismic survey with raypaths from a single shot of an airgun with streamers containing 5 hydrophones:	55
Figure 28: Showing the Fresnel zone for a low frequency and high frequency. Low frequency covers larger zones, while high frequencies cover smaller zones. From fig. 2.18 Badley( 1985).	57
Figure 29: Direct Hydrocarbon/ Fluid Indicators Løseth et al. (2009).	58
Figure 30: Map of Study Area with surrounding basin and associated landmasses.	62
Figure 31: showing a zoomed section of the study area, placement on the Norwegian Trench and corresponding seismic coverage Inline and Crosslines.	63
Figure 32: Spectral Analysis of data set to inspect for the dominating frequencies used in Table 1 and estimation of the vertical resolution of the 3D seismic data.	67
Figure 33: Showing examples of data's polarity with reference to the seafloor on 3D seismic cubes used in analysis.	68
Figure 34: Showing a difference between a Timeslice and a Horizon	70
Figure 35: showing workflow that was implemented during this project.	71
Figure 36: Basis of Stratigraphic Picks and Horizons (see section 4 of fig.10 for general seismic stratigraphy ). Inspired by Fig. 3. Horstad et al.( 1995). Note colour codes used and referenced with corresponding lithologies	73
Figure 37: shows Inline 3034 of reference Horizon picks only of ST11MZ07	74
Figure 38: Time depth map of horizon pick one across A.) ST11MZ07 B).ST98MZ C).NX0802. (Vertical Exaggeration: 1)	75
Figure 39: Time depth map of horizon pick two across A.) ST11MZ07 B).ST98MZ C).NX0802 (Vertical Exaggeration: 1)	76
Figure 40: Time depth map of horizon pick 3 across A.) ST11MZ07 B).ST98MZ C).NX0802 (Vertical Exaggeration: 1)	77
Figure 41: showing an interpreted seafloor surface of 3D seismic cubes corresponding to A). NX0802, B). ST98M7, and C). ST11MZ07 with a <b>vertical exaggeration of 25</b> .	81
Figure 42: Showing an image of A). Corresponding to the interpreted seafloor surface of ST98M7 B). Zoomed in section of seafloor surface with a random line (A- A') C). A random line showing an interpretation window transecting depressions on seafloor surface at a vertical exaggeration of 25 with a dashed line indicating the URU (Upper Regional Unconformity)	83
Figure 43: Showing an image of A). The corresponding surface of NX0802 B). Zoomed in section of seafloor surface with a random line (C- C*) C). A random line obtained from (B) seafloor surface at a vertical exaggeration of 25 with a dashed line indicating the URU (Upper Regional Unconformity) within the Quaternary.	85
Figure 44: Showing an image of A). The corresponding surface of ST11MZ07 B). Zoomed in section of seafloor surface with a random line (B- B') C). A random line was obtained from B seafloor surface at a vertical exaggeration 25.	87

Figure 45: showing shallow amplitude anomaly from a seismic 3D cube of ST11MZ07 mapped with a search window of 150ms (tw) above surface interval to map out shallow anomalies towards the seafloor. Line A-A\* represents an arbitrary line transecting shallow anomaly indicated by a red circle. (Note: the vertical exaggeration of the RMSA map is 7.5)..... 89

Figure 46: showing shallow amplitude anomaly from a seismic 3D cube of NX0802 mapped with RMSA with a search window of 160ms (tw) above to map out shallow anomalies towards the seafloor. Line (B-B\*) represents an arbitrary line transecting shallow anomaly indicated by a red circle. (Note: the vertical exaggeration of the RMSA map is 7.5). ..... 90

Figure 47: showing shallow amplitude anomaly from a seismic 3D cube of ST98M7 mapped with RMSA with a search window of 160ms (tw) to map out shallow anomalies towards the seafloor. Line (C-C\*) represents an arbitrary line transecting areas of shallow anomaly from one of the 3D seismic cubes. (Note: the vertical exaggeration of RMSA map is 7.5)..... 90

Figure 48: showing an interpretation window of inline 3034 from a 3D cube corresponding to ST11MZ07 showing amplitude anomalies, with horizon subdivisions and major (Large faults) faults and minor faults (basis as been previously established)..... 92

Figure 49: showing A). Distribution of v, w and winged-shaped anomaly with an RMSA time slice of 1632 from ST11MZ07 B). Zoomed in section of this anomaly on a RMSA at 1632 C). An ant tracking timeslice at 1800 with an adjusted RMSA opacity. D). An interpretation window showing an example of these anomalies with corresponding fractures beneath. .... 94

Figure 50: showing A). Distribution of v, w and winged-shaped anomaly with an RMSA time slice of 1473 from NX0802 B). inset image of this anomaly from RMSA at 1473ms C). An ant tracking attribute time slice was obtained at 1533ms with an adjusted RMSA opacity. D). An interpretation window showing an example of these anomalies with corresponding fractures highlighted beneath NX0802 ..... 95

Figure 51: showing A). Distribution of v, w and winged-shaped anomaly with an RMSA time slice of 1600ms from ST98M7 B). Inset image of this anomaly on an RMSA at a time slice of 1600ms C). An ant tracking attribute time slice obtained at 1740ms with adjusted RMSA opacity D). An interpretation window showing an example of these anomalies with corresponding fractures beneath. .... 96

Figure 52: shows a composite image of A). An RMSA attribute along interpreted surface (Horizon 1) of an uplifted structure located at a depth of -2250ms in two-way travel time, showing high amplitude anomalies along the interpreted horizon from ST11MZ07- 3D cube (note that no search window was used and concentric circles highlights brightened amplitude beneath) B). A combination of adjusted RMSA opacity and variance along this surface with discontinuities with a corresponding arbitrary line of (B-B\* on the interpretation window) and horizons/ surface are at a vertical exaggeration of 7.5)..... 98

Figure 53: showing Inline 3034 from T11MZ07, with manually picked fractures/ faults. Classified into minor faults, probable minor faults and large fault components observed at the base.. ..... 100

Figure 54: showing A). variance of -1001ms taken across the 3D cube (NX0802) B). showing a seismic sample with an inline 13871 (marked by the yellow line) with some examples of faulting imaged by the variance time slice. C). A close-up view of the variance time slice with several cross-cutting discontinuities imaged by the variance time slice. .... 102

Figure 55: showing A). variance of -1244ms taken across the 3D cube (ST11MZ07) B). A close-up view of the variance time slice at 1244ms in two-way travel time with cross-cutting discontinuities and discontinuities imaged by the variance time slice. C). showing a seismic sample with an inline 2963 with some examples of faulting imaged by the variance time slice. .... 103

Figure 56: showing A). Uplifted area with a decollement surface, interpreted fault with time-shifted surfaces and time slice B). A variance map along a time-shifted horizon (vertical exaggeration of 7.5) and a time slice of 3100ms to image significant fault components. Vertical Exaggeration:7.5) ..... 105

Figure 57: A composite image showing an example of potential structures underlying the base Cretaceous of ST11MZ07. A variance map across horizon (Vertical exaggeration:7.5) superimposed on an adjusted RMSA timeslice indicated on image showing an uplifted structure with several large fault components below the base Cretaceous. Note: Time-shifted horizon surface attributes was not shown, but added of boundary used in showing profile..... 107

Figure 58: A composite image showing an example of potential structures underlying base Cretaceous of NX0802. A variance map (Vertical exaggeration: 7.5) horizon 1 with an adjusted RMSA opacity map showing a sagging structure with dipped reflections. The time-shifted surfaces are just used in generating a profile showing a sag and loading. .... 108

Figure 59: showing A). An image from ST11MZ07 of inline-1225 with distinct seismic descriptions and an inset image (B). Terminologies used are from Loseth.al. (2009) ..... 109

Figure 60: Timeslice 432 from Fig.59 imaging several discontinuities and breaks in reflections. .... 112

Figure 61: showing A). Image from ST11MZ07 OF INLINE -3086 with associated seismic descriptions and an inset image (B, C and D) ..... 113

Figure 62: A time slice of 320 from Fig.62..... 117

Figure 63: Showing an A). RMSA map obtained of the seafloor showing high anomaly from against slope from the east B).RMSA map of interpreted seafloor superimposed with a flare data from cruise by NPD mapping out flares from the water column across an embankment north of the Northern Sea from a 2D window. .... 118

Figure 64: Showing an A). RMSA map obtained of the seafloor B). RMSA map of interpreted seafloor along with a cruise by NPD mapping out flares from the water column across an embankment north of the Northern Sea from a 2D window ..... 120

Figure 65: Shows an image of the impact of glaciers on the seafloor with A). Full glaciation of the Fennoscandian ice sheet B) Receding Glacier and Fast-moving ice streams C). A complete deglaciation showing the impact and action of glaciers..... 124

Figure 66: Proposed Mode and root points of possible fluid and pathways (Not to scale and not generalized) ..... 132